

Intra- and Intersegmental Coordination among Central Pattern Generating Networks in an Insect Walking System

Inaugural-Dissertation

zur

Erlangung des Doktorgrades

der Mathematisch-Naturwissenschaftlichen Fakultät

der Universität zu Köln

vorgelegt von

Charalampos Mantziaris

aus Kozani, Griechenland

Köln, 2018

Berichtersteller/in: Prof. Dr. Ansgar Büschges

Prof. Dr. Martin Nawrot

Tag der letzten mündlichen Prüfung: 14.06.2018

Zusammenfassung

In der thorakalen Ganglienkette der Stabheuschrecke *Carausius morosus* gibt es verschiedene neuronale Netzwerke, die eine oszillatorische Aktivität in Motoneuronen (MN) auslösen können und die als zentralen Mustergeneratoren (Central Pattern Generators, CPGs) bezeichnet werden. Diese treiben antagonistische Muskeln an den Beingelenken an. Für die Beincoordination während des Gehens ist eine korrekte Phasenkopplung zwischen Gelenk-CPGs notwendig. Die CPG-Kopplung kann durch intersegmentale Signale und lokale sensorische Rückkopplung vermittelt werden. Es können jedoch auch zentrale Mechanismen existieren und zur CPG-Kopplung beitragen.

Hier analysierte ich die Synchronisation, Phasendifferenz und Korrelation zwischen der Aktivität der contralateralen und ipsilateralen Depressor MN-Gruppen der deafferentierten thorakalen Ganglien, als Proxy für die intra- und intersegmentale Kopplung zwischen Coxa-Trochanter (CTr) Gelenk-CPGs, die den Depressor-Muskel von *C. morosus* antreiben.

Ich habe herausgefunden, dass eine Tendenz zu in- und anti-phasischer Aktivität zwischen kontralateralen Depressor MN Gruppen in den isolierten Meso- bzw. Metathorakalganglien besteht, dass es dagegen keine Hinweise auf eine koordinierte Aktivität zwischen den beiden Hälften des isolierten Prothorakalganglions gibt. In den miteinander verbundenen Ganglien wird die Koordination der Aktivität zwischen contralateralen Depressor MN Gruppen durch intersegmentale Einflüsse modifiziert. Ipsilaterale Depressor-MN-Gruppen der verbundenen meso- und metathorakalen Ganglien sind ebenfalls phasengekoppelt. Diese ipsilaterale Koordination wird darüber hinaus modifiziert, wenn alle drei thorakalen Ganglien miteinander verbunden sind. Die contralaterale Kopplung der Aktivität von Depressor MN Gruppen wird durch die Durchtrennung entweder der hinteren Kommissuren oder eines der Konnektive beeinflusst, jedoch nicht vollständig zerstört. Intrazellulär, zeigt die Depressor MN Aktivität dagegen keine mit dem kontralateralen Depressorzyklus korrelierte Modulation und eine Stimulation des Depressors MN beeinflusst die kontralaterale Aktivität nicht.

Zusammenfassend zeigen die Ergebnisse dieser Arbeit in einem Insektenpräparat, dem die phasische sensorische Eingänge fehlen, eine schwache Kopplung zwischen den CTr-Gelenk-CPGs, die die Depressor MN Gruppen antreiben. Die intra- und intersegmentalen Phasenbeziehungen zwischen den MN Gruppen sind jedoch nicht den Mustern ähnlich, die in einer sich verhaltenden Stabheuschrecke beobachtet werden. Daraus kann man schlussfolgern, dass eine zentrale CPG-Kopplung alleine nicht ausreichend ist, um eine Beincoordination während des Gehens zu erreichen.

In einem Nebenprojekt fand ich, dass Oszillationen im Membranpotential von Protractor MN bestehen bleiben, nachdem spannungsaktivierte Na^+ -Kanäle unter Verwendung des nicht-selektiven Blockers QX 314 blockiert wurden. Dies deutet darauf hin, dass diese Oszillationen nicht auf Aktionspotential-bezogenen ionischen Mechanismen basieren.

Abstract

In the thoracic nerve cord of the stick insect *Carausius morosus* there are distinct neural networks, known as central pattern generators (CPGs), which can induce oscillatory activity in motor neuron (MN) pools that drive the antagonistic muscles attached to the leg joints. Proper phase-coupling among joint-CPGs is necessary for intra- and interleg coordination during walking. CPG coupling can be mediated by intersegmental signals and local sensory input. However, central mechanisms may also exist and contribute to CPG coupling.

Here, I analyzed the synchronization, phase difference, and correlation between the activity of contralateral and ipsilateral depressor MN pools of the deafferented thoracic ganglia, as a proxy for intra- and intersegmental coupling among Coxa-Trochanter (CTr) joint-CPGs that drive the depressor muscle of *C. morosus*.

I found a tendency for in- and anti-phase activity between contralateral depressor MN pools in the isolated meso- and metathoracic ganglia respectively, and no evidence for coordinated activity in the isolated prothoracic ganglion. In the interconnected ganglia, coordination of contralateral depressor MN activity is modified by intersegmental input. Ipsilateral depressor MN pools in the interconnected meso- and metathoracic ganglia are also phase-coupled. Ipsilateral coordination is further modified when all three thoracic ganglia are interconnected. Contralateral coupling between depressor MN pool activity is affected by sectioning either the posterior commissures or one of the connectives, yet not fully disrupted. Finally, intracellular depressor MN activity shows no modulation correlated with the contralateral depressor cycle, and depressor MN stimulation does not influence contralateral activity.

Taken together, findings of this thesis reveal weak coupling among CTr-joint CPGs driving the depressor MN pools in an insect preparation lacking phasic sensory input. However, the intra- and intersegmental phase relationships between leg MN pools are not

similar to the activity patterns observed in a behaving stick insect. Therefore, central CPG coupling alone is insufficient to bring about leg coordination during walking.

In a side-project, I found that protractor MN membrane potential oscillations persist after blocking voltage-activated Na⁺ channels using the non-selective blocker QX 314. This indicates that oscillations are not based on action potential-related ionic mechanisms.

Table of contents

Zusammenfassung	2
Abstract.....	4
Table of Abbreviations.....	8
Introduction	9
<i>Neuronal oscillations and generation of rhythmic movement</i>	9
<i>CPGs and their role in walking</i>	10
<i>Central vs. sensory neural mechanisms in CPG coordination and walking generation</i>	12
<i>Intra- and interleg coordination in Carausius morosus</i>	16
<i>This thesis</i>	17
Materials and Methods	19
<i>Experimental Animals</i>	19
<i>Preparation</i>	19
<i>Electrophysiology</i>	21
<i>Analysis of coordination between rhythmically-active MN pools</i>	21
I. Phase analysis based on waveform transformation to a discrete-time analytic signal	22
II. Coordination analysis based on the spiking time series	25
III. Cross-correlation analysis of the spike time series	28
<i>Statistics</i>	29
Results.....	32
I. Intrasegmental CPG coordination	32
<i>Coordination of activity between contralateral depressor MN pools in the isolated mesothoracic ganglion</i>	32
<i>Coordination of activity between contralateral depressor MN pools in the isolated metathoracic ganglion</i>	35
<i>Intrasegmental coordination of depressor MN activity is influenced by intersegmental signals ...</i>	38
<i>Summary of the results concerning the intrasegmental CPG coupling in the meso- and metathoracic ganglia</i>	47
<i>Coordination of activity between contralateral depressor MN pools in the isolated prothoracic ganglion and the interconnected pro- and mesothoracic ganglia</i>	51
<i>Coordination between contralateral depressor MN pools in the complete deafferented thoracic nerve cord</i>	58
<i>Summary</i>	62
II. Intersegmental CPG coordination	64
<i>Intersegmental coordination of activity between depressor MN pools in the interconnected meso- and metathoracic ganglia</i>	64
<i>Intersegmental coordination of activity between depressor MN pools in the interconnected pro- and mesothoracic ganglia</i>	68
<i>Intersegmental coordination of activity between depressor MN pools in the complete deafferented thoracic nerve cord</i>	71

Summary	77
III. Neuronal mechanisms underlying intra and intersegmental CPG coordination.....	79
<i>Intrasegmental coordination of depressor MN activity after posterior midline section in the isolated mesothoracic ganglion.....</i>	79
<i>Intra- and intersegmental coordination of depressor MN activity after sectioning of one connective nerve in the interconnected meso- and metathoracic ganglia.....</i>	83
<i>Intracellular recordings of the fast and slow depressor motor neuron activity</i>	88
IV. Influence of QX 314 on motor neuron activity	91
Discussion	93
<i>Variability in pilocarpine-induced activity and analysis of CPG coupling</i>	94
<i>Contralateral CPG coordination in isolated thoracic ganglia.....</i>	97
<i>Influence of central intersegmental pathways on contralateral CPG coordination.....</i>	100
<i>Neural mechanisms underlying intrasegmental CPG coordination.....</i>	102
<i>Intersegmental CPG coordination and the underlying mechanisms</i>	105
<i>Speed-dependence of intersegmental coordination patterns.....</i>	109
<i>Motor neuron activity and the role of Ca²⁺</i>	110
References	112
Acknowledgments	125
Appendix.....	126

Table of Abbreviations

Abbreviation	Complete form
[Ca ²⁺] _i	Intracellular calcium concentration
5-HT	5-Hydroxytryptamin or Serotonin
ACh	Acetylcholine
ASC	Ascending interneuron in the crayfish swimmeret system
BAPTA	1,2-bis(<i>o</i> -aminophenoxy)ethane- <i>N,N,N',N'</i> -tetraacetic acid
BLs ⁻¹	Body lengths per second
circ_mean	Circular mean
circ_std	Circular standard deviation
CNS	Central nervous system
ComInt1	Commissural interneuron 1
CPG	Central pattern generator
CS	Campaniform sensilla
CTr	Coxa-Trochanter joint
DCI-DCVI	Dorsal commissures I to VI
dep	Depressor MN
DSC	Descending interneuron in the crayfish swimmeret system
fCO	Femoral chordotonal organ
FDTTr	Fast depressor trochanteris MN
FTi	Femur-Tibia joint
IN	Interneuron
mAChRs	Muscarinic acetylcholine receptors
meso	Mesothoracic ganglion
meta	Metathoracic ganglion
MN	Motor neuron
N	Number of animal preparations
n	Number of cycles
NMDA	<i>N</i> -methyl-D-aspartate
pro	Prothoracic ganglion
PVC	Posterior ventral commissure
QX 314	<i>N</i> -Ethylidocaine bromide
RSA	Rectified and smoothed activity
SDTr	Slow depressor trochanteris MN
SMC	Supramedian commissure
TCMRO	Thoraco-coxal muscle receptor organ
ThC	Thorax-Coxa joint
VCI-VCII	Ventral commissures I and II
ΔΦ	Phase difference
Φ	Phase

Introduction

Neuronal oscillations and generation of rhythmic movement

Oscillatory phenomena are commonly observed in nature and neural systems are not an exception (Singer, 2018). In fact, even single neurons behave as oscillators, swinging between an action potential (spike) release and a refractory period of inactivity. Depending on cellular and synaptic properties, neurons can periodically trigger a group of action potentials (burst), therefore acting as pacemakers or conditional “burststers”. Moreover, neurons synapse with each other and, based on various connectivity patterns, they form multifunctional oscillatory neural circuits (Getting, 1989). Such circuits are abundant both in complex systems, such as the mammalian brain cortex (Buzsáki and Draguhn, 2004; Grillner et al., 2005), as well as in simpler invertebrate neural systems (Selverston and Moulins, 1985). Proper phase coupling between neuronal oscillators has been related to important functions in the brain, such as sensory processing, attention and memory (Sadeh et al., 2014). Nevertheless, the functionality of coupling among neuronal oscillators is perfectly expressed in the generation and patterning of rhythmic motor activity during locomotion.

Rhythmic motor activity is at the core of everyday behavioral expressions, such as walking, swimming, breathing and chewing, which require repetitive muscle activation and are vital for animals and humans. As early as the beginning of the 20th century, scientists debated on whether a complex behavior, such as muscle alternation during leg stepping, purely resulted from sensory-based reflex action, or could as well be generated in the absence of sensory and descending commands (Brown, 1911; Sherrington, 1913). Today, we know that there are neural oscillatory networks located in the central nervous system that are intrinsically capable of generating rhythmic motor activity, without the contribution of descending or sensory phasic input, even though the latter can modulate and shape the intrinsic activity pattern (Delcomyn, 1980; Marder and Calabrese, 1996; Marder and Bucher, 2001; Katz and Hooper, 2007; Smith et al., 2013). These networks are called Central Pattern Generators (CPGs).

CPGs and their role in walking

CPGs have been implicated in the generation of various rhythmic animal behaviors: respiration in mammals (Smith et al., 1990, 2013); heartbeat in the lobster and the leech (Selverston and Moulins, 1985); gastric movements in Crustaceans (Marder and Calabrese, 1996); scratching in the turtle (Stein, 2018); swimming in the lamprey (Grillner, 2003), the tadpole (Arshavsky Yul et al., 1993) and various mollusks (Selverston and Moulins, 1985; Arshavsky Yul et al., 1993; Sakurai and Katz, 2016); flight in the locust (Ausborn et al., 2007); leg stepping in mammals (Grillner and Zangger, 1979; Whelan, 1996) etc.. The basic principles of motor control appear to be universal among animals (Pearson, 1993). Therefore, in the following paragraphs, I am going to cite a number of studies on both vertebrates and invertebrates, to introduce the role of CPGs in walking and present the main evidence on central generation of walking behavior.

CPGs are responsible for generating alternating muscle activity, which is essential for walking behavior. Evidence on centrally-generated walking patterns was first published in the 70's, with experiments on semi- or completely deafferented animal preparations, namely preparations partially or fully deprived of afferent input from sensory organs. Antagonistic activity in leg MNs could still be recorded in a semi-deafferented cockroach preparation, after elimination of input from leg sensory organs (Pearson and Iles, 1970; Pearson, 1972). Similarly, alternating activity in antagonistic leg motor neuron (MN) pools could also be induced upon tactile stimulation in the deafferented thoracic nervous system of the stick insect (Bässler and Wegner, 1983). Three years later, spontaneous oscillations of MN pools controlling leg muscles were observed in a crayfish preparation, consisting of the isolated thoracic ganglia with the proprioceptor TCMRO (thoraco-coxal muscle receptor organ) of the fourth leg attached (Sillar and Skorupski, 1986). The resulting rhythmic motor pattern resembled the muscle activity pattern expressed during forward walking by behaving crayfish. Thus, experiments on semi-intact preparations first revealed that walking patterns could be centrally generated.

Compelling evidence in support of the role of CPGs in walking generation came from experiments on deafferented nerve and spinal cord preparations *in vitro*, upon pharmacological activation. Bath application of oxotremorine or pilocarpine, two agonists of muscarinic acetylcholine receptors (mAChRs), on the thoracic nerve cord of various invertebrates resulted in rhythmic activation of antagonistic leg MN pools (Chrachri and Clarac, 1990; Ryckebusch and Laurent, 1993; Büschges et al., 1995). Pilocarpine application on the deafferented nerve cord of the stick insect resulted in tonic MN depolarization that was patterned by phasic inhibitory input, presumably from the CPG, identical to the MN activity after tactile stimulation of a semi-intact preparation (Büschges, 1998; Schmidt et al., 2001; Büschges et al., 2004). Furthermore, pilocarpine-induced motor patterns, extracellularly recorded from deafferented nerve cords of the cockroach and the hawk moth, resembled walking patterns that can be recorded from leg muscles of those animals during walking (Johnston and Levine, 2002; Fuchs et al., 2011). Such patterns of activity are called fictive motor patterns and underline the importance of central coupling among CPGs in generating walking behavior. Finally, in a more recent study on isolated spinal cords of neonatal mice, locomotor-like activity could be induced in the hind-leg MN pools using optogenetics (Hägglund et al., 2013). Thus, walking-like motor activity could be induced by pharmacological or light stimulation of certain neural networks in deafferented spinal or nerve cord preparations.

Regarding the CPG topology, five years before Pearson reported on the evidence for a walking CPG, Wendler had assumed the existence of individual phase-coupled oscillators for each leg of the stick insect (Wendler, 1965). Based on behavioral observations, Foth and Bässler also proposed that each leg of the stick insect should be individually controlled by its own walking pattern generator (Foth and Bässler, 1985). However, experiments on the hind limbs of the cat revealed variable activity patterns for different flexor muscles of the same leg (Grillner and Zangger, 1979) that could not have been generated by a single CPG. Thus, the “unit burst generator” hypothesis emerged, according to which a CPG consists of several generators. These generators assume distinct functions and they can be mutually coupled to

result in a coordinated motor output. In favor of this hypothesis, Büschges and colleagues demonstrated that MN pools corresponding to different joints of the same leg oscillate at different frequencies upon pilocarpine application in the stick insect deafferented mesothoracic ganglion, therefore proposing that distinct CPG modules should control the muscles of each leg joint (Büschges et al., 1995). Interestingly, the authors noticed spontaneous recurrent patterns (SRPs) of coordinated MN activity, as a result of transient coupling among CPGs. SRPs resembled activity patterns expressed during stepping transitions in walking animals. Only recently the “unit burst generator” model resurged with experiments on the neonatal spinal cord preparation of the mouse. Hägglund and colleagues demonstrated unilateral induction of locomotor-like oscillatory activity and independent activation of flexor- or extensor-related MN pools (Büschges and Borgmann, 2013; Hägglund et al., 2013).

Taken together, data published within the last 50 years have confirmed the existence of independent CPG modules in the CNS, which control and shape MN activity to generate rhythmic motor activity. In the stick insect, accumulating reports argue for at least one hemisegmental CPG devoted to the control of each of the main leg joints. Proper phase coupling among segmental CPGs is essential for generating a coordinated and behaviorally relevant walking motor pattern. However, the exact neural mechanisms underlying CPG coupling and coordination remain largely elusive in most animal preparations.

Central vs. sensory neural mechanisms in CPG coordination and walking generation

Fictive locomotor patterns have been recorded in a large number of deafferented nerve and spinal cord preparations (Delcomyn, 1980; Marder and Bucher, 2001). Assuming that deafferentation has no immediate compensatory side-effects, fictive locomotion would imply that sensory input is of relatively minor importance for CPG coupling, locomotor patterning and behavior (Marder, 2002). It is reasonable to argue that nature has endowed animals with central neural mechanisms, capable of entirely organizing a locomotor pattern, whereas the

role of afferent input would in that context be restricted in compensating for external perturbations, thus allowing animals to preserve their pivotal ability to move (Grillner and Zangger, 1975).

This is especially relevant to animals moving in homogeneous environments (e.g. aquatic). Intact lampreys swim with side-to-side undulations, having an intersegmental phase lag of about 1% of the undulatory cycle, identical to the phase difference between adjacent CPG motor outputs recorded after bath application of the NMDA receptor agonist D-glutamate on the isolated spinal cord (Grillner, 2003; Hill et al., 2003). Similarly, in the crayfish swimmeret system, the intra- and intersegmental phase relationships of the abdominal limbs observed in behavior are maintained by the deafferented abdominal nerve cord preparation (Mulloney and Smarandache-Wellmann, 2012). In contrast, leeches show a phase lag of about 20° between adjacent body segments during dorsal-ventral undulatory swimming, which substantially differs from the 8° phase lag recorded in the isolated ganglia chain *in vitro* (Hill et al., 2003). However, even in leeches, the basic swimming coordination pattern is preserved. To conclude, fictive swimming patterns are quite similar to the behaviorally expressed coordination patterns.

True as this may be for some aquatic animal preparations, it does not apply in the case of terrestrial animals. The motor pattern recorded in the deafferented nerve cord of the adult hawk moth preparation after pilocarpine application resembled a typical leg coordination pattern during insect walking (Johnston and Levine, 2002). Interestingly though, the intra- and intersegmental phase relationships of this fictive motor pattern are only rarely represented in the hawk moth behavior repertoire (Johnston and Levine, 1996a). In the deafferented thoracic nerve cord of the crayfish, although coordination of MN pools within a hemisegment resembled the coordination between leg muscles during forward-walking, in most thoracic ganglia examined, ipsilateral MN pools of different segments were active in-phase, dissimilar to the coordination expressed by the intact animal (Sillar et al., 1987; Chrachri and Clarac, 1990). Moreover, pilocarpine-induced fictive motor patterns that resembled walking coordination patterns have been reported for the deafferented thoracic

nerve cords of the locust and the cockroach (Ryckebusch and Laurent, 1993; Fuchs et al., 2011). However, analysis of the former was confined to recording intervals that showed regular rhythmicity, and the latter solely took into consideration the “temporal characteristics of the rhythmic bursts” (see Fuchs et al., 2011, p. 4).

A more recent study on the cockroach substantiated earlier findings concerning a fictive walking pattern in this system and proposed a central connectivity model adequate to reproduce fictive walking (David et al., 2016). In contrast, findings of Ryckebusch and Laurent (1993) concerning fictive walking patterns in the locust were not substantiated. A recent study in the locust deafferented system reported a tendency for intra- and intersegmental in-phase activity between homologous MN pools, a pattern that is never observed during insect walking (Knebel et al., 2016). Tendency for in-phase intersegmental coordination between homologous MNs had been earlier reported for the stick insect, yet not systematically analyzed (Büschges et al., 1995). Nevertheless, neither a cycle-to-cycle interjoint coupling nor a strong intra- or intersegmental coupling was observed in stick insect preparations. Finally, flexor-/extensor-like and left/right alternation could reliably be induced after transfusion with 5-HT/NMDA in the lumbar spinal cords of mice and rats, only at the neonatal or embryonic stage (Talpalar et al., 2013; Beliez et al., 2015). All the above taken into consideration, generation of intra- and intersegmental coordination in the absence of sensory input appears to be rather complex in nerve and spinal cord preparations of adult terrestrial animals. Central CPG coupling is not sufficient to support a persistent and complete fictive motor pattern that would resemble the muscle activity pattern during walking. Thus, sensory input plays a crucial role in CPG coupling and coordination in terrestrial locomotion.

The role of sensory input in CPG coupling and coordination has been routinely investigated in semi-intact invertebrate preparations. Sillar and colleagues showed that in the crayfish, stimulation of the TCMRO at the fourth thoracic hemiganglion resulted in in-phase entrainment of MN activity in the third and fourth ipsilateral hemiganglia (Sillar et al., 1987). Similarly, sensory input from a stepping front leg resulted in tonic depolarization and rhythmic

modulation of the ipsilateral mesothoracic MN pools of the stick insect (Ludwar et al., 2005a, 2005b). Modulation in MN activity correlated with front leg movement, resulting however in a non-functional coordination pattern. Moreover, pilocarpine activation of the MN pools in the deafferented prothoracic ganglion did not affect mesothoracic MN activity, implying that front leg afferent signaling is necessary for mesothoracic CPG activation and coordination (Ludwar et al., 2005a). In line with previous studies, stepping of a single middle or hind leg also affected MN activity in adjacent ganglia (Borgmann et al., 2007), and afferent signaling from a stepping front or hind leg entrained in-phase the pharmacologically-induced MN activity in the posterior or anterior thoracic ganglia respectively (Borgmann et al., 2009; Grabowska, 2014). Interestingly, local sensory input from a middle leg stump could override intersegmental front leg signaling and interfered with the in-phase entrainment this leg imposed (Borgmann et al., 2009, 2011). This indicated that local afferent input exerts a stronger influence on CPGs than intersegmental input. Consistent with these results, leg proprioceptive feedback influenced the activity of neighboring CPGs in the cockroach (Fuchs et al., 2011, 2012; Ayali et al., 2015). Finally, signals from trochanteral campaniform sensilla (CS), leg sensory organs that detect force and load, entrained the centrally-generated motor activity of the ipsilateral hemiganglion (Akay et al., 2007). Thus, input from leg sensory organs exerts intra- and intersegmental coordinating influence on CPGs that are responsible for walking.

To conclude, neurophysiological data have demonstrated that leg coordination during walking is based on a combination of intersegmental signal processing and local sensory input, both acting on centrally generated motor patterns. Centrally generated motor patterns differ among deafferented animal preparations, indicating potential differences in the relative contribution of central and peripheral signaling in CPG coordination. Intersegmental interactions among CPGs, the underlying neuronal mechanisms and their importance for walking generation still need to be investigated. Nevertheless, the state-of-the-art knowledge allows us to describe coordination between CPGs controlling muscles of the main joints in within a leg of the stick insect *Carausius morosus*.

*Intra- and interleg coordination in *Carausius morosus**

The neural control mechanisms of single-leg stepping have been thoroughly described for the middle leg of the stick insect (Büschges et al., 2008). *C. morosus* has six long, functionally uniform legs equipped with a palette of distinct sensory organs (Bässler and Büschges, 1998; Tuthill and Wilson, 2016). Each leg consists of five independent segments: the coxa; the trochanter; the femur; the tibia and the tarsus. The three main leg joints are the thorax-coxa (ThC), the coxa-trochanter (CTr), and the femur-tibia (FTi) joint, each controlled by a pair of antagonistic muscles: the protractor/retractor coxae; the levator/depressor trochanteris and the flexor/extensor tibiae. A step cycle consists of two phases: the stance phase, during which the leg has ground contact, and while moving to one direction it creates forces that propel the animal to the opposite direction; and the swing phase, during which the leg is in the air and moves back to its initial position to complete the cycle. Leg kinematics and muscle activation patterns differ among legs of the stick insect and depend on walking direction (Gruhn et al., 2009; Rosenbaum et al., 2010). Thus, neural mechanisms underlying leg stepping may also be accordingly different.

During forward-straight walking, extension of the middle-leg tibia is detected by the femoral chordotonal organ (fCO). The fCO has access to the CTr-joint CPG and results in coordinated activation of the depressor and flexor MNs (Hess and Büschges, 1999). Upon leg touchdown, activation of tarsal CS results in synergistic activation of the retractor unguis, the depressor and the flexor muscles, whose action enables substrate grip (Zill et al., 2015). At the same time, load signals detected by trochanteral and femoral CS initiate the retractor and flexor activity respectively, while the protractor muscle is deactivated and levator activity switches to depressor (Akay et al., 2001, 2004; Borgmann et al., 2011; Zill et al., 2017). Flexion of the tibia during the step is detected by the femoral chordotonal organ (fCO) that activates the levator and extensor MNs to lift the leg from the ground and complete the cycle (Hess and Büschges, 1999). Thus, a number of leg sensory organs couple the activity of CPGs that control single joints and result in muscle synergies that enable coordinated movement of the leg during stepping.

Stepping of one leg needs to be coordinated with the rest of the legs of an insect to induce versatile walking behavior. Depending on their walking speed, insects express a continuum of walking patterns that range from the “wave gait” at low speeds, where only one leg is in swing phase when all other legs touch the ground (Hughes, 1952; Graham, 1985; Wosnitza et al., 2013), to tetrapod and tripod coordination patterns at higher speeds, where two or three legs are in swing at the same time, respectively (Hughes, 1952; Wilson, 1966; Mendes et al., 2013; Wosnitza et al., 2013; Berendes et al., 2016). These walking patterns are reminiscent of the energetically optimal gaits observed in vertebrates (Hoyt and Taylor, 1981; Alexander, 1989). However, it is still not known how different coordination patterns are generated and what neural mechanisms underlie the transition in coordination throughout this walking pattern continuum.

Behavioral experiments on walking stick insects have contributed a lot in our understanding of the mechanisms for leg coordination. These experiments resulted in a list of consistent coordinating interactions observed among legs, known as the “Cruse rules” (Cruse, 1990): 1) a leg in swing phase suppresses lift-off of its anterior neighboring leg; 2) upon touchdown a leg promotes lift-off of its anterior neighboring and its contralateral leg; 3) a leg in late stance phase promotes lift-off of its posterior or contralateral leg; 4) a leg’s touchdown position affects the upcoming touchdown position of its posterior neighboring leg; 5) load increase in one leg results in co-contraction and stance prolongation of all other legs. The “Cruse rules” comprised the basis upon which an artificial neural network for hexapod walking was built (Schilling et al., 2013). However, the neural mechanisms underlying the above behavioral observations are not known yet.

This thesis

In the introduction, out a few limitations of previous neurophysiological studies on deafferented insect preparations were pointed out and gaps of knowledge on how interleg coordination in insects is organized at the neuronal level were reported. In the past, in an

attempt to anticipate the highly noisy, pharmacologically-induced activity in deafferented preparations, researchers inevitably restricted their analysis on certain easily identifiable motor patterns. Consequently, this resulted in the assumption that walking coordination patterns, like the tripod pattern, are generated centrally in the thoracic ganglia, without the need of sensory input. In fact, there were numerous studies on fictive swimming patterns to support this notion. However, Büschges and colleagues (1995) did not observe fixed phase relationships between protractor MN pools in the deafferented thoracic ganglia of the stick insect. The authors reported instead a tendency for in-phase activity throughout recording intervals ranging from 5 to 25 consecutive cycles. Thus, CPGs driving the protractor MN pools in the stick insect appear to transiently interact with each other, in the absence of sensory input, to give rise to a non-functional motor pattern.

Within the scope of the present thesis, it was hypothesized that the CTr-joint CPGs driving the depressor MN pools of the stick insect are centrally coupled with each other and this results in coordinated MN activity, as previously observed for the protractor MN pools by Büschges and colleagues (1995). To test this, pharmacologically-induced depressor MN activity was investigated in the deafferented thoracic nerve cord of the stick insect. The investigation process was carried out for the first time throughout long recording intervals by means of three different methods of analysis. Moreover, this thesis concentrated on the neuronal mechanisms underlying CPG coupling and their role in walking pattern generation. Finally, based on the finding that calcium transients mirror MN activity and persist after blocking the generation of action potentials (Goldammer, 2013), persistence of MN membrane potential oscillations was also assessed. To achieve that, intracellular MN activity was recorded and a non-specific channel blocker known to interfere with action potential generation was applied.

Materials and Methods

Experimental Animals

For all experiments in this thesis, adult female Indian stick insects of the species *Carausius morosus* were used. The animals were bred in a colony at the Biocenter, University of Cologne. The colony is maintained at 22 to 26°C and 45 to 55% humidity, under a 12 h light/12 h dark cycle. The experimental procedures described below comply with the German National and State Regulations for Animal Welfare and Animal Experiments.

Preparation

The experimental procedures for inducing and recording rhythmic activity of MN pools has been previously published (Büschges et al., 1995). CPG activity was induced by bath application of pilocarpine, and was assessed by recording extracellular activity of leg MN pools. Extracellular electrodes were placed on the coxal branch 1 and 2 nerves (C1 and C2) of the main leg nerve nervus cruris (ncr) (Graham, 1985). C1 and C2 nerves carry the axons that innervate the levator and depressor trochanteris muscles of the stick insect, respectively (Bässler et al. 1983; Goldammer et al., 2012). The levator and depressor trochanteris muscles allow the leg to move downwards and upwards respectively, about the Coxa-Trochanter (CTr) joint. All lateral nerves at the ganglia of interest were either crushed or cut, to avoid that peripheral sensory input influences the pharmacologically-induced motor activity. Both the intrasegmental coordination between contralateral MN pools of each deafferented thoracic ganglion, when isolated or interconnected with other thoracic ganglia, and the intersegmental coordination between ipsilateral MN pools located in different interconnected thoracic ganglia were analyzed. The first abdominal ganglion was always left interconnected to the metathoracic ganglion. Finally, in split-bath experiments, the animal's body cavity was separated by a Vaseline-barrier, to allow targeted drug application on a specific ganglion.

Rhythmic activity in levator and depressor MN pools is strictly alternating (Büschges, 1995; Büschges et al., 1995). Thus, rhythmicity in either of these MN pools can be monitored by exclusively recording and analyzing the activity of just the one of them. Analysis was focused on the CTr joint and especially the depressor MN for three reasons: the activity of the muscles controlling movement of the CTr joint defines the stance and swing phases of each leg's stepping cycle, irrespective of the walking direction and orientation of locomotion (Rosenbaum et al., 2010); there are only two excitatory MNs innervating the depressor trochanteris muscle in each hemisegment, a slow (SDTr) and a fast (FDTr) MN, rendering the data analysis easier and more accurate; and there is a plethora of publications investigating MN and muscle activity of the same joint in other preparations (Ryckebusch and Laurent, 1994; Johnston and Levine, 2002; Knebel et al., 2016).

The preparation procedure for intracellular recordings has been described in detail elsewhere (Büschges, 1990). For the investigation of Ca²⁺ influx mechanisms, extracellular recordings from the leg nerves were combined with intracellular recordings of MN activity. Extracellular electrodes were placed on the lateral nerves 2c and 5 (nl2c and nl5). Nerves nl2 and nl5 carry the axons innervating the protractor and retractor coxae muscles of the stick insect, respectively. The protractor and retractor coxae muscles allow the leg to move forwards or backwards about the Thorax-Coxa (ThC) joint. Intracellular retractor or protractor MN activity was recorded ipsilateral to the extracellular recordings, and pilocarpine was applied either before or after the intracellular recording had been established.

Pilocarpine concentration depended on the preparation. Unlike intracellular recording preparations, for extracellular recordings the neural lamella and the perineurium, the main diffusion barrier between neurons and the hemolymph, were left intact (Treherne and Schofield, 1981; Schofield and Treherne, 1984). Therefore, for extracellular recordings, 3 to 7 mM pilocarpine in saline was applied, whereas for intracellular recordings the concentration was at least ten times lower, ranging from 0.1 to 0.5 mM. Pilocarpine concentration always corresponded to the minimum concentration that could reliably induce rhythmicity in MN pools of the ganglia under investigation.

Electrophysiology

Extracellular MN activity was recorded with hook electrodes (Schmitz et al., 1988). The signal was 100-fold pre-amplified by isolated low-noise preamplifiers (model PA101, Electronics workshop, Zoological Institute, Cologne). It was further ten-fold amplified to reach an overall gain of 1000 and filtered (low-cut: 200 Hz, high-cut: 3 kHz) using a standard 4-channel amplifier/signal conditioner (model MA102, Electronics workshop, Zoological Institute, Cologne). Finally, the signal was digitized at a sampling rate of 12 kHz, using the Micro 1401-3 acquisition unit (CED, Cambridge, UK) and it was monitored using the Spike2 software (CED, Cambridge, UK).

Intracellular recordings were performed in bridge mode (intracellular amplifier SEC-10L, npi electronics, Tamm, Germany). Sharp electrodes were made of thin-walled borosilicate glass capillaries, pulled using the Sutter Micropuller (P-1000, Sutter Instruments, Novato, CA, USA). They were filled with a 3M KAc/0.1M KCl solution, and depending on the experimental procedure, either 5% Neurobiotin or 100 mM QX 314 bromide, a non-selective blocker of voltage-activated Na⁺ channels (Biotrend Chemicals AG) was added to it (Connors and Prince, 1982). Electrode resistances ranged between 15 and 35 MΩ. QX 314 was injected in the cell via positive holding current and/or current pulses of 1 to 2 nA.

Analysis of coordination between rhythmically-active MN pools

Three different methods of analysis were applied. In recordings that showed regular bursting with clearly defined cycle periods, a phase analysis was applied to test for coordination and phase relationships between recording traces, and make assumptions about possible coupling interactions of the underlying networks. In noisy recordings that showed irregular bursting patterns interrupted by intervals of tonic activity, spiking activity of the one trace was plotted against the activity of the other to identify recurrent bursting patterns throughout the recording and cross-correlation was used to test for interdependence of activity.

I. Phase analysis based on waveform transformation to a discrete-time analytic signal

To investigate potential central interactions between meso- and metathoracic CPGs that drive the trochanteral MN pools, a time-series analysis method widely used in electro-diagnostic medicine and functional neuroimaging techniques was adapted. This method has been successfully applied for the analysis of non-stationary, extracellularly recorded rhythmic motor activity (Tass et al., 1998; Pikovsky et al., 2001; Kralemann et al., 2008).

A recording interval of the activity between contralateral depressor MN pools in the isolated mesothoracic ganglion after application of 5 mM pilocarpine was used here to exemplify this method, as both waveforms depict regular bursting with clear cycle onsets (Fig. 1, a). First, the DC offset was removed and each extracellular waveform signal was rectified and smoothed with a time constant of 0.05 s using the Spike 2 toolbox (version 7.17; Cambridge Electronic Design, Cambridge, UK) (Fig. 1, b). Next, waveforms were re-sampled at a rate of 100 Hz and data time-series were imported into MATLAB R2014b (MathWorks, Inc., Natick, MA, USA). Based on the formula $x = x_r + i * x_i$ (x_r is the real part corresponding to the original data and x_i the imaginary part containing the Hilbert transform), the real data sequence was transformed to a discrete-time analytic signal (Fig. 1, c). This signal retains the amplitude, frequency content and phase information of the original data. The Poincaré section (Fig. 1, c, grey vertical line) was then used to determine the instantaneous-wrapped phase increasing from 0 to 1 for each cycle (Fig. 1, d). Finally, to analyze the phase development over time for each MN activity, the phase was unwrapped and let continuously grow from one cycle to the next, giving rise to the infinite phase that was plotted over the recording time for each waveform of the Fig. 1, a (Fig. 1, e). The phase difference development between the two rhythms was calculated by subtraction of the infinite phase values concerning the one nerve activity from those concerning the other (Fig. 1, f). Furthermore, the phase difference between the two rhythmic activities was calculated, by defining the relative phase between corresponding cycle onsets of the two activity traces

(Fig. 1, g). The resulting angles were binned in 18 bins (20° per bin) and plotted as a phase difference distribution, after normalizing the number of events of each bin to the sum of the events (Fig. 1, h). To conclude, with this method cycles were automatically marked throughout the recording, and the phase difference between rhythmically-active MN pools could be reliably analyzed.

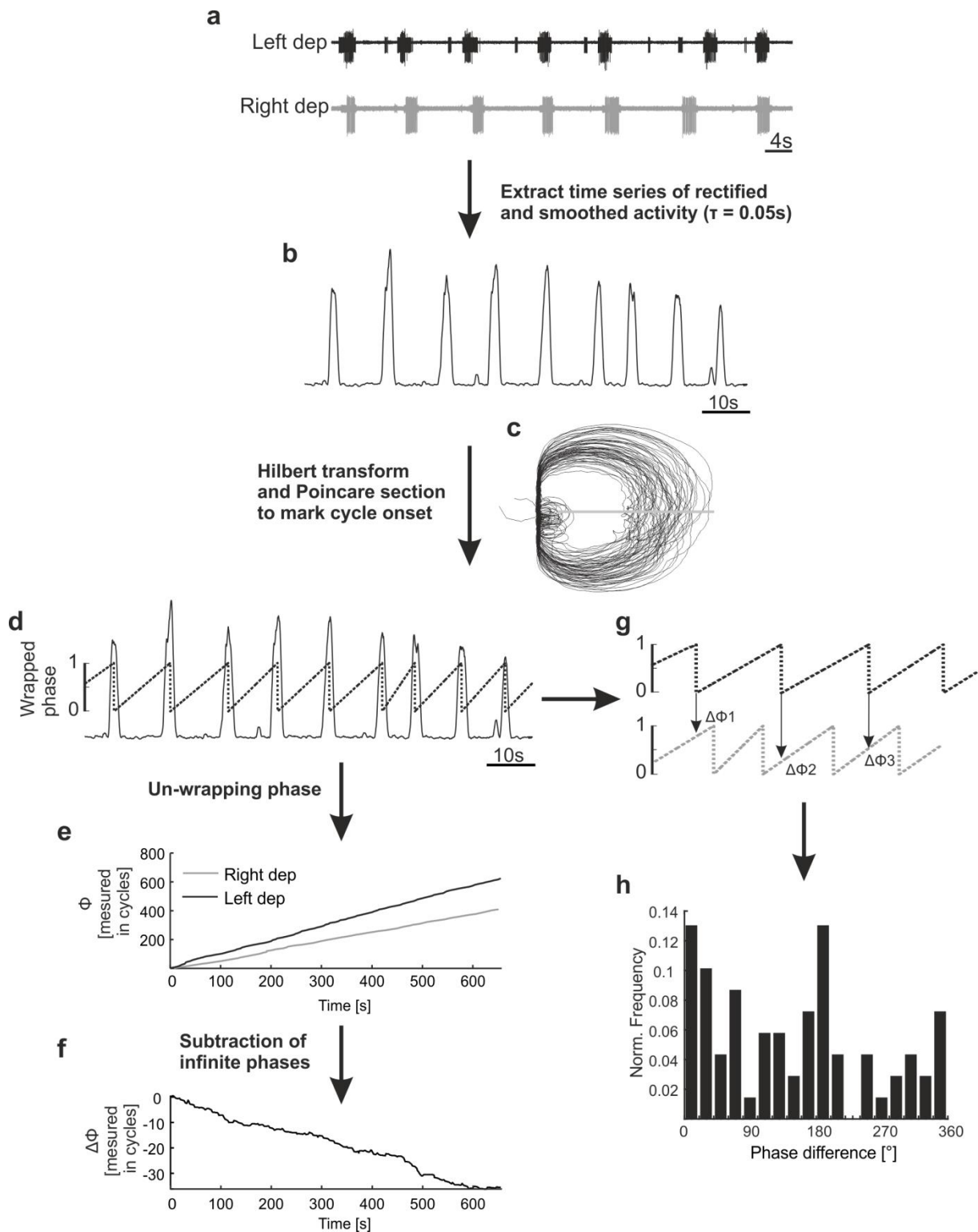


Figure 1: Phase analysis of activity between contralateral depressor MN pools, based on waveform transformation to a discrete-time analytic signal. **a:** Extracellular recording of the activity of contralateral MN pools that innervate the depressor muscles of the stick insect. Rhythmic activity was induced by bath application of 5 mM pilocarpine. **b:** Rectified and smoothed trace. **c:** Discrete-time analytic signal using the Hilbert transform. The amplitude, frequency and phase information of the real data are here preserved. Cycles were defined according to the Poincaré section. **d:** Wrapped phase defined on the circle from 0 to 1. **e:** Infinite (cumulative) phase (Φ) of each nerve. **f:** Phase difference ($\Delta\Phi$) development throughout the recording measured in cycles, after subtraction between the infinite phase curves. **g:** Calculation of the relative phase ($\Delta\Phi_1 \rightarrow \Delta\Phi_n$) of the cycle onset of the one activity to the cycle of the other activity **h:** Relative phase values were allocated in 18 bins; the frequency of values in each bin was normalized to the sum of all bins, and was plotted in as a phase difference distribution.

II. Coordination analysis based on the spiking time series

To identify recurrent activity patterns that resulted from synchronized bursting throughout a recording of highly variable MN activity, spiking activity of the one trace was plotted against the activity of the other. For this, all spike events of the recordings were marked and the corresponding time series were extracted at a sampling rate of 1000 Hz (Fig. 2, a1). Then the spike time series were smoothed by convolving with a 1001-point Gaussian window (Fig. 2, a2). Last, both resultant time series were identically interpolated at a rate of 100 Hz and for each time point the spike activity of the one waveform was plotted against the spike activity of the other (Fig. 2, b1 and b2).

To illustrate the possibilities of this method, a recording showing anti-phase coordination and another showing a clear tendency for in-phase coordination were analyzed. Asynchronous spiking events, related to anti-phase bursting, correspond to data points that move between the x and y axes and result in data clustering along them (Fig. 2, c1). Conversely, synchronous spiking events, related to in-phase bursting, correspond to data points that periodically move from zero towards the center of the plot, until maximum spike activity is reached, and back to zero, mainly resulting in data clustering at the center of the plot (Fig. 2, d1). Completely random spiking events, corresponding to uncoordinated nerve activity would result in data scattered throughout the plot with unclear pattern and no distinct clusters. For better result illustration, data were binned in a 15-by-15 grid and 2D probability distributions were plotted (Fig. 2, c2 and d2). To increase contrast, all data corresponding to single or double spikes, which resulted in normalized activity between 0 and 0.1, and were considered to result from noise in the nervous system, were omitted from the plots. The map scale was adjusted accordingly for all figures in this thesis and is depicted only once in Fig. 2, c2.

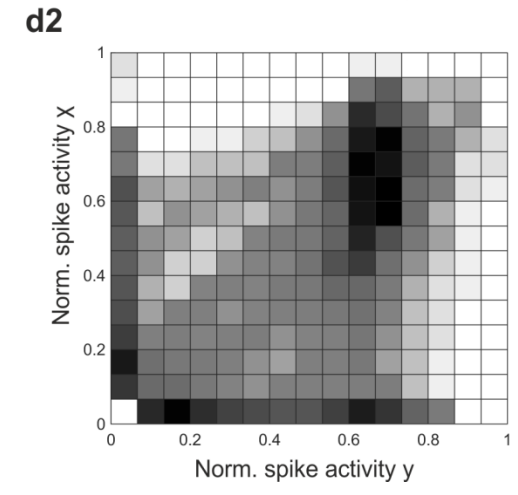
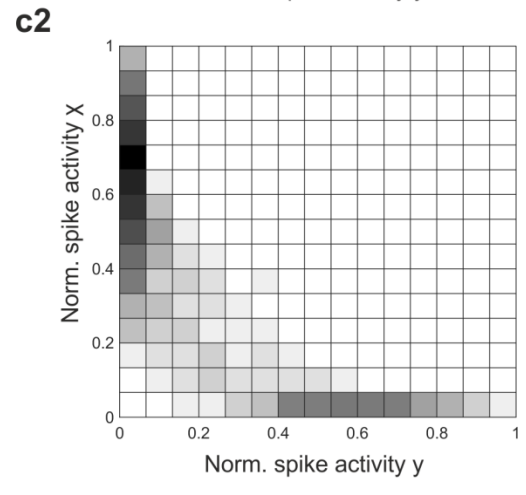
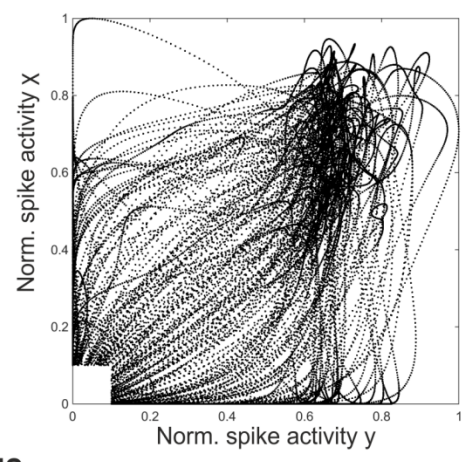
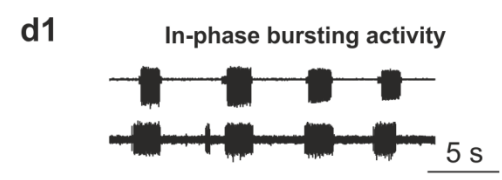
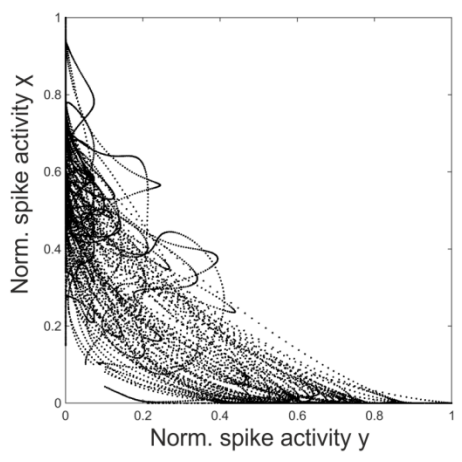
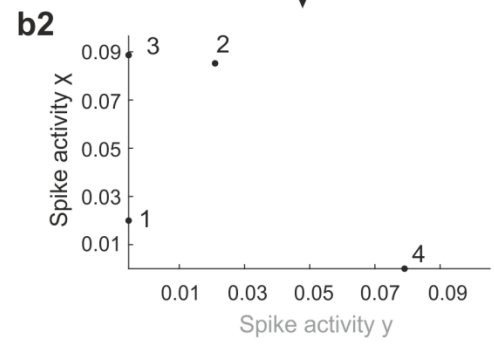
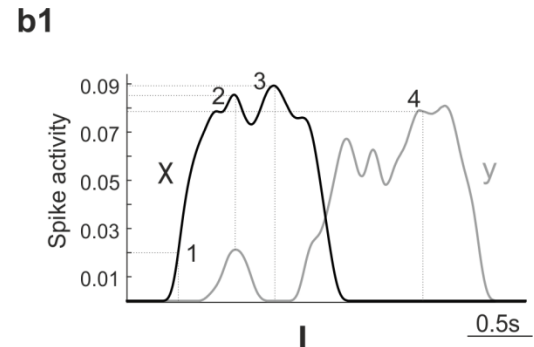
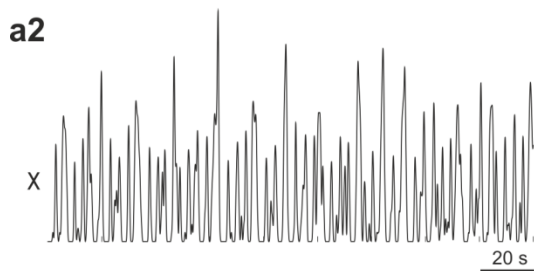
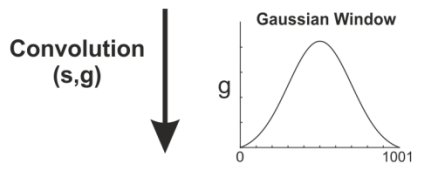


Figure 2: Coordination analysis based on the spiking time series. **a1:** Time series of spike events, extracted at a sampling rate of 1000 Hz. **a2:** Smoothed data after convolution with a 1001-point Gaussian window (only one trace is shown). **b1 and b2:** After interpolation at a rate of 100 Hz, spike activity of the two traces was compared throughout the recording and was plotted against each other. **c1:** Plot of the normalized spike activity of each data trace against activity of another. In anti-phase bursting, high spike activity in one nerve corresponds to low activity in the contralateral nerve and thus data points move between the x and y axes of the plot, resulting in clear clusters at the two axes. **c2:** Data points of the plot in c1 were allocated in 15 bins and the frequency of data in each bin was normalized to the maximum frequency. The map scale was adjusted accordingly for all figures in this thesis and is depicted only once here. To increase contrast, all data corresponding to single or double spikes, which resulted in normalized activity between 0 and 0.1, were omitted from the plot. **d1:** In in-phase bursting, high spike activity in one nerve corresponds to high activity in the contralateral nerve and thus data points move between 0 activity towards the center of the plot, resulting in a clear cluster. **d2:** Data points of the plot in c2 were allocated in 15 bins and the frequency of data in each bin was normalized to the maximum frequency. Data formed a clear cluster in the center of the plot, indicating synchronous spiking activity.

III. Cross-correlation analysis of the spike time series

For the cross-correlation analysis all spike events of each extracellular waveform were marked and the corresponding spiking time series were extracted at a sampling rate of 1000 Hz. Then data was smoothed after undergoing convolution with a 1001-point Gaussian window. All data points of the smoothed traces were centered to have a mean equal to 0 and scaled to have standard deviation equal to 1 by calculating the z-score. Cross-correlation analysis was applied on the smoothed and normalized spiking time series at 40 s-time windows that moved with 1 s steps throughout the recording (Fig. 3, a). In recording intervals, during which the two activity traces correlated with each other, cross-correlation showed symmetric oscillations with a period that corresponded to the period of the original recordings, and a clear peak at the time lag of maximum correlation (Fig. 3, b1). Conversely, in recordings showing irregular activity, or intervals of uncoordinated activity, the cross-correlation signal was noisier, non-symmetric and peaked at lower correlation coefficients (Fig. 3, b2). In each window moving throughout the recording, the absolute value of the correlation coefficient corresponding to the highest peak or trough was extracted and plotted against time (Fig. 3, c1).

To preclude the possibility that the moderate to high correlation coefficients were calculated due to random correlation between similar rhythmic motifs, cross-correlations between unrelated recording traces from similar preparations of other specimens were plotted in comparison (Fig. 3, c1: black traces). Maximum correlation coefficients of all control cross-correlations were allocated into 50 bins; the density of each was normalized to the sum of distribution densities of all bins and then plotted as a horizontal histogram (Fig. 3, c2). Finally, the cumulative distribution of the histogram was calculated and its complementary distribution (1-cdf) was plotted (Fig. 3, c3). This curve shows the probability (P) that an “x” correlation coefficient value is smaller than a correlation coefficient value “X” of the distribution ($P(X > x)$). A threshold was set at the correlation coefficient value that corresponded to a probability as small as 0.01 (Fig.3: horizontal red lines) and all maximal correlation coefficients above this threshold were regarded as significantly different from the

control correlation coefficients of the distribution (Fig. 3, c1: red intervals of the blue trace). To increase discernability of these plots, the curves corresponding to the maximal correlation coefficients of the controls were omitted in all figures of the Results and the mean maximal correlation coefficient of each window (\pm standard deviation) was plotted instead. Finally, the percentage of the 40 s-windows that showed significant peaks was calculated for each recording and for the pooled data, so that comparison with other ganglia preparations could be possible.

Statistics

For statistical analysis of circular data the MATLAB toolbox CircStat was used (Berens, 2009). The mean phase difference with 95% confidence interval and the angular deviation from the mean direction were calculated. The resultant vector length (r vector) was estimated as a measure of the spread around the mean. Finally, circular uniformity was assessed using the Hodges-Ajne test (omnibus test) and the mean directedness of the data distributions towards specific angles was tested using a circular statistic's test resembling the one-sample t-test on a linear scale (circ_mttest).

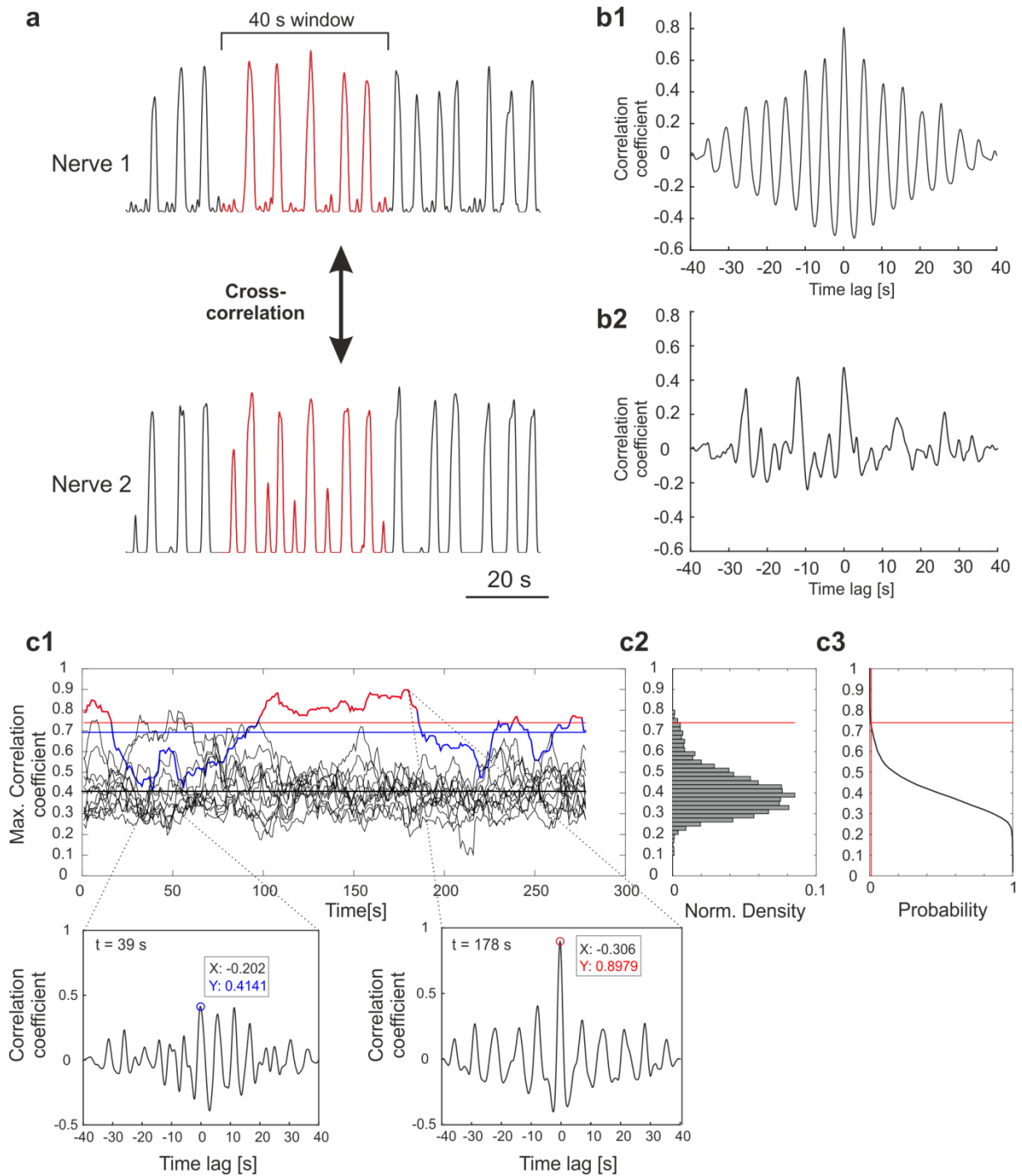


Figure 3: Cross-correlation analysis of the spike time series. **a:** Cross-correlation between smoothed and normalized spike time series at 40 s gliding time-windows every 1 s throughout the recording. **b1:** Cross-correlation in a window during which the two activity traces strongly correlated with each other. Note the peak at highest correlation coefficient close to 0 time lag and the symmetric oscillations, which show peaks at time intervals equal to the period of the original recording. **b2:** Cross-correlation in a window, during which the two activity traces weakly correlated with each other. In contrast to b1, cross-correlation signal is noisier, non-symmetric and forms peaks at lower correlation coefficients. **c1:** In each 40 s-window throughout the recording, the absolute correlation coefficient value corresponding to the highest peak or trough was extracted and plotted against time (blue-red trace). This is exemplified by two windows showing low and high cross-correlation at time points $t = 39$ s and $t = 178$ s of the recording, respectively. The mean max correlation coefficient is also plotted (blue horizontal line). The black traces are used as controls and resulted from cross-correlation between Nerve 1 activity and activity of unrelated recording traces from similar ganglion preparations of other specimens. In all other figures in this thesis only the average max correlation coefficient (\pm standard deviation) of the control traces in each window is plotted. **c2:** Distribution of the control max correlation coefficients (50 bins), normalized to the sum of distribution densities of all bins. **c3:** The complementary cumulative distribution of the

histogram in c2. The x coordinate of each point on this curve represents the probability that the respective correlation coefficient (y coordinate) is smaller than a random correlation coefficient value of the control distribution. Here we consider significant only the max correlation coefficients that are larger than the 99.9% of the control, namely we set a threshold (vertical red line) at probability equal to 0.01. The cross-section between this threshold and the complementary cumulative distribution curve gives the minimum significant max correlation coefficient (horizontal red lines in all plots). All max correlation coefficients above the horizontal red line are significantly different from the control correlation coefficients of the distribution (red parts of the blue curve in c1).

Results

I. Intrasegmental CPG coordination

Coordination of activity between contralateral depressor MN pools in the isolated mesothoracic ganglion

To determine whether contralateral networks driving MN activity in a single ganglion are centrally coupled, activity of contralateral depressor MN pools of the completely isolated and deafferented mesothoracic ganglion was recorded after pilocarpine application (N = 4). Pilocarpine induced rhythmic bursting in depressor MN pools in all four preparations, exactly as described in previous reports (Büschges et al., 1995). The average of the mean cycle period of all preparations was 4.6 ± 1.4 s. In accordance with Büschges and colleagues (1995), systematic cycle-to-cycle coupling of activity between the left and right depressor MNs was not observed in any of the recordings. However, a series of results indicated weak coupling of activity between contralateral depressor MNs. First, contralateral depressor MNs often exhibited synchronous bursts or intervals of in-phase activity (Fig. 4, a, black and gray traces). Second, the corresponding infinite phase showed almost parallel, linear phase development throughout the recording, as indicated by the slopes of the two phase curves (Fig. 4, b1). Third, the instantaneous frequency ratio of the two rhythms fluctuated at around 1, indicating similar bursting frequencies throughout the recording (data not shown). Finally, the phase difference between contralateral depressor MN pools remained partially constant throughout the recording (Fig. 4, b2). Consistent, however, with the apparent bursting variability observed in the activity of contralateral depressor MNs, only 2.3% of the windows showed a maximum correlation coefficient that was higher than 99.9% of the control values (Fig. 4, c). Overall, significant correlation coefficients were reported for 1.8% of the windows of all four preparations. Therefore, although cycle periods of contralateral depressor MN pools of the isolated mesothoracic ganglion were weakly coupled in intervals throughout the recording, their activity on the whole did not significantly correlate.

The overall phase difference distribution, calculated throughout the recording, showed distinct peaks (Fig. 4, d, solid line). Despite the high variability in phase differences, the distribution significantly deviated from circular uniformity ($p < 0.001$). The mean direction was 352° (95% CI: 328° to 15°), the circular angular deviation 64.5° and the r-vector 0.37. About half of the cycles (48%) showed a phase difference within the interval of 315° to 45° ($0^\circ \pm 45^\circ$), suggesting that the networks that drive the contralateral depressor MNs interact only weakly in the mesothoracic ganglion. Overall distributions of two out of the four preparations significantly deviated from the uniform distribution ($p < 0.001$) and showed clear tendency for in-phase cycle coupling (Table 1, Rec. 2 and 4). All preparations showed distinct peaks at 0° (Fig. 2C, dashed lines) and the statistical hypothesis for mean direction towards 0° could not be rejected in any preparation at the 5% level (Table 1). Pooling the data from all four animals ($n = 262$ cycles), resulted in a non-uniform phase difference distribution ($p < 0.001$) with a mean angle of 5° (95% CI: 347° to 22°), 69° angular deviation and 0.28 r-vector length (Fig. 4, e). However, only 44% of the cycles showed a phase difference of $0^\circ \pm 45^\circ$. Hence, interactions between contralateral depressor MN networks are weak, as peaks may appear at various angles in a phase distribution. Taken together, these observations suggest that the CPGs generating rhythmic activity in depressor MNs on either side of the isolated and deafferented mesothoracic ganglion are weakly coupled and show a tendency for in-phase activity.

Table 1: Phase analysis of activity between contralateral depressor MN pools in the isolated mesothoracic ganglion. Each recording corresponds to a different animal preparation. Circ_mean (90%C.I.): Circular mean of the angles with the 90% confidence interval into brackets. Circ_Std: Angular deviation. The p-value resulted from the Hodges-Ajne test (omnibus test) for circular uniformity ($\alpha = 0.001$). The smaller this value, the less uniform is the distribution. The $h0^\circ$ and $h180^\circ$ test whether the population mean is equal to 0° or 180° , respectively. This hypothesis is accepted when $h = 0$ and rejected when $h = 1$.

Rec.	Cycles (n)	Circ_mean (90%C.I.) [°]	Circ_Std [°]	r-vector	p-value	$h0^\circ$	$h180^\circ$
1	69	63.9 (339.1 , 148.7)	73.9	0.17	0.4	0	1
2	85	351.74 (328.2 , 15.3)	64.5	0.37	0.001	0	1
3	40	29.6 (NaN , NaN)	74.5	0.16	0.5	0	0
4	68	355.06 (335.33 , 14.79)	58.8	0.47	0	0	1
Pool	262	4.8 (347.42 , 22.28)	68.7	0.28	0	0	1

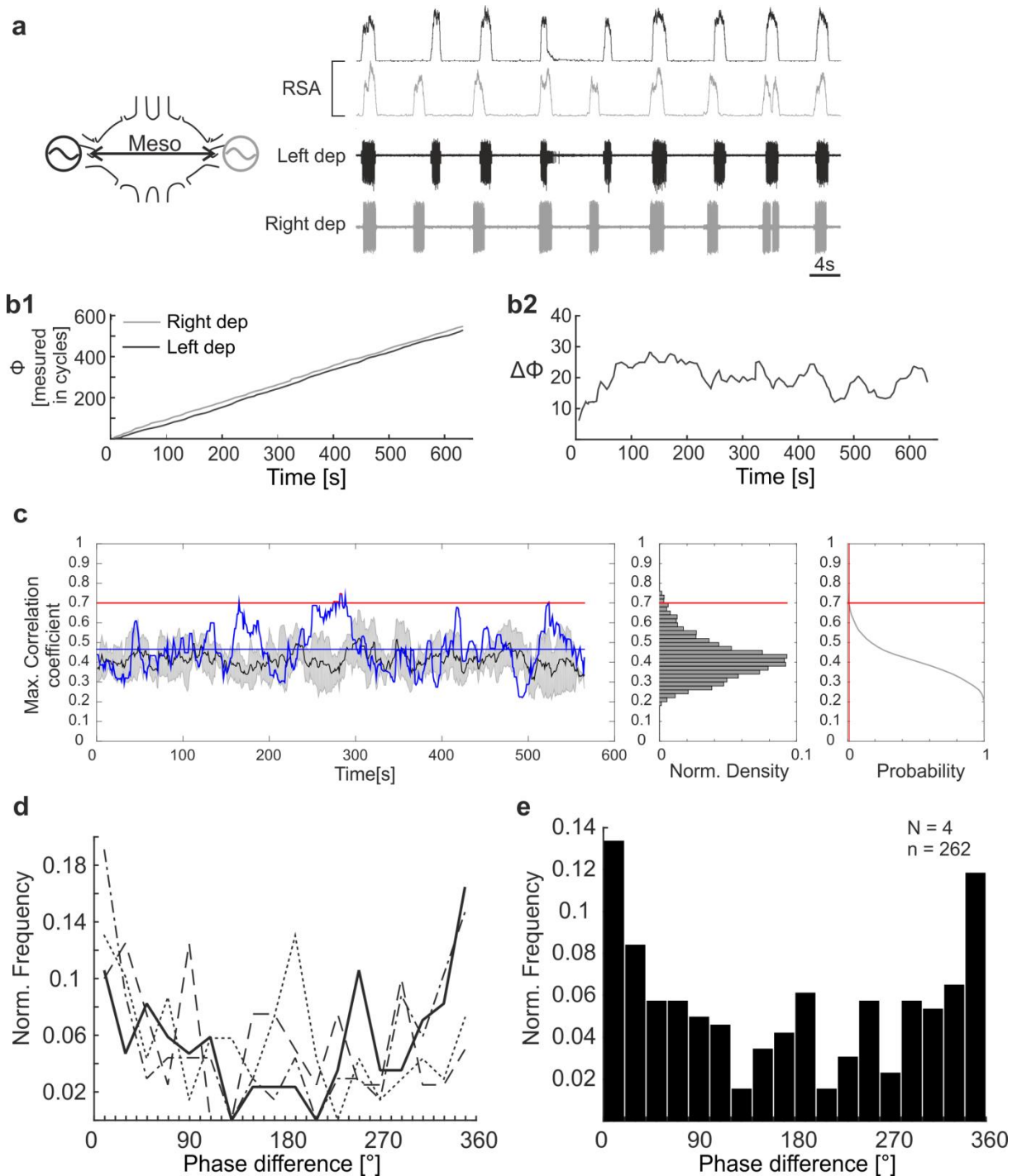


Figure 4: Phase analysis of activity in the isolated mesothoracic ganglion. **a:** Extracellular recording of left (black) and right (gray) depressor MN activity in the isolated mesothoracic ganglion after application of 5mM pilocarpine. RSA: Rectified and smoothed activity. **b1:** The infinite phase (Φ) curves show parallel-almost linear development throughout the recording of the left and right depressor MN activity. **b2:** Phase difference ($\Delta\Phi$) between activity of the left and right depressor MN pools remains largely bounded throughout the recording. **c:** Activity of contralateral depressor MNs is significantly correlated (max correlation coefficient larger than the 99.9% of the control values) in only 2.3% of the windows throughout the recording (red parts of the blue curve). Black curves correspond to the mean of the max correlation coefficients of six control cross-correlations (\pm standard deviation in grey). **d:** Phase difference distributions for four animal preparations plotted on top of each other. Overall distributions of two out of the four preparations show clear tendency for in-phase cycle coupling. The solid line corresponds to the preparation analyzed in previous subfigures. **e:** Normalized and pooled data from all four preparations resulted in a non-uniform phase difference distribution ($p < 0.001$) with a mean angle of 5° (95% CI: 347° to 22°), 69° angular deviation and 0.28 r-vector length. 44% of the cycles are within the interval $[315^\circ, 45^\circ]$. N: number of animal preparations; n: number of cycles.

Coordination of activity between contralateral depressor MN pools in the isolated metathoracic ganglion

Next, the same approach was applied to analyze the phase relationships between contralateral rhythmically active depressor MNs in the isolated metathoracic ganglion (N = 4). The average of the mean cycle periods of all four preparations was 4.9 ± 1.4 s. Similar to the situation in the mesothoracic ganglion, systematic cycle-to-cycle coupling of activity between contralateral depressor MN pools was not observed in the metathoracic ganglion. However, unlike the isolated mesothoracic ganglion preparation, contralateral depressor MN bursts in the isolated metathoracic ganglion were often found to be in anti-phase (Fig. 5, a). The infinite phase of the two rhythmically active metathoracic depressor MN pools also developed linearly. However, the corresponding phase curves had different slopes, indicating different phase development for each of the two MN rhythms (Fig. 5, b1). In spite of this, their frequency ratio was at around 1, indicating similar but not systematically coupled frequencies (data not shown). Moreover, the phase difference between activity of contralateral depressor MN pools continuously drifted throughout the recording, showing only few and very short intervals, during which the two rhythms nearly retained a constant phase relationship (Fig. 5, b2). Only 3.9% of the windows showed a significantly higher maximum correlation coefficient compared to the controls (Fig. 5, c), indicating a rather weak correlation of activity throughout the recording. An overall 2.9% of the windows of all four preparations showed significant cross-correlation.

The overall phase difference distribution, calculated throughout the recording, showed slight peaks at 0° , 90° and towards 270° , with a higher peak at 180° (Fig. 5, d, solid line). This distribution was the only one among the four preparations that significantly deviated from uniformity ($p < 0.001$). The mean direction was 165° (95% CI: 138° to 192°), the angular deviation 66° and the r-vector 0.34. 43% of the cycles showed a phase difference within the interval of 135° to 225° ($180^\circ \pm 45^\circ$). In the distributions of two out of the four preparations the statistical hypothesis for mean direction towards 180° could not be rejected at the 5% level, whereas the hypothesis for mean direction towards 0° was rejected (Table 2, Rec. 1

and 3). A clear peak close to the start of the cycle was observed in only one preparation (Fig. 5, d, dashed line). Pooling the data from all four animals, with a total recording time of approximately 2500 s ($n = 378$), resulted in a more uniform phase difference distribution than that of the isolated mesothoracic ganglion, as indicated by the higher p-value ($0.001 < p < 0.01$), with a mean angle of 166° (95% CI: 137.5° to 195°), 75° angular deviation and 0.15 r-vector length (Fig. 5, e). Only 33% of the cycles of the pooled data showed clear anti-phase activity, with phase differences in the interval between 135° and 225° ($180^\circ \pm 45^\circ$). Thus, consistent with the results presented for the mesothoracic ganglion, contralateral CPGs driving the depressor MN activity of the isolated metathoracic ganglion are coupled. However, interactions among the underlying networks are apparently extremely weak, as activity shows no significant cross-correlation, phase relationships are very variable among preparations and do not point to the same direction. Nevertheless, two out of the four recordings and the pooled data show a slight tendency for anti-phase activity.

Table 2: Phase analysis of activity between contralateral depressor MN pools in the isolated metathoracic ganglion.

Rec.	Cycles	Circ_mean (90%C.I.) [°]	Circ_Std [°]	r-vector	P-value	h0°	h180°
1	79	165 (138, 192)	66	0.34	0.000	1	0
2	125	204.3 (NaN , NaN)	79.8	0.03	0.94	0	0
3	90	162.7 (96 , 229.3)	74.3	0.16	0.1	1	0
4	84	162.4 (NaN , NaN)	75	0.14	0.32	0	0
Pool	378	166.3 (137.5 , 195.1)	74.8	0.15	0.003	1	0

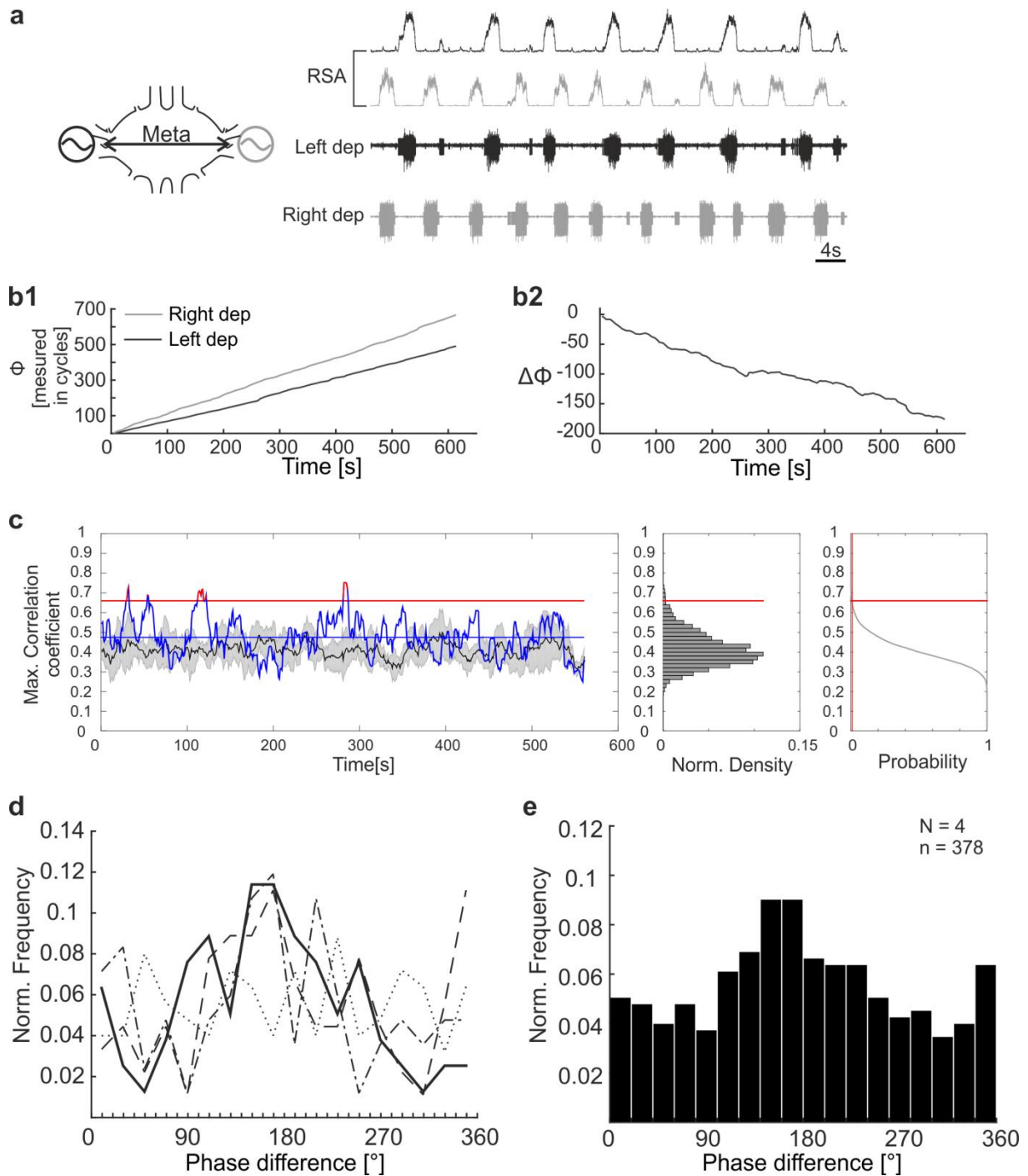


Figure 5: Phase analysis of activity in the isolated metathoracic ganglion. **a:** Extracellular recording of left (black) and right (gray) depressor MN activity after application of 5mM pilocarpine. RSA: Rectified and smoothed activity. **b1:** The infinite phases (Φ) curves show no systematic phase coupling throughout the recording. **b2:** Phase difference ($\Delta\Phi$) between activity of the left and right depressor MN pools remains bounded only at short intervals throughout the recording. **c:** Activity of contralateral depressor MNs is significantly correlated in only 3.9% of the windows throughout the recording (red parts of the blue curve). Black curves correspond to the mean of the max correlation coefficients of six control cross-correlations (\pm standard deviation in grey). **d:** Phase difference distributions for four animal preparations plotted on top of each other. Two of the four distributions show tendency for anti-phase coupling, and none of them shows tendency for in-phase coupling. The solid line corresponds to the preparation analyzed in previous subfigures. **e:** Normalized and pooled data from all four preparations resulted in a non-uniform phase difference distribution ($0.001 < p < 0.01$) with a mean angle of 166° (95% CI: 137.5° to 195°), 75° angular deviation and 0.15 r-vector length. 33% of the cycles of the pooled data showed clear anti-phase activity, with phase differences in the interval $[135^\circ$ and $225^\circ]$. N: number of animal preparations; n: number of cycles.

Intrasegmental coordination of depressor MN activity is influenced by intersegmental signals

Next, the influence of potential intersegmental signaling on contralateral coordination was studied in the interconnected meso- and metathoracic ganglia. For this, the phase relationship of the activity between contralateral depressor MN pools was analyzed after pilocarpine application. Interestingly, contralateral depressors in both the meso- and metathoracic ganglia were active in-phase for many consecutive cycles (Fig. 6, a). Intrasegmental coordination would recover within a few cycles after natural-occurring gaps in activity or double bursts (see asterisks in Fig. 6, a), indicating coordinating interactions between the underlying networks.

Phase analysis of the activity between contralateral depressor MN pools in the mesothoracic ganglion revealed similar bursting frequencies throughout long recording intervals (data not shown), during which the phase difference remained constant for more than 200 s (Fig. 6, b). Notably, such long periods of coupled activity have never been detected in isolated ganglia. Contralateral rhythmic activity in the interconnected metathoracic ganglion was more variable, and intervals of coupled intrasegmental activity were shorter in duration compared to those of the interconnected mesothoracic ganglion (Fig. 6, c). Cross-correlation of contralateral activity throughout the recording resulted in significant maximum correlation coefficients in 81.3% and 11.1% of the meso- and metathoracic windows, respectively (Fig. 6, d and e). Correlation coefficients often exceeded 0.6, indicating moderate to strong cross-correlation of contralateral activity. Overall, significant correlation-coefficients were found in 33.3% and 18.2% of the windows of seven mesothoracic and ten metathoracic recordings, respectively. The lower correlation of activity is indicative of the higher variability in pilocarpine-induced rhythmicity between contralateral MN pools of the metathoracic ganglion. All the above taken into consideration, intersegmental signals appear to influence contralateral depressor MN activity and contralateral coupling between CTr joint CPGs in both interconnected ganglia.

Table 3: Phase analysis of activity between contralateral depressor MN pools in the interconnected meso- and metathoracic ganglia.

Rec.	Cycles	Circ_mean (90%C.I.) [°]	Circ_Std [°]	r-vector	P-value	h0°	h180°
1	84	340.1 (322.3, 357.9)	59	0.47	0	1	1
2	58	3 (332.4 , 33.7)	65.4	0.35	0.016	0	1
3	71	349.3 (3.8 , 334.9)	51.2	0.60	0	0	1
4	77	30.4 (12.8 , 48)	57.7	0.49	0	1	1
5	46	22.8 (9.6 , 36.1)	39.7	0.76	0	1	1
6	108	0.3 (352.8 , 7.9)	33.8	0.83	0	0	1
7	136	349.3 (340.4 , 358.2)	45.9	0.68	0	1	1
Pool	580	359.3 (354.3 , 4.4)	51.7	0.59	0	0	1

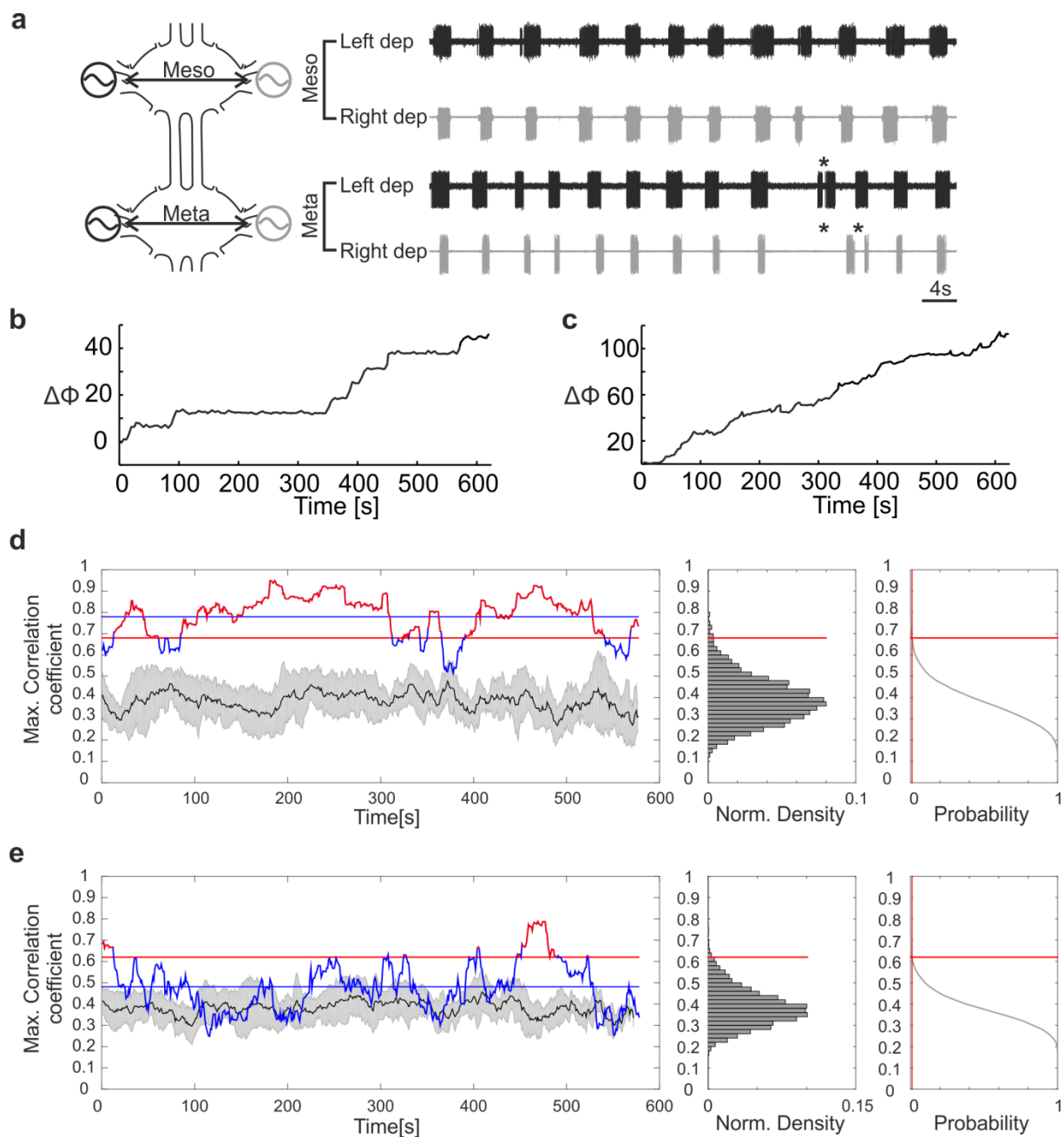


Figure 6: Phase analysis and cross-correlation of activity in the interconnected meso- and metathoracic ganglia. a: Extracellular recording of left (black) and right (gray) depressor MN activity of both ganglia after application of 5mM pilocarpine. In-phase bursting between contralateral depressor MN pools is observed in both ganglia. Asterisks denote bursting variability in the metathoracic ganglion. **b:** Phase difference ($\Delta\Phi$) between activity of contralateral mesothoracic depressor MN pools remains bounded a very long interval. Phase slips are due to disturbances that last for one or two cycles. **c:** Phase difference ($\Delta\Phi$) between activity of contralateral metathoracic depressor MN pools fluctuates more, but remain bounded at intervals throughout the recording. **d:** Activity of contralateral mesothoracic depressor MNs is significantly correlated in 81.3% of the windows throughout the recording and shows a very high mean of max correlation coefficients (horizontal blue line). Black curves correspond to the mean of the max correlation coefficients of 12 control cross-correlations (\pm standard deviation in grey). **e:** Activity of contralateral metathoracic depressor MNs is significantly correlated in 11.3% of the windows throughout the recording and has a lower mean of the max correlation coefficients (horizontal blue line), indicative of the higher variability of the metathoracic activity. Black curves correspond to the mean of the max correlation coefficients of 18 control cross-correlations (\pm standard deviation in grey).

The intrasegmental phase differences between contralateral depressor MN pools of the meso- and metathoracic ganglia was also calculated and the respective phase difference distributions were plotted. All distributions of the mesothoracic ganglion (N = 7) and eight out of ten metathoracic preparations differed significantly from the uniform distribution at the 95% level (Tables 3 and 4). They all showed clear peaks at or close to 0° (Fig. 7, a1 and b2). As exemplified in Fig. 6, contralateral depressor MNs in the interconnected mesothoracic ganglion were active in-phase with a mean phase difference of 0° (95% CI: 353° to 8°), an angular deviation of 34° , and an r-vector length of 0.83. Contralateral depressor rhythms in the interconnected metathoracic ganglion in the same recording showed a mean phase difference of 23° (95% CI: 7.5° to 39°) with a deviation of 61° and an r-vector length of 0.44. Pooled data corresponding to analysis of 3588 s of recording time, depicted strict in-phase coordination between intrasegmental depressor MN pools in the mesothoracic ganglion with a mean angle of 360° (95% CI: 354.5° to 4.5°), angular deviation 52° , and r-vector length 0.59 (Fig. 7, a2). More than half of the cycles (66%) had a phase difference of $0^\circ \pm 45^\circ$. Pooled data from the interconnected metathoracic ganglion showed a mean angle of 10° (95% CI: 2° to 18°), angular deviation 67.4° , and r-vector length equal to 0.31 (Fig. 7, b2). Contralateral depressor MNs in the interconnected metathoracic ganglion presented a phase difference within the interval of $0^\circ \pm 45^\circ$ in 43% of the cycles.

Taken together, intersegmentally transmitted neural signals not only stabilize contralateral CPG phase relationships in the mesothoracic ganglion (compare Fig. 4, e and 7, a2), but also affect contralateral CPG coordination in the metathoracic ganglion, leading to long intervals of in-phase activity between contralateral MN pools in both segments (compare Fig. 5, e and 7, b2).

Table 4: Phase analysis of activity between contralateral depressor MN pools in the interconnected metathoracic ganglion.

Rec.	Cycles	Circ_mean (90%C.I.) [°]	Circ_Std [°]	r-vector	P-value	h0°	h180°
1	58	351 (331.4, 10.6)	56.7	0.51	0.000	0	1
2	50	25.5 (11, 39.9)	44.8	0.69	0.000	1	1
3	57	19.6 (352.7, 46.5)	63.1	0.39	0.004	0	1
4	98	335.2 (298.4, 12)	71	0.23	0.015	0	1
5	104	31.4 (341.8, 81)	73.5	0.18	0.158	0	1
6	50	338.6 (308.6, 8.6)	63.8	0.38	0.002	0	1
7	159	31.5 (9.2, 53.7)	68.5	0.29	0.000	1	1
8	121	23.2 (7.5, 38.9)	60.5	0.44	0.000	1	1
9	156	347 (335.7, 358.3)	55.7	0.53	0.000	1	1
10	128	111.7 (NaN, NaN)	76	0.12	0.185	0	0
Pool	981	9.82 (1.8, 17.9)	67.4	0.31	0	0	1

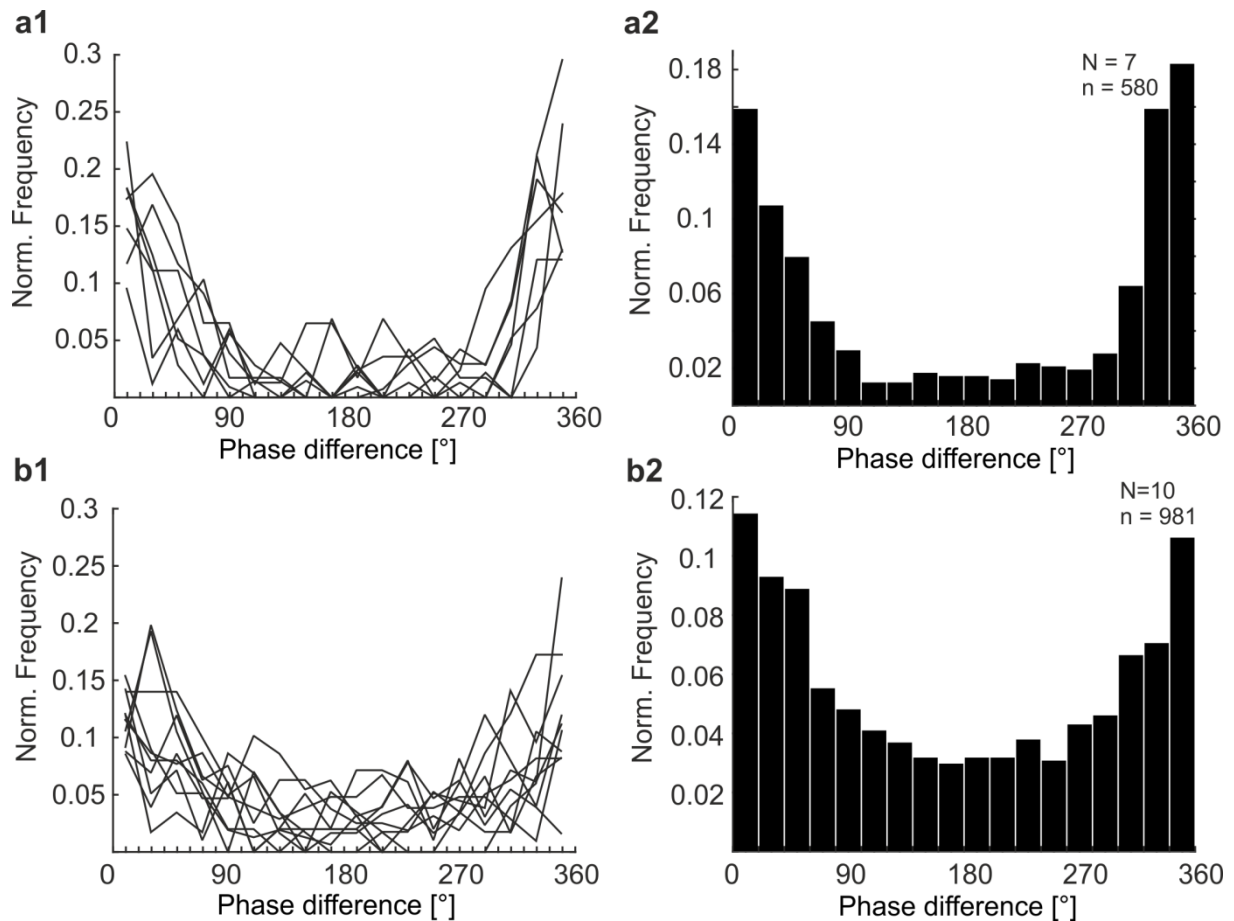


Figure 7: Distributions of the phase difference between contralateral mesothoracic and metathoracic depressor MN pools. **a1:** Phase difference distributions between contralateral depressor MN pools of the interconnected mesothoracic ganglion for seven animal preparations plotted on top of each other. All distributions of the mesothoracic ganglion differed significantly from the uniform distribution at the 95% level. They all showed clear peaks at or close to 0° . **a2:** The distribution of normalized and pooled data from all seven preparations of the interconnected mesothoracic ganglion had a mean angle of 360° (95% CI: 354.5° to 4.5°), angular deviation 52° , and r-vector length 0.59. 66% of the cycles of the pooled data showed clear in-phase activity, with phase differences in the interval $[315^\circ, 45^\circ]$. **b1:** Phase difference distributions between contralateral depressor MN pools of the interconnected metathoracic ganglion for ten animal preparations plotted on top of each other. Eight out of ten distributions of the metathoracic ganglion differed significantly from the uniform distribution at the 95% level. They all showed clear peaks at or close to 0° . **b2:** The distribution of normalized and pooled data from all seven preparations of the interconnected mesothoracic ganglion had a mean angle of 10° (95% CI: 2° to 18°), angular deviation 67.4° , and r-vector length equal to 0.31. 43% of the cycles of the pooled data showed clear in-phase activity, with phase differences in the interval $[315^\circ, 45^\circ]$. N: number of animal preparations; n: number of cycles.

To substantiate the latter observation, according to which intersegmental neural signaling affected contralateral coordination of activity between MN pools, a split-bath preparation was used. Pilocarpine was applied on the metathoracic ganglion first, and subsequently, the mesothoracic CPGs were also activated. Notably, spiking activity was never observed in mesothoracic ganglion after pilocarpine application on the metathoracic ganglion (N = 6, Fig. 8, a). Activation only of the metathoracic ganglion, in six different preparations, resulted in variable peaks at different angles throughout the cycle (Fig. 8, b1). In two preparations, peaks were formed either at 180°, or between 0° and 90° and close to 270°, whereas distributions of all other preparations did not show peaks at these angles. The phase distribution of one preparation showed a clear tendency for anti-phase activity (Table 5, Rec. 4). Pilocarpine application on the mesothoracic ganglion resulted in rhythmic activity of the depressor MN pools in this segment, and affected metathoracic intrasegmental coordination (Fig. 8, a). Activity in four out of six preparations showed a tendency for in-phase relationship (Fig. 8, b2). The phase distributions corresponding to these preparations showed a significant preferred direction towards 0°, and the hypothesis for mean direction towards 180° was rejected (Table 6, Rec. 1, 2, 3, and 6). Before activation of rhythmic activity in the mesothoracic ganglion, pooled phase differences concerning the contralateral metathoracic depressors formed a uniform distribution ($p = 0.954$) with a very low r-vector length equal to 0.01 (Fig. 8, c1). Only 26% of the cycles had phase differences in the range between $0^\circ \pm 45^\circ$, a percentage that is close to the expected 25% of a uniform distribution. After activation of the mesothoracic CPGs, the phase difference distribution concerning the metathoracic MN activity was significantly non-uniform ($p < 0.001$) with a mean angle of 10° (95% CI: 352° to 27°), r-vector length as high as 0.24, and 38% of the data within the interval $0^\circ \pm 45^\circ$, indicating a higher tendency for in-phase activity (Fig. 8, c2). Therefore, intersegmental neural signals transmitted through the connectives affect CPG coupling and promote weak in-phase coordination of activity between contralateral depressor MN pools in the meso- and metathoracic ganglia.

Table 5: Split-bath experiment. Phase analysis of activity between contralateral depressor MN pools in the interconnected metathoracic ganglion, before pilocarpine application on the mesothoracic ganglion.

Rec.	Cycles	Circ_mean (90%C.I.) [°]	Circ_Std [°]	r-vector	P-value	h0°	h180°
1	79	212.4 (NaN , NaN)	79.1	0.05	0.97	0	0
2	111	340.2 (NaN , NaN)	78	0.07	0.92	0	0
3	102	29.6 (NaN , NaN)	76.2	0.12	0.15	0	0
4	122	189.2 (166.2 , 212.2)	67.1	0.31	0	1	0
5	76	342.9 (NaN , NaN)	77.1	0.10	0.7	0	0
6	48	28.9 (2.9 , 55)	60.8	0.44	0	1	1
Pool	538	54.7 (NaN , NaN)	80.7	0.01	0.95	0	0

Table 6: Split-bath experiment. Phase analysis of activity between contralateral depressor MN pools in the interconnected metathoracic ganglion, after pilocarpine application on the mesothoracic ganglion.

Rec.	Cycles	Circ_mean (90%C.I.) [°]	Circ_Std [°]	r-vector	P-value	h0°	h180°
1	112	10.5 (337.5 , 43.6)	70.8	0.24	0.02	0	1
2	34	358.7 (322.9 , 34.5)	63	0.40	0.04	0	1
3	46	337.1 (288.5 , 25.8)	69.2	0.27	0.06	0	1
4	86	66.1 (29.8 , 102.4)	70.2	0.25	0.03	1	1
5	65	332.3 (308.1 , 356.5)	62.5	0.40	0.002	1	1
6	34	59.6 (356.2 , 123.1)	69.5	0.26	0.01	0	1
Pool	377	9.7 (352.3 , 27.1)	70.8	0.24	0	0	1

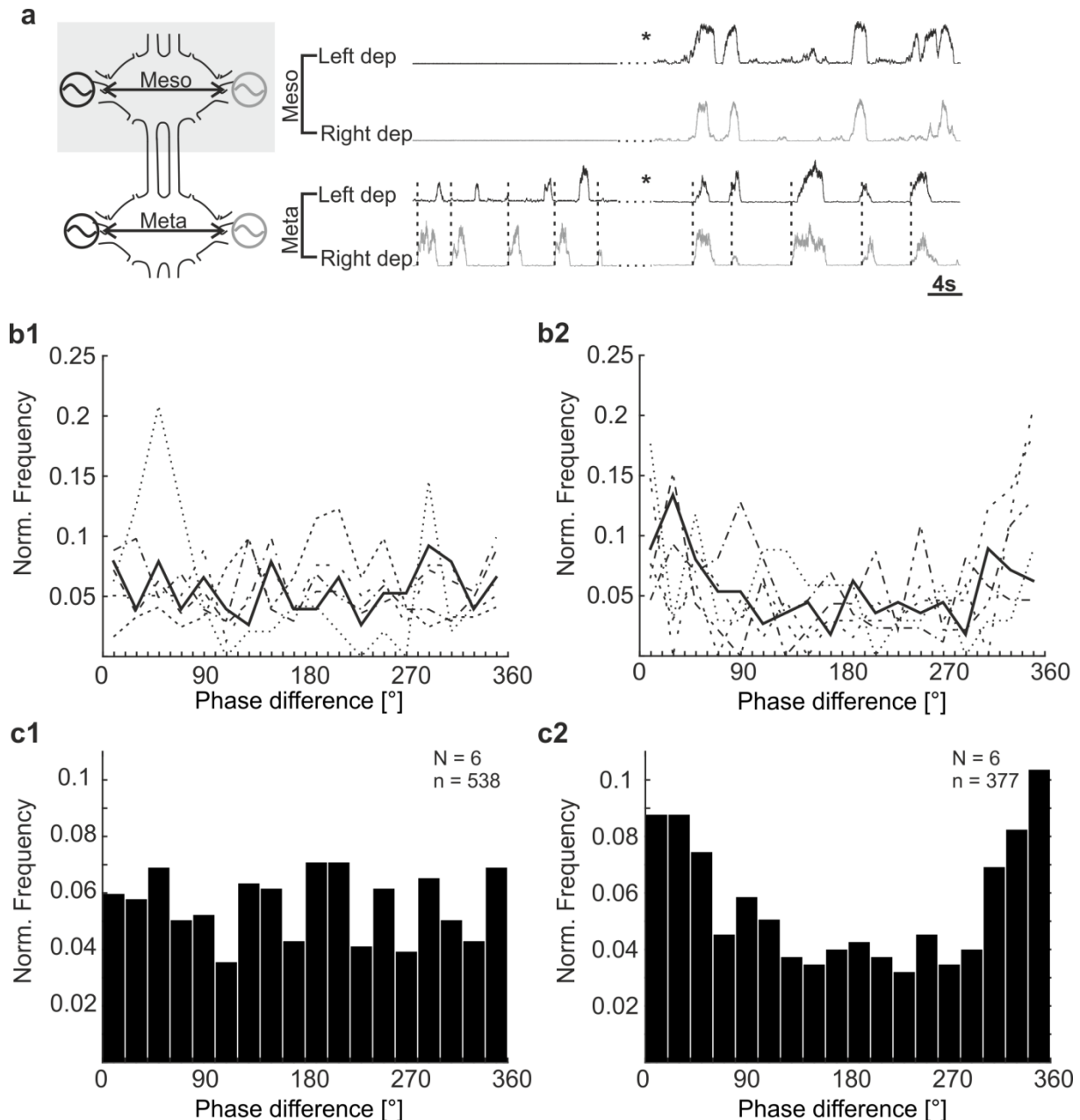


Figure 8: Phase analysis of activity in the interconnected metathoracic ganglion before and after activation of the mesothoracic networks. **a:** Rectified and smoothed activity of contralateral depressor MN pools in the interconnected meso- and metathoracic ganglia. Bath was split by a Vaseline-barrier between the two ganglia. 5mM pilocarpine was applied first on the meta- (before the asterisks) and subsequently on the mesothoracic ganglion (after the asterisks). Note the change in contralateral coordination of metathoracic activity. **b1:** Phase difference distributions between contralateral depressor MN pools of the interconnected metathoracic ganglion before activation of the mesothoracic CPGs, plotted on top of each other ($N = 6$). Only two distributions were significantly non-uniform at the 95% level, with the one showing a tendency for anti-phase activity. **b2:** Phase difference distributions between contralateral depressor MN pools of the interconnected metathoracic ganglion after activation of the mesothoracic CPGs, plotted on top of each other ($N = 6$). Half of the distributions were non-uniform ($\alpha = 0.05$) and showed a tendency for in-phase activity. **c1:** The distribution of normalized and pooled data of the interconnected metathoracic ganglion before activation of the mesothoracic CPGs, was uniform ($p = 0.954$), and had r-vector length equal to 0.01. Only, 26% of the cycles had phase differences in the interval $[315^\circ, 45^\circ]$. **c2:** The distribution of normalized and pooled data of the interconnected metathoracic ganglion, after activation of the mesothoracic CPGs, was significantly non-uniform ($p < 0.001$), had a mean angle of 10° (95% CI: 352° to 27°), and r-vector length 0.24. 38% of the cycles had phase differences in the interval $[315^\circ, 45^\circ]$. N : number of animal preparations; n : number of cycles.

Summary of the results concerning the intrasegmental CPG coupling in the meso- and metathoracic ganglia

To summarize, activity of contralateral depressor MNs was mostly in-phase in the isolated mesothoracic ganglion (Fig. 9, a) and anti-phase in the isolated metathoracic ganglion (Fig. 9, b). R-vectors were generally longer in the mesothoracic polar plot, highlighting the lower variability in intrasegmental coordination compared to the metathoracic ganglion. Plotting of the pooled spike activity of contralateral depressor MNs against each other, resulted in a clear data cluster in the right upper part of the plot for the mesothoracic ganglion, indicating synchronous spiking of contralateral depressors (Fig. 9, c), whereas metathoracic data were only clustered at the two axes and no clear cluster could be observed, indicating a higher frequency of out-of-phase spiking events (Fig. 9, d).

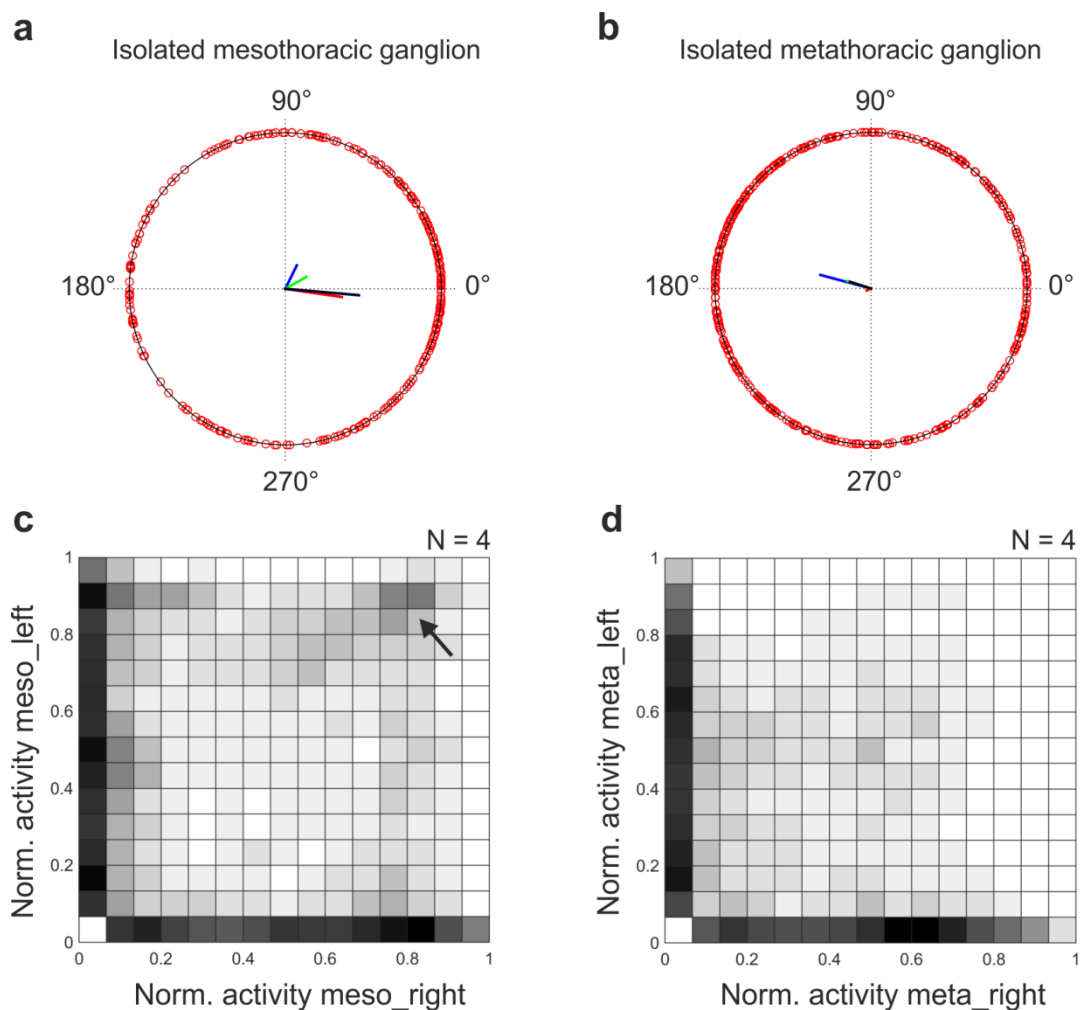


Figure 9: Results summary concerning coordination of activity between contralateral depressor MN pools of the isolated meso- and metathoracic ganglia. a: Polar plot of four different isolated mesothoracic ganglion preparations. Half of

the preparations show a higher tendency for in-phase coordination between contralateral depressor MN pools, as exemplified by the relatively long r-vectors. **b**: Polar plot of four different isolated metathoracic ganglion preparations. R-vectors are shorter than in (a), indicating higher variability in phase relationships between contralateral depressor MNs of the metathoracic ganglion. They all point towards 180°. **c**: Normalized spiking activity of the left depressor MN pools is plotted against normalized spiking activity of the right depressor MN pools in the isolated mesothoracic ganglion. The data cluster in the upper right part of the plot (see arrow) is indicative of a tendency synchronous spiking activity. **d**: Normalized spiking activity of the left depressor MN pools is plotted against normalized spiking activity of the right depressor MN pools in the isolated metathoracic ganglion. Sparse data in the plot are indicative of high variability in spiking relationships of contralateral depressor MNs.

The phase difference between cycle periods of contralateral depressor MN pools in both the interconnected meso- and metathoracic ganglia pointed towards 0° (Fig. 10, a and b). R-vectors were considerably longer compared to those of the isolated ganglia (compare with Fig. 9, a and b). Plotting of pooled spiking activity of contralateral depressor MNs against each other resulted in a clear cluster concerning the interconnected mesothoracic ganglion, and a broader, less pronounced cluster concerning the metathoracic ganglion (Fig. 10 c and d). This corresponds to the higher variability observed in the activity dynamics of the depressor MNs in the interconnected metathoracic ganglion.

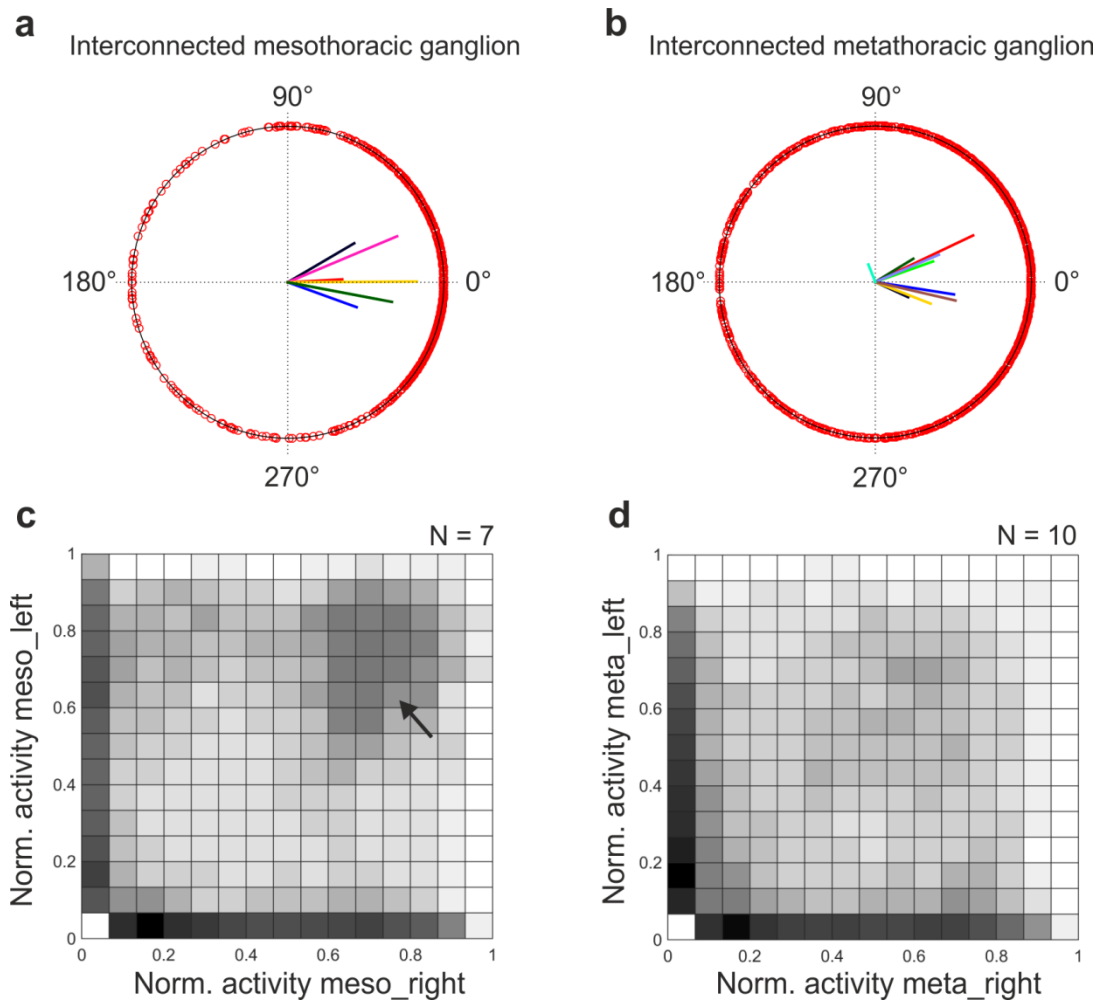


Figure 10: Results summary concerning coordination of activity between contralateral depressor MN pools of the interconnected meso- and metathoracic ganglia. a: Polar plot of seven different interconnected mesothoracic ganglion preparations. All preparations show a higher tendency for in-phase coordination between contralateral depressor MN pools, with substantially longer r-vectors in comparison to the isolated mesothoracic ganglion (Fig. 9, a). **b:** Polar plot of ten different interconnected metathoracic ganglion preparations. Nine of the r-vectors point towards 0°, in contrast to the isolated metathoracic ganglion. R-vectors are shorter than in (a), indicating higher variability in phase relationships between contralateral depressor MNs of the metathoracic ganglion. **c:** Normalized spiking activity of the left depressor MN pools is plotted against normalized spiking activity of the right depressor MN pools in the interconnected mesothoracic ganglion. The data cluster in the upper right part of the plot (see arrow) is indicative of a tendency synchronous spiking activity. **d:** Normalized spiking activity of the left depressor MN pools is plotted against normalized spiking activity of the right depressor MN pools in the interconnected metathoracic ganglion. Data form a cluster in the center of the plot, with more sparse distribution in comparison to (c). This is indicative of the higher variability in spiking relationships of contralateral depressor MNs in the metathoracic ganglion.

Finally, before activation of the mesothoracic CPGs, the cycle periods of contralateral depressor MN pools of the interconnected metathoracic ganglion showed uniformly-distributed phase relationships all over the cycle (Fig. 11, a1), and the spiking activity showed no clear patterning (Fig. 11, b1). After activation of the mesothoracic CPGs, four out

of six r-vectors pointed towards 0° (Fig. 11, a2) and although spiking coordination was still unclear, an indistinct cluster became apparent (Fig. 11, b2).

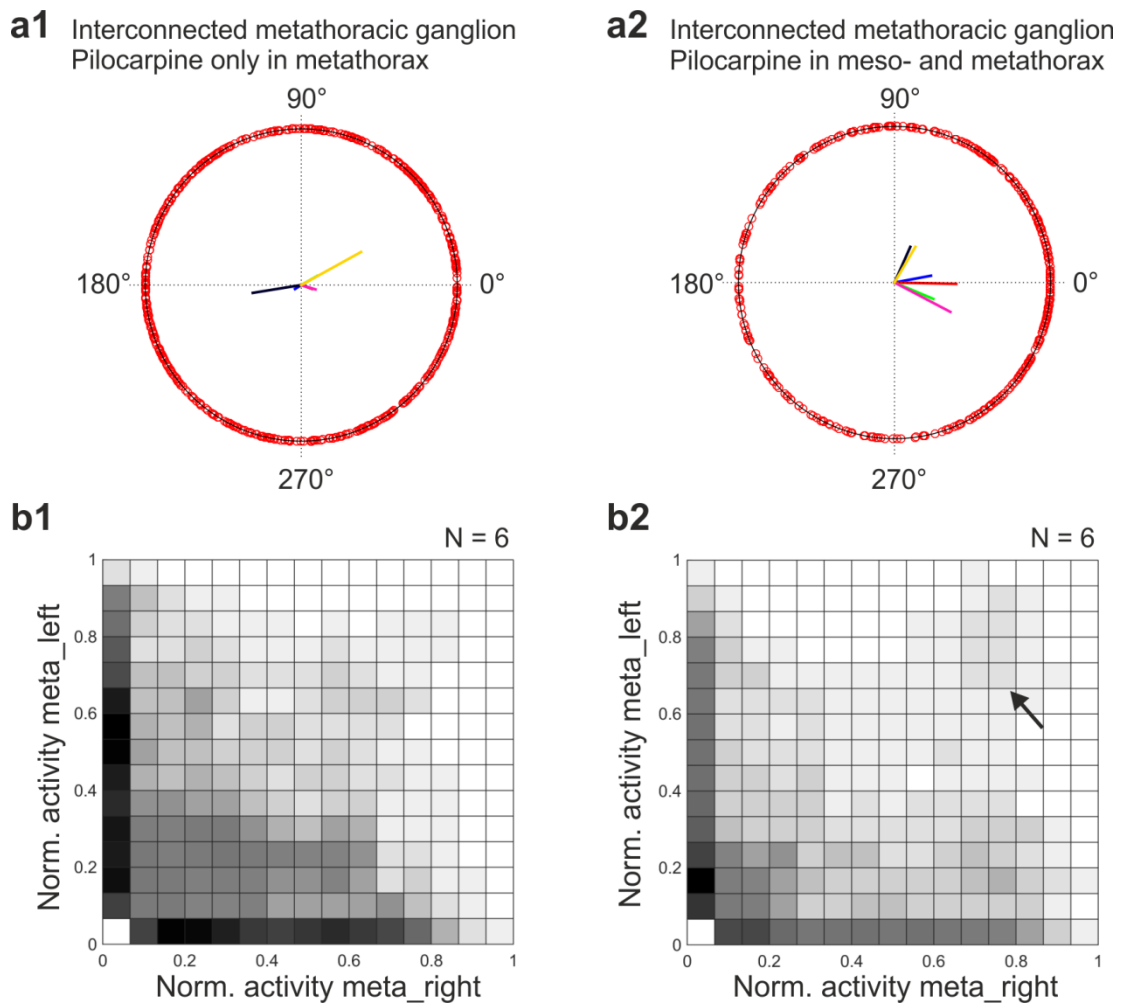


Figure 11: Results summary concerning coordination of activity between contralateral depressor MN pools in the interconnected metathoracic ganglion in split-bath preparations. **a1:** Polar plot of six different interconnected metathoracic ganglion preparations, before activation of the mesothoracic CPGs with 5 mM pilocarpine. Each of the r-vectors, corresponding to a different animal preparation, points towards a different angle. Two of the r-vectors are too short to be discerned in the figure. One of the preparations showed tendency for anti-phase activity. **a2:** Polar plot of six different interconnected metathoracic ganglion preparations, after activation of the mesothoracic CPGs with 5 mM pilocarpine. R-vectors are generally longer compared to (a1). Four out of the six r-vectors point towards a 0°. Two of the r-vectors are too short to be discerned in the figure. One of the preparations showed tendency for anti-phase activity. **b1:** Normalized spiking activity of the left depressor MN pools is plotted against normalized spiking activity of the right depressor MN pools in the interconnected metathoracic ganglion, before activation of the mesothoracic CPGs with 5 mM pilocarpine. Data show a rather sparse, random distribution, with higher concentration around point 0, suggesting uncorrelated activity between contralateral depressor MNs. **b2:** Normalized spiking activity of the left depressor MN pools is plotted against normalized spiking activity of the right depressor MN pools in the interconnected metathoracic ganglion, after activation of the mesothoracic CPGs with 5 mM pilocarpine. In comparison to (b1), data show substantially lower frequency at the axes of the plot and around point 0. The faint cluster pointed by the arrow suggests more correlated activity between contralateral depressor MNs, after activation of the mesothoracic CPGs.

Coordination of activity between contralateral depressor MN pools in the isolated prothoracic ganglion and the interconnected pro- and mesothoracic ganglia

Contralateral coordination of pilocarpine-induced activity in depressor MN pools was investigated in the isolated prothoracic ganglion. The average of the mean cycle periods of six different preparations was 1.79 ± 0.24 s, about 60% shorter than the mean cycle periods of the other isolated thoracic ganglia. Pilocarpine-induced activity in the prothoracic MN pools was more variable compared to the activity in other ganglia. Recording intervals with bursts consisting of both the SDTr and FDTr units alternated with long SDTr bursts, and, thus, the cycle onsets could not be clearly defined throughout the recording (Fig. 12, a). Moreover, five out-of six recordings did not present distinct patterns of coordinated MN activity. Recurrent bursting patterns were detected in one preparation only, implying that weak central CPG interactions may exist in the prothoracic ganglion as well (Fig. 13, a). In the aforementioned preparation, cross-correlation analysis revealed moderate to strong cross-correlation between contralateral depressors in 63.5% of the windows throughout the recording (Fig. 13, b), whereas the same percentage in the other five preparations was in average just 2.5%. Spike activity plots substantiated the above observations. In the preparation that showed uncoordinated depressor MN activity, data were randomly distributed and did not show clear clusters or any sort of a pattern (Fig. 12, c1 and c2). However, the same plots in the coordinated preparation, showed random data distribution in the 0.2×0.2 area, and also clusters at the two axes, which corresponded to the apparent out-of-phase bursting patterns (Fig. 13, a) that were characterized by FDTr activation (Fig. 13, c1 and c2). To conclude, five out of six preparations generally showed uncoordinated activity between contralateral depressor MN pools. Plotting the pooled activity of contralateral depressor MN pools against each other for all five preparations resulted in randomly distributed data and no clusters (Fig. 12, d1 and d2). Thus, contralateral CTr-joint CPGs appear not to be consistently coupled and result in unclear coordination in the isolated prothoracic ganglion.

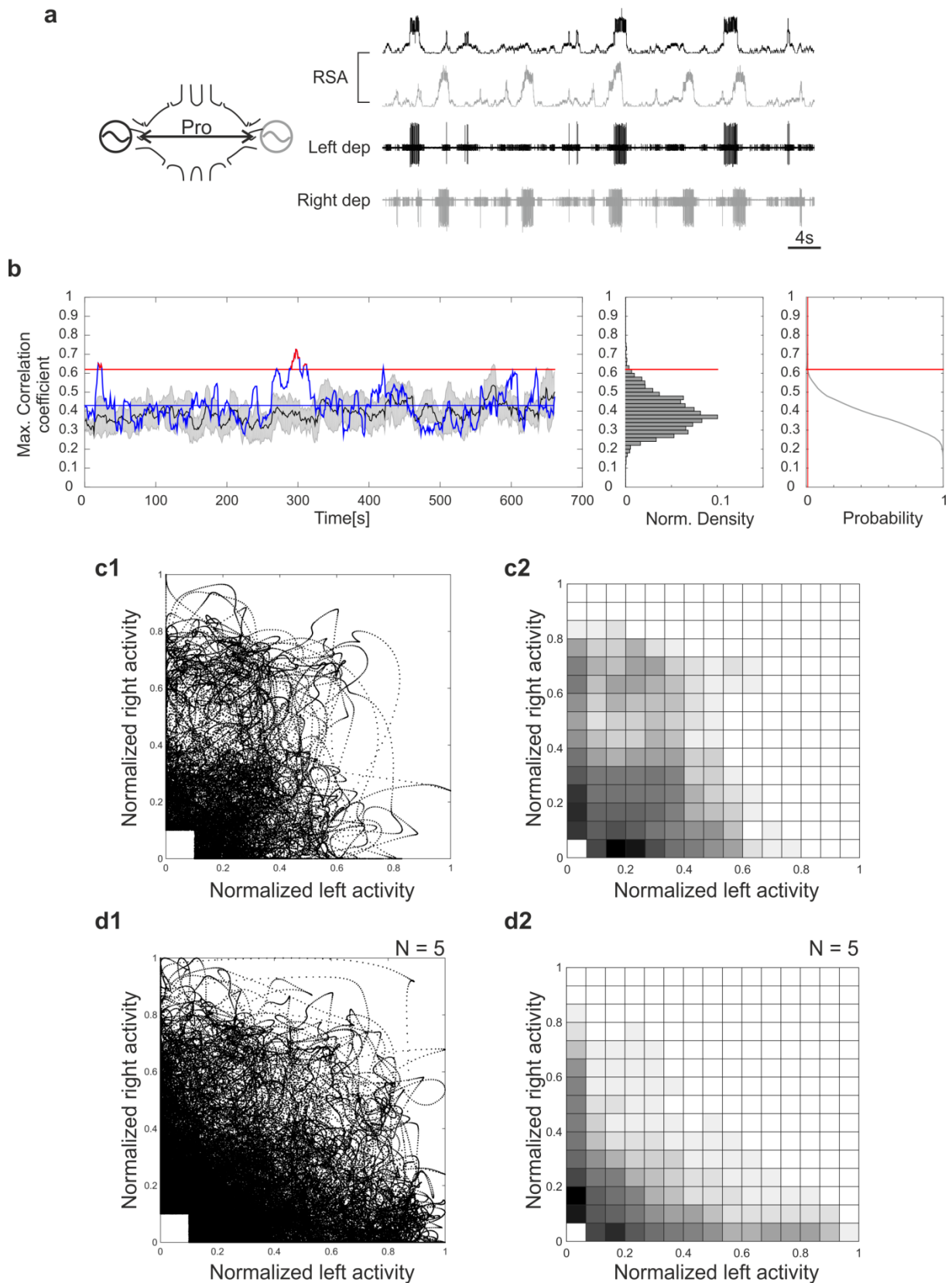


Figure 12: Coordination analysis of spiking activity in the isolated prothoracic ganglion. **a:** Extracellular recording of contralateral depressor MN activity in the isolated prothoracic ganglion. Rhythmic activity was induced by application of 5 mM pilocarpine in saline. Five out of six preparations showed no obvious intrasegmental coordinating pattern. RSA: rectified and smoothed activity. **b:** Activity of contralateral depressor MNs is significantly correlated in only 4.1% of the windows throughout the recording (red parts of the blue curve). Black curves correspond to the mean of the max correlation coefficients of eight

control cross-correlations (\pm standard deviation in grey). **c1 and c2:** Normalized spiking activity of the left depressor MN pools is plotted against normalized spiking activity of the right depressor MN pools in the interconnected metathoracic ganglion. Data are sparse around point 0 and show no distinct clusters. **d1 and d2:** Pooled data from all five recordings show also no distinct clusters.

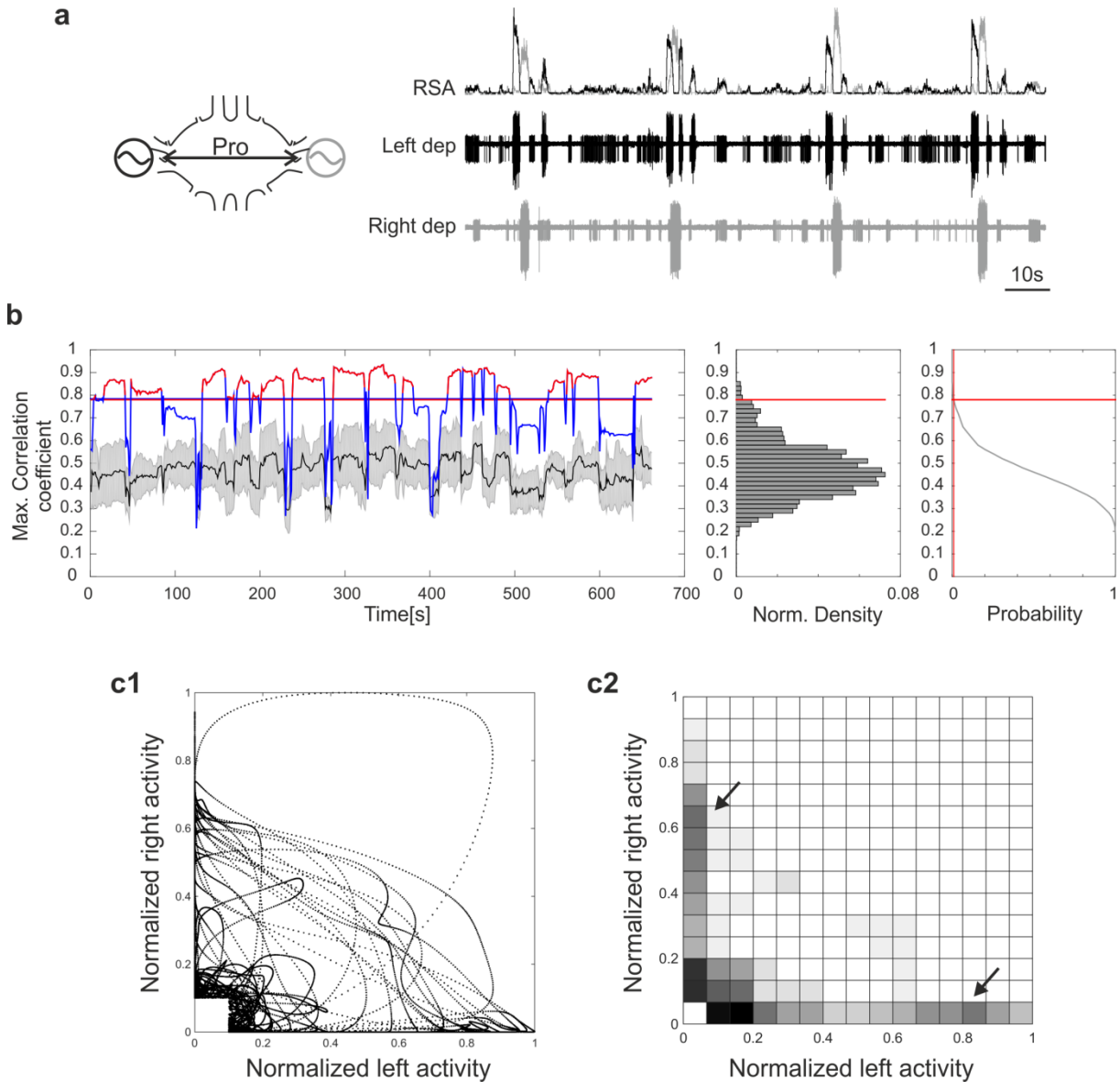


Figure 13: Coordination analysis of spiking activity in the isolated prothoracic ganglion. **a:** The only extracellular recording that showed recurrent patterns of coordinated activity between contralateral depressor MN pools of the isolated prothoracic ganglion. Rhythmic activity was induced by application of 7 mM pilocarpine in saline. RSA: rectified and smoothed activity. **b:** Activity of contralateral depressor MNs is significantly correlated in only 63.5% of the windows throughout the recording (red parts of the blue curve). Black curves correspond to the mean of the max correlation coefficients of ten control cross-correlations (\pm standard deviation in grey). **c1:** Normalized spiking activity of the left depressor MN pools is plotted against normalized spiking activity of the right depressor MN pools in the interconnected metathoracic ganglion. There are either randomly distributed at around point 0, or cluster at the x and y axes and move from the one axis to the other. Random data close to point 0 correspond to low-spiking, uncoordinated activity, due to SDTr activation. Data on the axes correspond to the intervals of patterned activity, during which bursts of both FDTTr and SDTr activity alternate between the two depressor MN pools (see (a)). **c2:** 2D-grid after allocating the data of (c1) in 15 bins. Arrows point to the data clusters at the axes, which suggests a tendency for alternating activity.

Next, the influence of intersegmental signals from the mesothoracic ganglion on contralateral coordination of prothoracic depressor MN activity was investigated (N = 5). Contralateral depressor MN activity of the interconnected pro- and mesothoracic ganglia was recorded after pilocarpine application. Generally, recurrent patterns of coordinated MN activity were not observed (Fig. 14, a). Cross-correlation of activity between contralateral prothoracic depressor MN pools revealed significant maximum correlation coefficients only in 2% of the windows throughout the recording (Fig. 14, b). In overall 5.5% of the windows of all five recordings, activity of the contralateral depressor MN pools of the prothoracic ganglion was significantly correlated. Cross-correlation of the activity of contralateral mesothoracic depressor MNs showed significant maximum correlation coefficients in 22.5% of the windows throughout the recording (Fig. 14, c). However, only 6.3% of the windows of all five recordings showed significant cross-correlation of the activity of contralateral mesothoracic depressor MNs. Thus, activity of contralateral prothoracic depressor MN pools was more coordinated in the interconnected compared to the isolated pro- and mesothoracic ganglia, and activity of contralateral mesothoracic depressor activity was less coordinated compared to the interconnected meso- and metathoracic ganglia preparation. Plotting of the normalized activity of the two contralateral prothoracic depressor MN pools against each other revealed not only data points close to the two axes, but also a higher frequency of data points in the center of the plot at the same level (around 0.6) of normalized activity (Fig. 14, d). This clustering of spiking activity implied a higher likelihood for synchronous spiking between the two depressor MN pools, and therefore an intersegmental influence on contralateral coordination of MN pools in the interconnected prothoracic ganglion. Plotting of the normalized activity of contralateral depressor MNs of the mesothoracic ganglion against each other resulted in two clusters, proximal to, but not at the axes (Fig. 14, e). Thus, mesothoracic networks tended to be active in alternation.

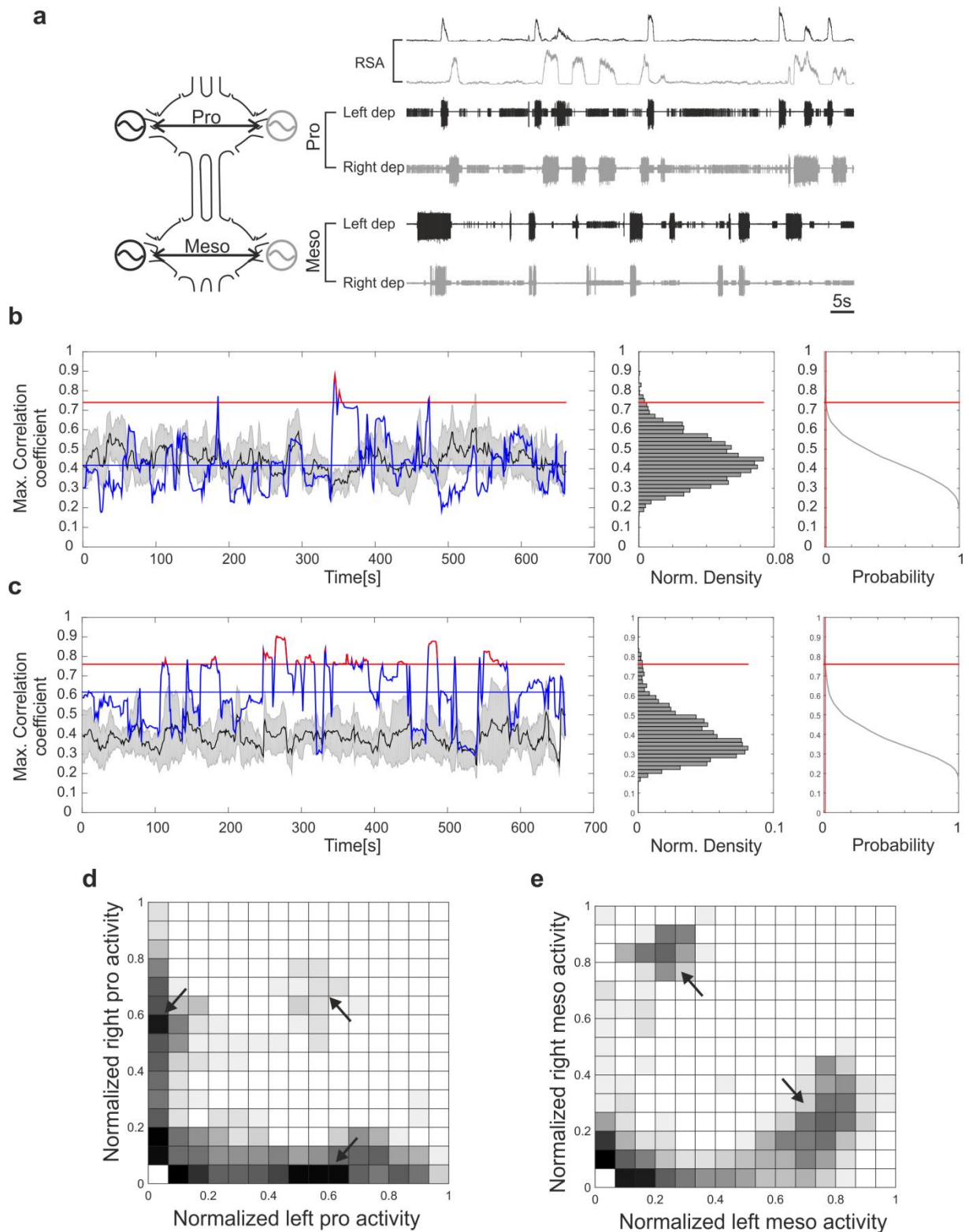


Figure 14: Coordination analysis of activity in the interconnected pro- and mesothoracic ganglia. a: Extracellular recording of contralateral depressor MN activity in the interconnected pro- and mesothoracic ganglia. Rhythmic activity was induced by application of 5 mM pilocarpine. Intervals of regular bursting activity alternate with prolonged SDTr activation in both ganglia. RSA: rectified and smoothed activity of contralateral prothoracic depressor MN pools. **b:** Activity of contralateral depressor MNs of the interconnected prothoracic ganglion is significantly correlated in only 2% of the windows throughout the recording (red parts of the blue curve). **c:** Activity of contralateral depressor MNs of the interconnected mesothoracic ganglion is significantly correlated in 22.5% of the windows throughout the recording (red parts of the blue curve). Black curves correspond to the mean of the max correlation coefficients of eight control cross-correlations (\pm standard deviation in grey). **d:** Normalized

spiking activity of the left depressor MN pools is plotted against normalized spiking activity of the right depressor MN pools in the interconnected prothoracic ganglion. Data are mainly clustered at the axes and there is also a faint cluster in the center of the plot (see arrows). Thus, there is a tendency for out-of-phase activity and a much lower frequency of synchronous spike events.

e: Normalized spiking activity of the left depressor MN pools is plotted against normalized spiking activity of the right depressor MN pools in the interconnected mesothoracic ganglion. There are two clusters close to the axes (see arrows). Thus, contralateral mesothoracic depressor MN pools are active mainly out-of-phase, when the mesothoracic ganglion is interconnected to the prothoracic ganglion.

Data clusters indicating synchronous and asynchronous spiking activity were still obvious after pooling the data from all five preparations with a total recording length of approximately 3400 s (Fig. 15, a1 and a2). Contralateral prothoracic activity in the interconnected ganglia showed distinct clusters and apparently was more coordinated compared to the activity in the isolated ganglion (compare Fig. 15, a1 and a2 to Fig. 12, d1 and d2). Mesothoracic spiking activity formed data clusters indicative of alternating activity (Fig. 15, b1 and b2). These results suggest that on the one hand coordination between contralateral depressor CPGs in the prothoracic ganglion can be influenced by intersegmental signals from the mesothoracic ganglion, and on the other hand coordination between contralateral mesothoracic depressor CPGs is affected, as contralateral depressor MNs show a higher tendency for asynchronous spiking rather than synchronous.

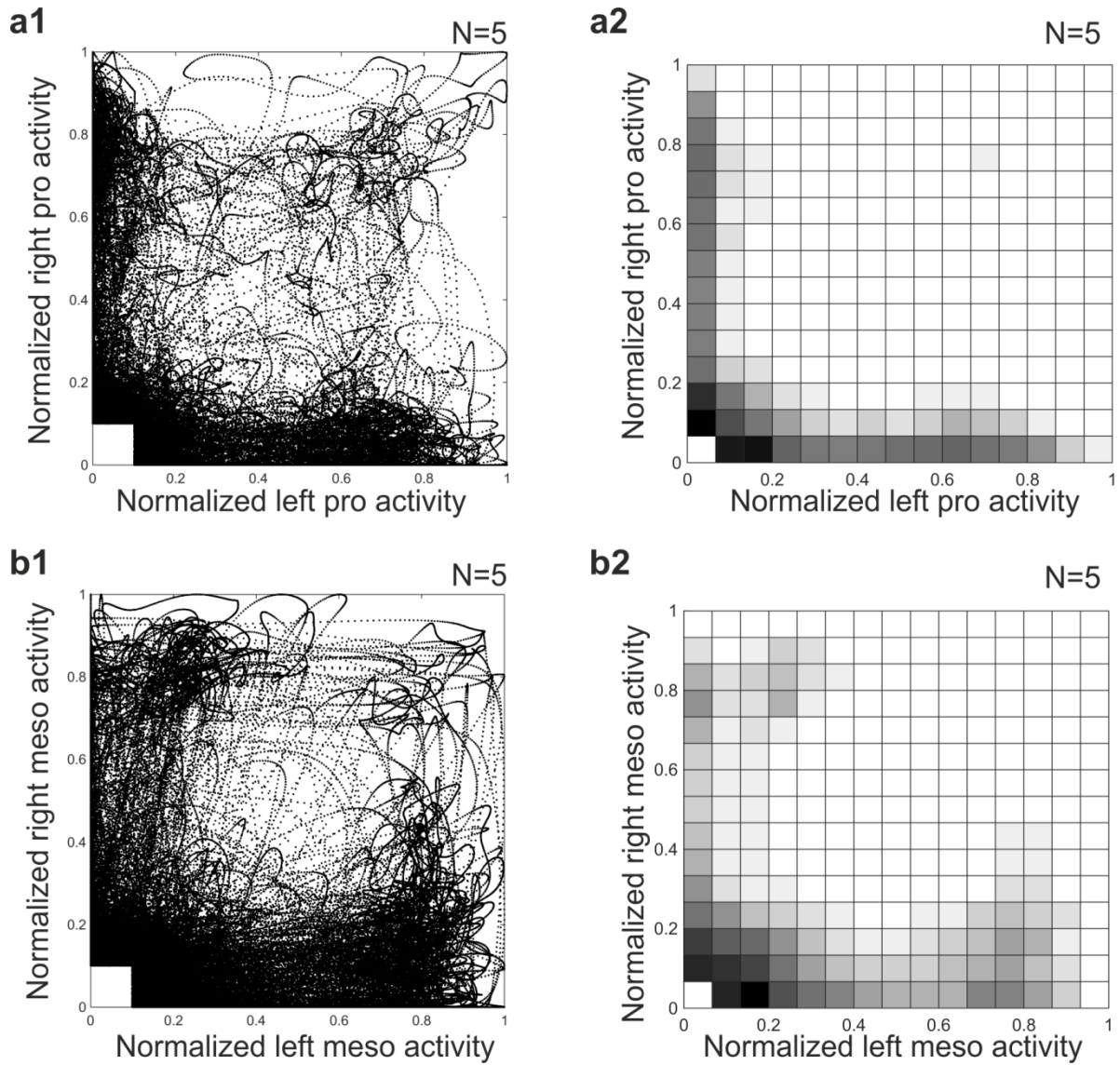


Figure 15: Coordination analysis of spiking activity in the interconnected pro- and mesothoracic ganglia (pooled data). **a1 and a2:** Normalized spiking activity of the left depressor MN pools is plotted against normalized spiking activity of the right depressor MN pools in the interconnected prothoracic ganglion. Data of overall five preparations are plotted on top of each other. Data are mainly clustered at the axes, suggesting a higher likelihood for out-of-phase activity. **b1 and b2:** Normalized spiking activity of the left depressor MN pools is plotted against normalized spiking activity of the right depressor MN pools in the interconnected mesothoracic ganglion. Data of overall five preparations are plotted on top of each other. There are two clusters close to the axes. Contralateral mesothoracic depressor MN pools are active mainly out-of-phase, when the mesothoracic ganglion is interconnected to the prothoracic ganglion.

Coordination between contralateral depressor MN pools in the complete deafferented thoracic nerve cord

After analyzing coordination of activity between contralateral depressor MN pools in isolated thoracic ganglia and ganglia pairs, coordination was also investigated in the complete thoracic nerve cord. Contralateral depressor MN activity was recorded from the interconnected pro- (N = 5), meso- (N = 5), and metathoracic ganglia (N = 3) chain, after pilocarpine application. Reliable rhythm could be induced with 5 to 7 mM pilocarpine in only 20% of the preparations. Generally, except a slight tendency for in-phase bursting, no clear coordinating pattern could be observed in the activity of contralateral depressor MNs, as exemplified by the recording in Fig. 16, a. Cross-correlation of the activity between contralateral depressor MN pools of the prothoracic ganglion revealed significant maximum correlation coefficients in 10.7% of the windows throughout the recording (Fig. 16, b). In all five recordings, in 12.7% of the total number of windows, MN activity was significantly correlated. Cross-correlation of the activity between contralateral depressor MN pools of the mesothoracic ganglion showed significant maximum correlation coefficients in only 3.2% of the windows throughout the recording and the maximum correlation coefficient did not exceed 0.5 (Fig. 16, c). However, in all five recordings, 12.4% of the windows showed significant cross-correlation of activity between contralateral depressor MN pools. Activity of contralateral depressor MN pools of the metathoracic ganglion was significantly correlated in 48.1% of the windows throughout the recording (Fig. 16, d). However, with percentages of 0% and 0.9%, the other two preparations could not substantiate this result. Plotting of the pooled normalized activity of contralateral depressor MNs resulted in clustered data only for the pro- and mesothoracic ganglia (Fig. 17, a1, a2 and b1, b2). The spike activity plots concerning the interconnected prothoracic ganglion showed more clustered data compared to the isolated ganglion plot (compare Fig. 12, d1, d2 with Fig. 17 a1, a2). In the mesothoracic ganglion, the two clusters close to the axes at normalized activity equal to 0.8 and a cluster in the center of the plot at the same height corresponded to asynchronous and synchronous bursts, respectively (Fig. 17, b1 and b2). However, low normalized spiking

activity of mesothoracic depressor MNs does not appear to be coordinated (Fig. 17, b2). Finally, normalized activity of contralateral depressor MNs of the metathoracic ganglion did not show clear clusters (Fig. 17, c1 and c2). To summarize, contralateral coordination of activity between depressor MNs in the prothoracic ganglion was improved by intersegmental signals. Contralateral coordination between depressor MNs in the mesothoracic ganglion showed higher frequency of asynchronous or random spiking, compared to the isolated mesothoracic ganglion. Metathoracic depressors showed a tendency for in-phase coordination in only one out-of three preparations (Fig. 16, a and d). Taken together, contralateral CPG coordination improved only in the prothoracic ganglion, due to intersegmental input from other thoracic ganglia.

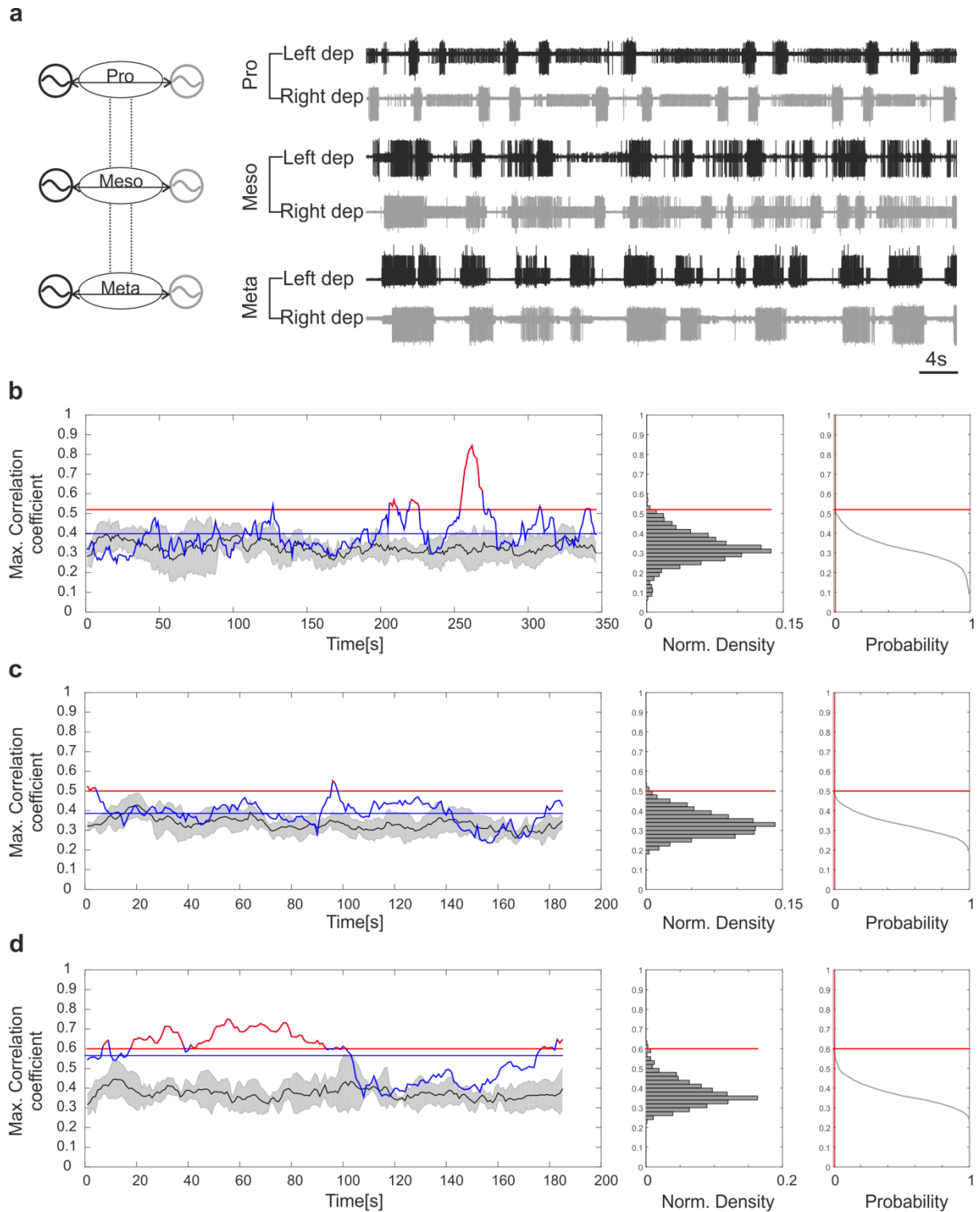


Figure 16: Cross-correlation analysis of activity between contralateral depressor MNs of all ganglia in the complete thoracic ganglia chain. a: Extracellular recording of contralateral depressor MN activity in the complete chain of thoracic ganglia. Rhythmic activity was induced by application of 5 mM pilocarpine. There is no evidence of recurrent patterns of coordinated activity, or coordination patterns that resemble those expressed during behavior. In this recording, there is a tendency for in-phase bursting between contralateral metathoracic depressor MN pools. **b:** Activity of contralateral depressor MNs of the interconnected prothoracic ganglion is significantly correlated in 10.7% of the windows throughout the recording (red parts of the blue curve). **c:** Activity of contralateral depressor MNs of the interconnected mesothoracic ganglion is significantly correlated in only 3.2% of the windows throughout the recording. **d:** Activity of contralateral depressor MNs of the interconnected metathoracic ganglion is significantly correlated in 48.1% of the windows throughout the recording. However, two other preparations could not substantiate such a strong correlation. Black curves: Mean out of eight control Cross-correlations.

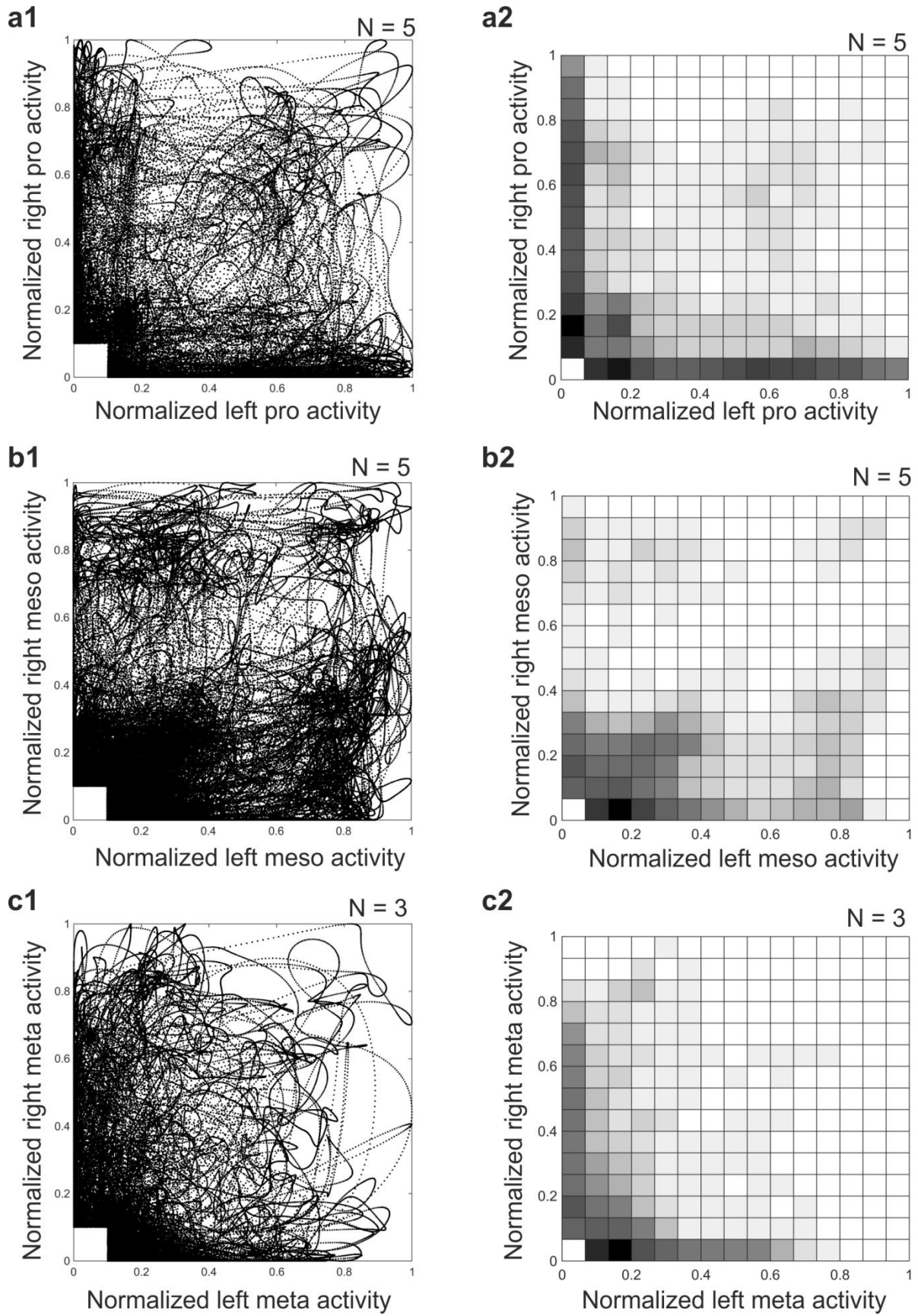


Figure 17: Coordination analysis of spiking activity between contralateral depressor MNs of all ganglia in the complete thoracic ganglia chain (pooled data). a1 and a2: Normalized spiking activity of the left depressor MN pools is plotted against normalized spiking activity of the right depressor MN pools in the interconnected prothoracic ganglion. Data of overall five preparations are plotted on top of each other. Data are sparsely clustered at the axes, suggesting a higher likelihood for out-of-

phase activity. Data appear to be more clustered in comparison to the isolated ganglion (Fig. 12, d1 and d2). **b1 and b2:** Normalized spiking activity of the left depressor MN pools is plotted against normalized spiking activity of the right depressor MN pools in the interconnected mesothoracic ganglion. Data of overall five preparations are plotted on top of each other. There are two clusters close to the axes at normalized activity equal to 0.8 and a cluster in the center of the plot at the same height of activity. There is a high frequency around point 0, indicative of random, uncorrelated spiking between contralateral mesothoracic MN pools. **c1 and c2:** Normalized spiking activity of the left depressor MN pools is plotted against normalized spiking activity of the right depressor MN pools in the interconnected metathoracic ganglion. Data of overall three preparations are plotted on top of each other. There are no clear clusters presented here.

Summary

To summarize, the phase of contralateral depressor MN pools was weakly coupled in the isolated meso- and metathoracic ganglia (Fig. 9, a and b). However, in all isolated ganglia, activity of contralateral depressor MN pools was not significantly correlated throughout the recording (Fig. 18). R-vector length was higher in the interconnected compared to the isolated meso- and metathoracic ganglia (Fig. 10 a and b), and the percentage of windows showing significant cross-correlation of the activity between contralateral depressor MNs was also found to be increased for all interconnected ganglia pairs (Fig. 18). Activity of contralateral depressor MNs in the interconnected prothoracic ganglion was more correlated compared to the activity in the isolated ganglion. In contrast, coordination of activity of contralateral depressor MNs in the interconnected meso- and metathoracic ganglia was weaker when the prothoracic ganglion was attached. However, the percentage of windows showing significant cross-correlation for the meso- and metathoracic ganglia was still higher, when all ganglia were connected, compared to the isolated ganglia (Fig. 18). Thus, the interdependence between CPGs that drive the prothoracic depressor MNs was increased by intersegmental signaling among ganglia. Overall, the activity of contralateral depressor MNs was more strongly correlated in the interconnected meso- and metathoracic ganglia, thereby implying interaction between the underlying CPGs. Prothoracic input to the meso- and metathoracic ganglia increased variability of the pilocarpine-induced rhythm and resulted in lower correlation of activity between contralateral CPGs.

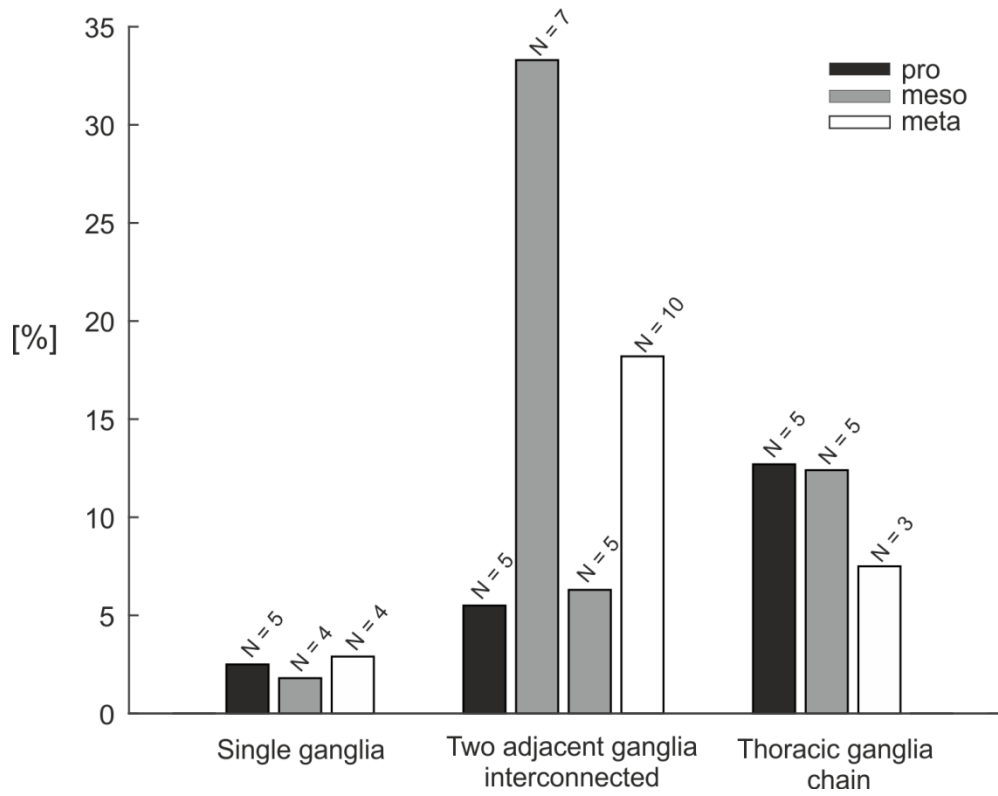


Figure 18: Results summary of the cross-correlation between activity of contralateral depressor MN pools in the isolated and interconnected thoracic ganglia. The percentage of windows that showed significantly correlated activity of contralateral depressor MN pools in the total number of preparations (N) is depicted on the y-axis. Generally, activity of contralateral MNs was more correlated in interconnected than in isolated ganglia.

II. Intersegmental CPG coordination

Intersegmental coordination of activity between depressor MN pools in the interconnected meso- and metathoracic ganglia

To investigate intersegmental coordination between ipsilateral depressor MN pools of the interconnected meso- and metathoracic ganglia, MN activity was extracellularly recorded and its time series were extracted and analyzed for phase coupling and cross correlation. The analysis of activity between ipsilateral depressor MNs of the Rec. 4 (Table 7) is described below. Pilocarpine-induced rhythm was regular in all recordings and MN activity often showed intervals of in-phase bursting (Fig. 19, a). This coordination pattern could be interrupted by intervals of uncoordinated or even tonic activity, especially when the prothoracic ganglion was interconnected. Phase analysis of the activity between right depressor MN pools revealed parallel development of the infinite phases of the meso- and metathoracic depressors (Fig. 19, b). The phase difference showed only few phase slips and largely remained bounded, indicating coupling of activity between ipsilateral meso- and metathoracic depressor MN pools throughout the recording (Fig. 19, b). The phase difference distribution significantly deviated from uniformity ($p < 0.001$), had a circular mean of 331.5 (95% CI: 317.2 to 345.9°) and the r-vector length was 0.49 (Fig. 19, c). Cross correlation in a gliding window of 40 s in steps of 1 s throughout the recording revealed a moderate to strong correlation of intersegmental activity between depressor MN pools with significant correlation coefficients in 21.6% of the windows (Fig. 19, d). Overall, in a total number of eight preparations, 12.2% of the windows showed significant maximum correlation coefficients. Finally, plotting of the normalized activity of the mesothoracic depressor MN pool against that of the ipsilateral metathoracic MN pool resulted in data clustering, indicative of coordinated activity and synchronous bursting (Fig. 19, e1 and e2).

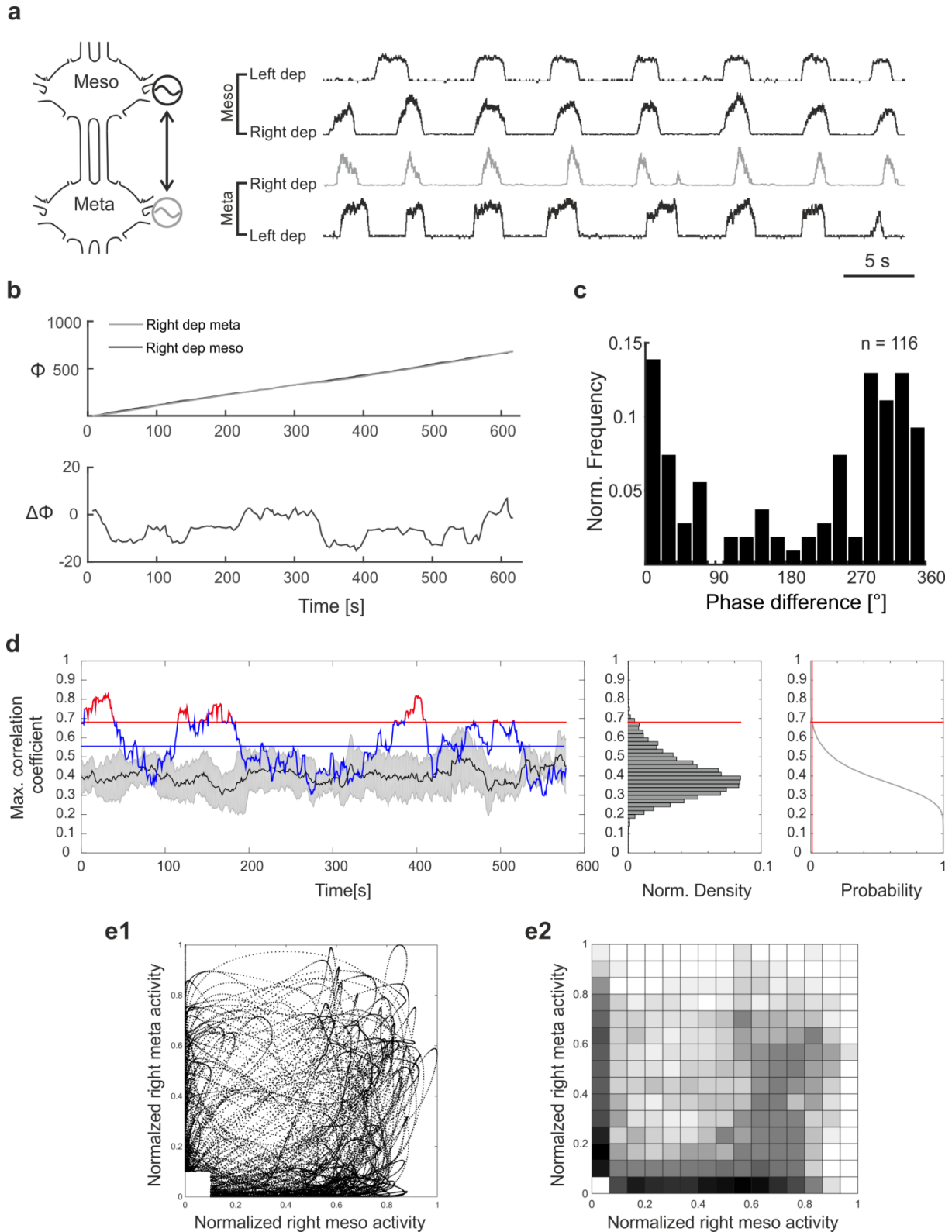


Figure 19: Phase and coordination analysis of intersegmental activity between depressor MN pools in the interconnected meso- and metathoracic ganglia. **a:** Exemplary extracellular recording of the left and right depressor MN activity in both ganglia after application of 5 mM pilocarpine. The ipsilateral right depressor MN activity is here analyzed for intersegmental phase coupling, cross-correlation and synchronization throughout the recording. **b:** The infinite phase (Φ) curves show parallel-almost linear development and the phase difference ($\Delta\Phi$) between activity of contralateral mesothoracic depressor MN pools remains relatively bounded for long intervals throughout the recording. **c:** The distribution of phase differences between the cycles of the mesothoracic and the ipsilateral metathoracic depressor MN pools had a circular mean of 331.5 (95% CI: 317.2 to 345.9°) and the r-vector length was 0.49. n: number of cycles. **d:** Activity of ipsilateral depressor MNs is

significantly correlated in 21.6% of the windows throughout the recording. Black curves correspond to the mean of the max correlation coefficients of 14 control cross-correlations (\pm standard deviation in grey). **e1 and e2**: Normalized spiking activity of the right metathoracic depressor MN pools is plotted against normalized spiking activity of the ipsilateral mesothoracic depressor MN pools. Data are sparsely clustered towards the center of the plot at the height of normalized activity equal to 0.6.

Table 7: Phase analysis of activity between ipsilateral depressor MN pools of the interconnected meso- and metathoracic ganglia. Each recording corresponds to a different animal preparation. Circ_mean (90%C.I.): Circular mean of the angles with the 90% confidence interval into brackets. Circ_Std: Angular deviation. The p-value resulted from the Hodges-Ajne test (omnibus test) for circular uniformity ($\alpha = 0.001$). The smaller this value, the less uniform is the distribution. The h_0° and h_{180} test whether the population mean is equal to 0° or 180° , respectively. This hypothesis is accepted when $h = 0$ and rejected when $h = 1$.

Rec.	Cycles	Circ_mean (90%C.I.) [°]	Circ_Std [°]	r-vector	P-value	h_0°	h_{180°
1	46	332.7 (312.1 , 353.2)	54.8	0.5	0.2e-03	1	1
2	108	25.5 (6.4 , 44.6)	63.1	0.39	5.7e-08	1	1
3	44	8.4 (353.2 , 23.6)	44.4	0.7	4.3e-09	0	1
4	116	331.5 (317.2 , 345.9)	57.9	0.49	2.1e-09	1	1
5	106	359.1 (343.2 , 15)	59.2	0.46	1.2e-08	0	1
6	100	326.7 (285.7 , 7.8)	72	0.21	0.05	0	1
7	57	38.8 (22.6 , 54.9)	51.1	0.6	1.8e-07	1	1
8	81	39.9 (16.8 , 63)	63.7	0.38	10e-06	1	1
9	50	11.9 (314.2 , 21.9)	65.6	0.34	0.015	0	1
10	109	15.8 (350 , 41.5)	67.8	0.3	0.003	0	1
11	106	15.4 (5.1 , 25.6)	46.5	0.67	1.9e-15	1	1
12	177	29.8 (14.6 , 45)	63.7	0.38	1.4e-08	1	1
13	48	151.7 (100 , 203.3)	70	0.25	0.069	1	0
Pool	1148	10.3 (4.2 , 16.3)	64	0.37	8.8e-58	1	1

In total, the phase of the activity between ipsilateral depressor MN pools was analyzed in thirteen recordings (Table 7). More precisely, phase analysis resulted in significantly non-uniform distributions in nine of the recordings ($p < 0.001$). Two out of the nine non-uniform phase difference distributions showed significant direction towards 0° , namely a tendency for in-phase activity, whereas none of them showed a significant tendency for anti-phase activity. The rest of the non-uniform distributions showed mean angles spanning from 331.5° to 39.9° . Pooled data corresponding to 1148 cycles resulted in a peaked distribution ($p < 0.001$) with a circular mean of 10° (95% CI: 4.2° to 16.3°) and a r-vector value of 0.37 (Fig. 20, a). 44.9% of the data included in this distribution are within the interval $0^\circ \pm 45^\circ$. The pooled normalized spike activity of the mesothoracic depressor MN was plotted against that

of the ipsilateral metathoracic depressor MN ($N = 8$). This plot depicted a high frequency of synchronous spiking activity, exemplified by the sparse data away from the two axes and towards the center of the plot (Fig. 20, b). However, these data did not form a distinct cluster, thus indicating that compared to the contralateral, ipsilateral depressor MN activity may be less coordinated throughout the recording. To sum up, activity of ipsilateral depressor MN pool was weakly phase coupled with a tendency for in-phase rather than out-of-phase relationship. The percentage of the windows showing significantly correlated activity throughout the recordings was comparable to those observed for the intrasegmental analysis. To conclude, CTr joint CPGs, driving ipsilateral depressor MN pools are weakly coupled in the interconnected meso- and metathoracic ganglia.

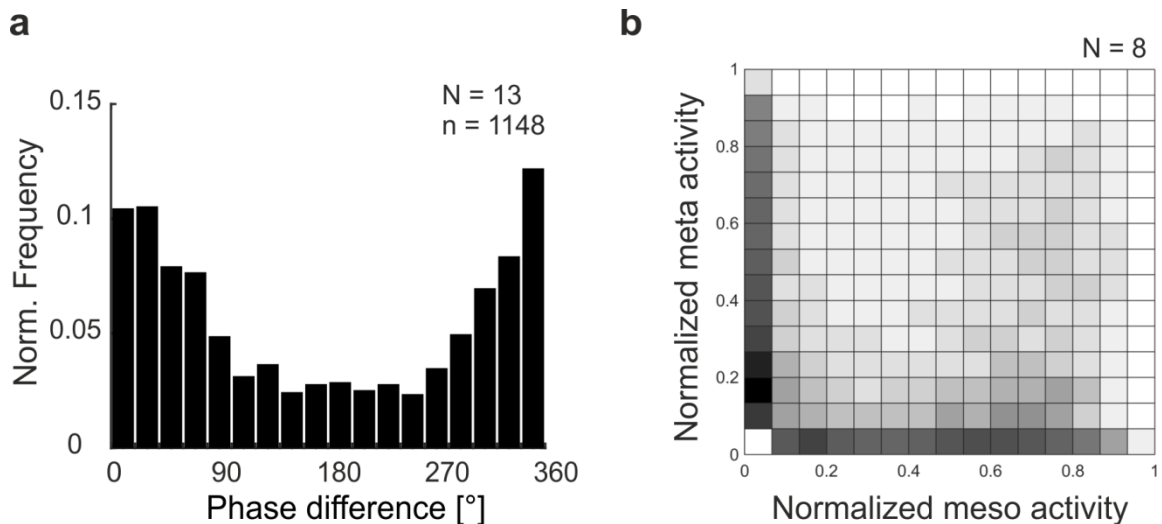


Figure 20: Analysis of intersegmental coupling of activity between depressor MN pools in the interconnected meso- and metathoracic ganglia. **a:** Pooled phase difference values resulted in a peaked distribution ($p < 0.001$) with a circular mean of 10° (95% CI: 4.2° to 16.3°) and r-vector value of 0.37. 44.9% of the data included in this distribution are within the interval $[315^\circ, 45^\circ]$. **b:** Pooled normalized spiking activity of the metathoracic depressor MN pools is plotted against pooled normalized spiking activity of the ipsilateral mesothoracic depressor MNs. Data are sparsely clustered in the central area of the plot, indicating rather weak intersegmental coordination between spike activity of ipsilateral depressor MN pools.

Intersegmental coordination of activity between depressor MN pools in the interconnected pro- and mesothoracic ganglia

Next, intersegmental CPG coordination and interdependence was analyzed by cross-correlating the activity between the ipsilateral pro- and mesothoracic depressor MN pools. Pilocarpine-induced activity showed high variability. Recordings were characterized by bursts consisting of both the slow and fast depressor MN units that alternated with intervals of slow unit activity, and by the complete absence of recurrent coordinated patterns of activity. An exemplary recording is illustrated in Fig. 21, a. In this recording, activity of ipsilateral left depressor MNs significantly correlated in only 1.8% of the windows tested (Fig. 21, b) and in only 2.2% of the windows throughout all seven recordings. Plotting of the spiking activity of the left prothoracic depressor MN pools against the activity of the ipsilateral mesothoracic depressor MN pools resulted in data clustering along the x and y axes and not in the center of the plot, suggesting a tendency for out-of phase activity (Fig. 21, c1 and c2). Similarly, plotting of the pooled prothoracic spiking activity against the ipsilateral mesothoracic activity resulted in the same pattern (Fig. 21, d1 and d2). Taken together, these results indicate that depressor MN activity of the intersegmental pro- and mesothoracic ganglia is only very weakly correlated. Unlike coordination of activity concerning the meso- and metathoracic depressor MN pools, there is no evidence to support synchronous bursting or any other coordination pattern, expressed throughout the recording. However, there is apparently a tendency for anti-phase spiking between ipsilateral pro- and mesothoracic depressors.

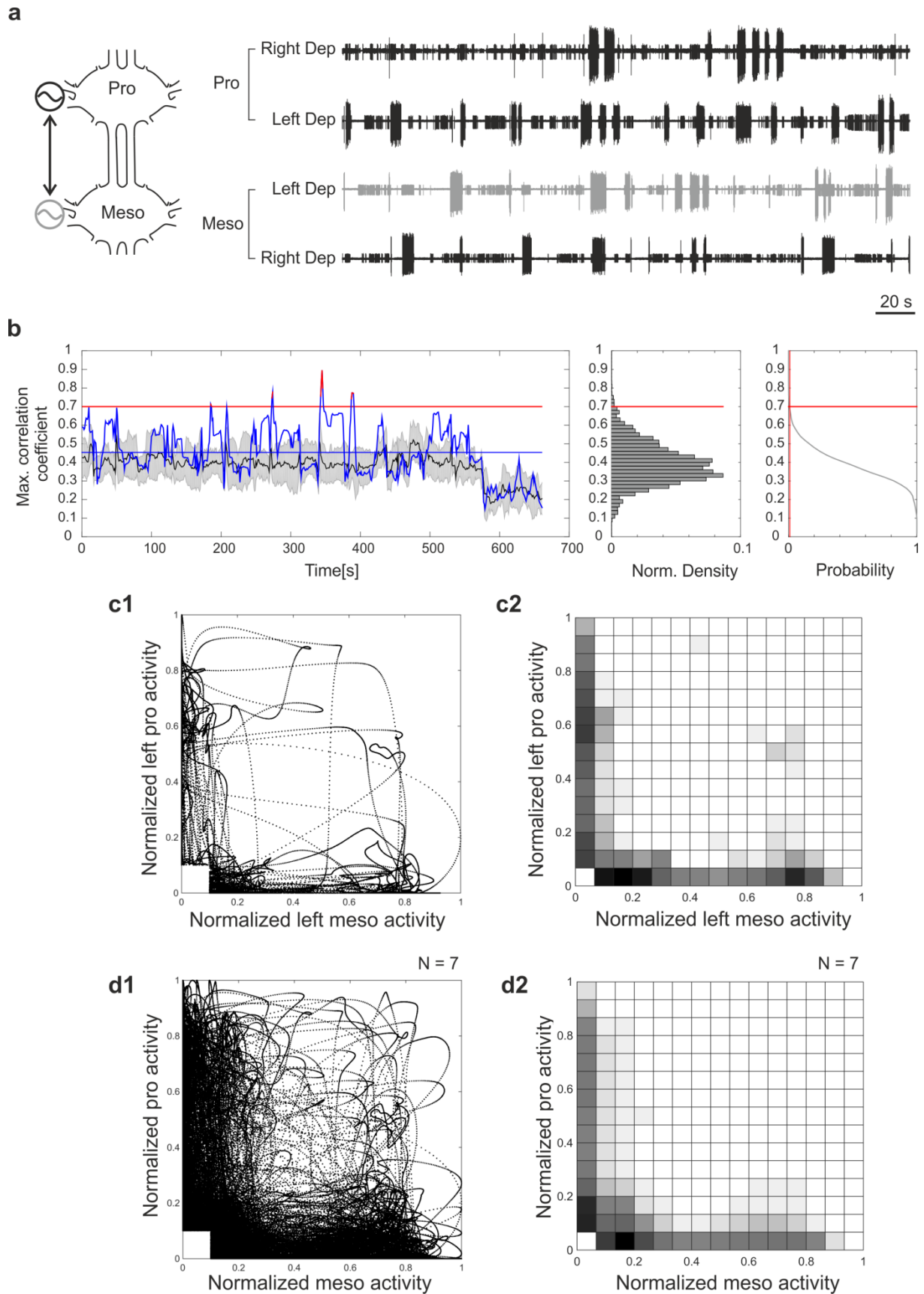


Figure 21: Coordination of intersegmental activity between depressor MN pools of the interconnected pro- and mesothoracic ganglia. a: Exemplary extracellular recording of the left and right depressor MN activity in both ganglia after application of 7 mM pilocarpine. The ipsilateral left depressor MN activity is here analyzed for intersegmental cross-correlation and synchronization throughout the recording. **b:** Activity of ipsilateral depressor MNs is significantly correlated in only 1.8% of

the windows throughout the recording. Black curves correspond to the mean of the max correlation coefficients of 12 control cross-correlations (\pm standard deviation in grey). **c1 and c2:** Normalized spiking activity of the left prothoracic depressor MN pools is plotted against normalized spiking activity of the ipsilateral mesothoracic depressor MN pools. There are two clusters, close to the x- and y-axis each, at normalized activity equal to 0.8 and 0.6, respectively. These data indicate out-of-phase spiking between ipsilateral depressor MNs. **d1 and d2:** Normalized spiking activity of the prothoracic depressor MN pools is plotted against normalized spiking activity of the ipsilateral mesothoracic depressor MN pools. Data of overall seven preparations are plotted on top of each other. Clusters close to the x- and y-axis show sparse distribution. These data indicate tendency for out-of-phase activity and high variability between ipsilateral depressor MNs.

Intersegmental coordination of activity between depressor MN pools in the complete deafferented thoracic nerve cord

Finally, intersegmental coordination of depressor MN activity was analyzed when all thoracic ganglia were left interconnected. An exemplary recording of ipsilateral depressor MN activity of all three thoracic ganglia is illustrated in Fig. 22, a. Similar to the activity patterns observed in the recording of the interconnected pro- and mesothoracic ganglia, depressor MN pools in the complete thoracic ganglia chain did not show any recurrent patterns of coordinated activity (Fig. 22, a). Cross-correlation did not show any interdependence among activity of the pro-, meso- and metathoracic depressor MNs (Fig. 22b, c and d). In a total number of seven recordings, the activity of the pro- and mesothoracic MN pools was significantly correlated in 5.7% of the windows; the activity of the meso- and metathoracic MN pools was significantly correlated in 5.6% of the windows; and the prothoracic depressor MN activity significantly correlated with the metathoracic MN activity in only 2.1% of the windows. Plotting of the pooled normalized spiking activity of the depressor MN pools against the spiking activity of the MN pools of the adjacent ganglion resulted in no clear data clustering, highlighting the lack of coordinated activity (Fig. 23). All plots mainly showed sparse distribution of data at the two axes and data broadly distributed in the center of the plot, at spike activity around 0.6 to 0.8. These findings suggest a higher tendency for asynchronous, out-of-phase spike activity between ipsilateral depressor MN pools in the interconnected thoracic ganglia.

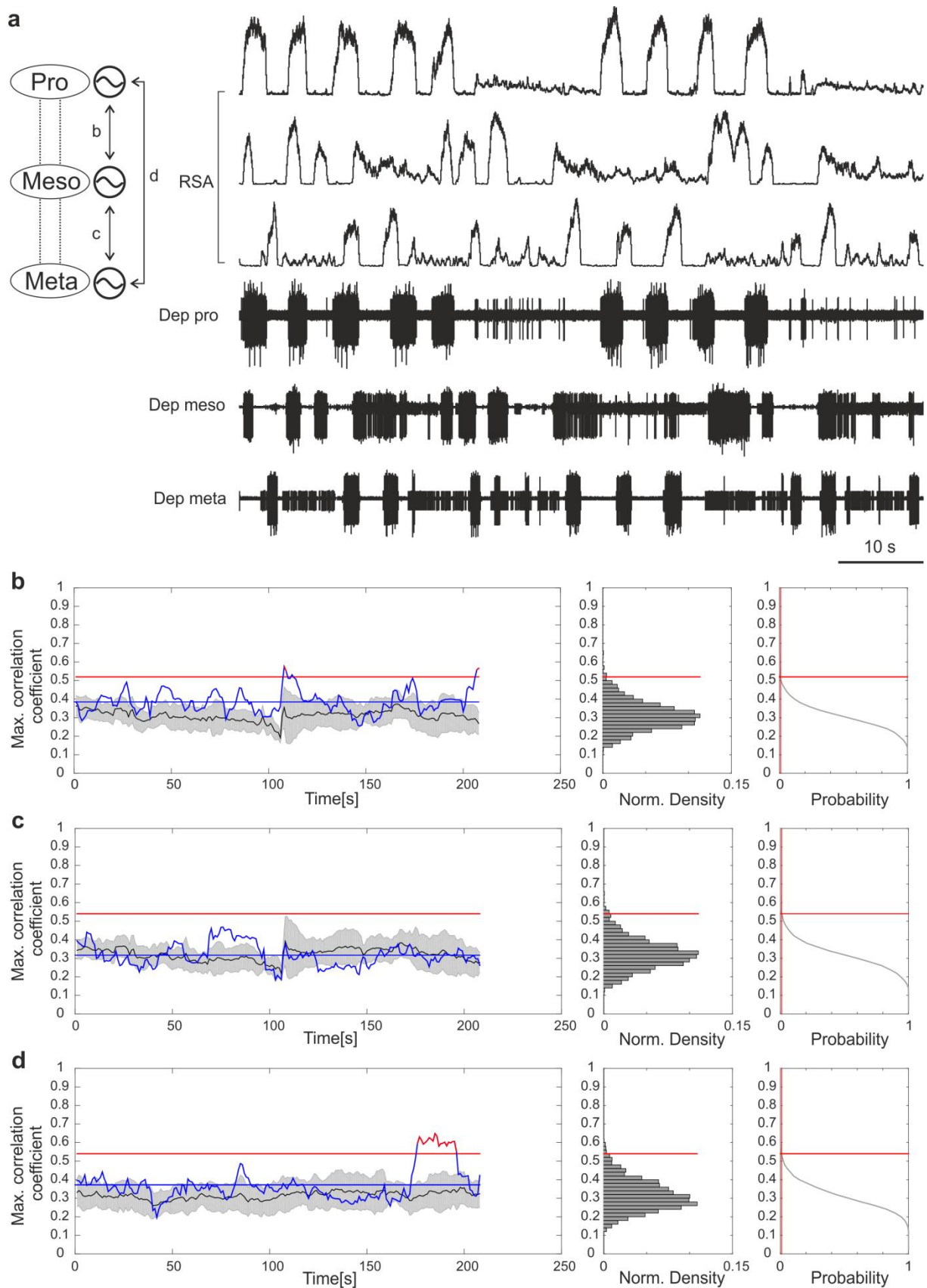


Figure 22: Cross-correlation analysis of the activity between ipsilateral depressor MNs of all ganglia in the complete thoracic ganglia chain. a: Extracellular recording of the activity of all ipsilateral depressor MN pools of all thoracic ganglia after application of 5 mM pilocarpine. No recurrent coordination pattern of ipsilateral depressor activity can be observed. RSA: Rectified and smoothed activity ($\tau = 0.05$). **b:** Activity of ipsilateral pro- and mesothoracic depressor MNs is significantly correlated in only 2.4% of the windows throughout the recording. **c:** Activity of ipsilateral meso- and metathoracic depressor

MNs is not significantly correlated throughout the recording. **d**: Activity of ipsilateral pro- and metathoracic depressor MNs is significantly correlated during a 25 s interval throughout the recording. Black curves correspond to the mean of the max correlation coefficients of 12 control cross-correlations (\pm standard deviation in grey).

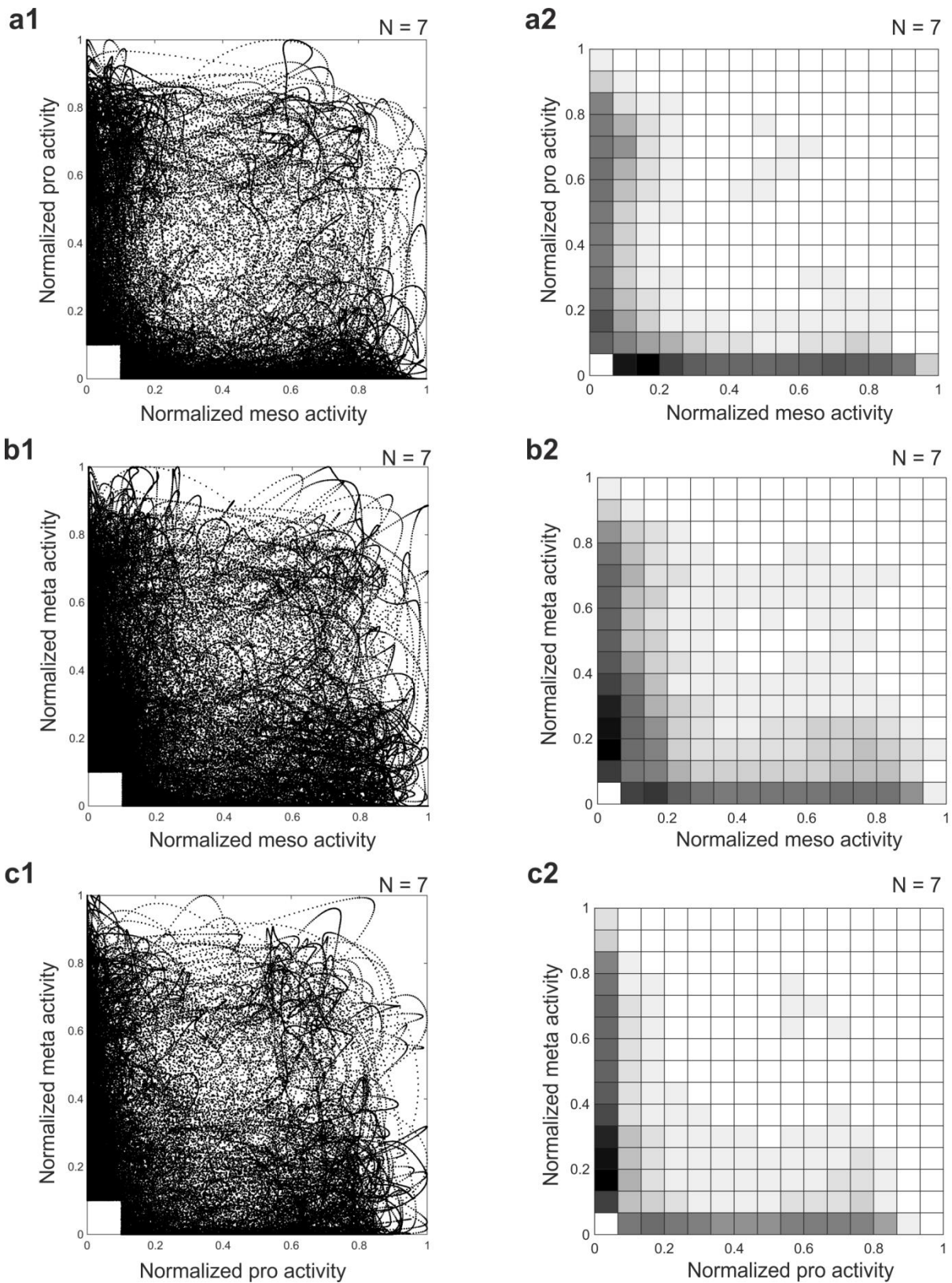


Figure 23: Coordination analysis of spiking activity between ipsilateral depressor MN pools of all ganglia in the complete thoracic ganglia chain (pooled data). **a1 and a2:** Normalized spiking activity of the prothoracic depressor MN pools is plotted against normalized spiking activity of the ipsilateral mesothoracic depressor MN pools. Data of overall seven preparations are plotted on top of each other. Data are sparsely clustered at the axes, suggesting a higher likelihood for out-of-phase activity. There is a faint cluster in the center of the plot. **b1 and b2:** Normalized spiking activity of the metathoracic depressor MN pools is plotted against normalized spiking activity of the ipsilateral mesothoracic depressor MN pools. Data of

overall seven preparations are plotted on top of each other. Data are mainly distributed close to the axes, suggesting a higher likelihood for out-of-phase activity. However, data distribution is quite sparse and indicates high variability in ipsilateral coordination. **c1 and c2:** Normalized spiking activity of the metathoracic depressor MN pools is plotted against normalized spiking activity of the ipsilateral prothoracic depressor MN pools. Data of overall seven preparations are plotted on top of each other. Data are sparsely distributed close to the axes and there is no clear pattern of spike coordination observed. N: number of animal preparations.

To test whether lack of intersegmental coordination of activity between ipsilateral depressor MN pools of the meso- and metathoracic ganglia is related to the signals transmitted by the prothoracic ganglion, the bath of the prothoracic ganglion was isolated from the rest of the thoracic ganglia, and pilocarpine was selectively first applied on the meso- and metathoracic ganglia (N = 3). In two out of three recordings activity of ipsilateral depressor MNs of the meso- and metathoracic ganglia was not significantly coordinated throughout the recording (Fig. 24, b). After activation of the prothoracic CPGs, rhythmicity and intersegmental coordination between depressor MN pools developed differently for each of the three recordings. In a preparation, coordination of depressor MN activity between the meso- and metathoracic ganglia partially improved (Fig. 24, c); in a second preparation, activity remained uncorrelated throughout the recording; and in a third preparation the percentage of the windows that showed significant cross-correlation decreased from 10.6% to 5.4%. Plots showing the pooled meso- and metathoracic spiking activities plotted against each other, before (Fig. 24, d), and after (Fig. 24, e) activating the prothoracic CPGs indicated an overall lack of coordinated activity, as no clear data clusters were depicted. Thus, these results indicate that intersegmental signals from the prothoracic CPGs contribute to the bursting variability of the meso- and metathoracic activity and affect the in-phase coordination between the meso- and metathoracic CTr-joint CPGs .

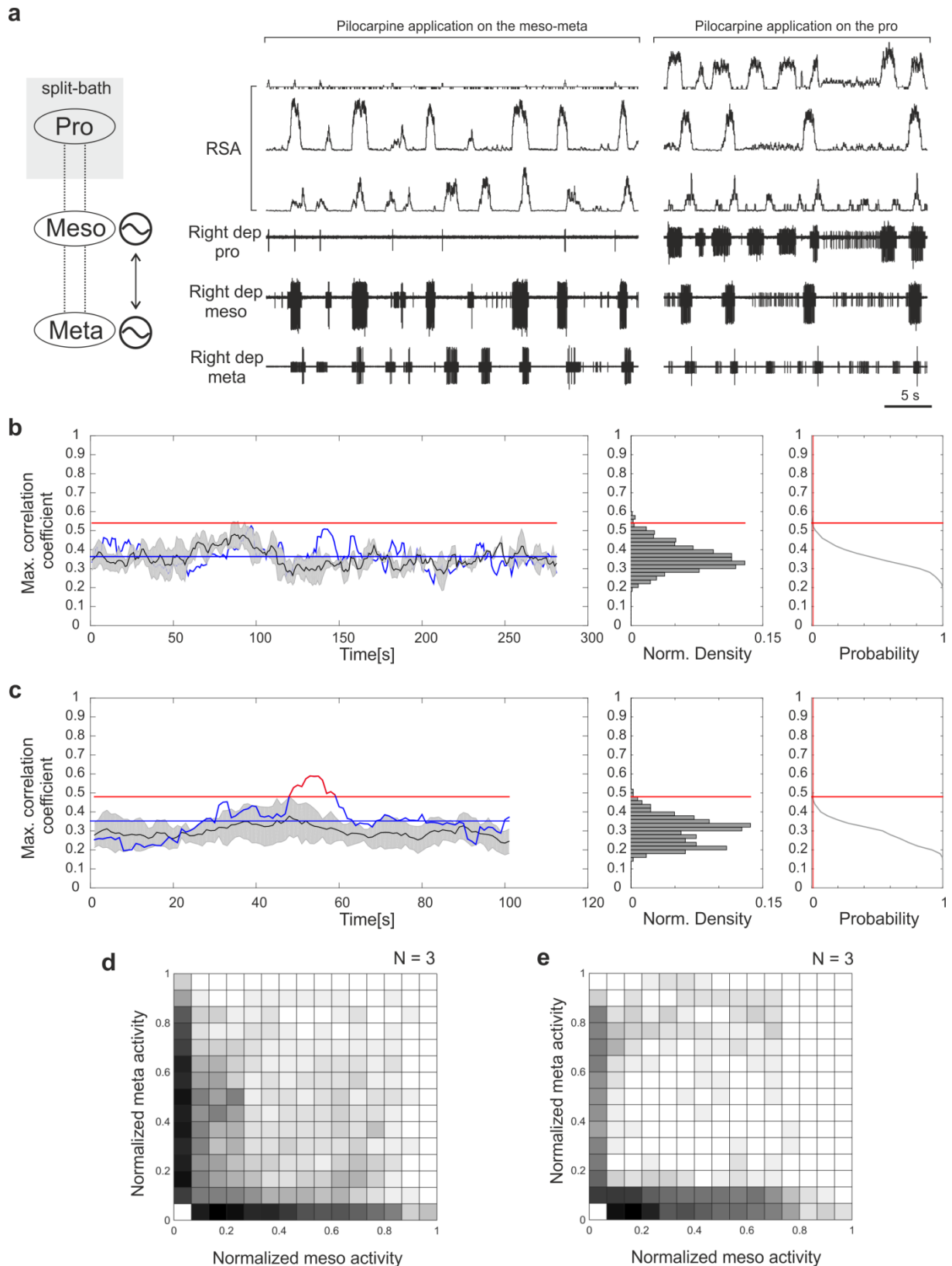


Figure 24: Coordination analysis of intersegmental activity between depressor MN pools of the meso- and metathoracic ganglia, before and after activation of the prothoracic CPGs (split-bath). **a:** Exemplary extracellular recording of the right depressor MN activity in all thoracic ganglia. Rhythmic activity in the meso- and metathoracic MN pools was induced by application of 5 mM pilocarpine. Prothoracic CPGs were activated by application of 6 mM pilocarpine. **b:** Activity of ipsilateral meso- and metathoracic depressor MNs is not significantly correlated throughout the recording before pilocarpine application in the prothoracic ganglion. Black curves correspond to the mean of the max correlation coefficients of four control cross-correlations (\pm standard deviation in grey). **c:** Activity of ipsilateral meso- and metathoracic depressor MNs is significantly

correlated for about only 10 s throughout the recording, after pilocarpine application in the prothoracic ganglion. Black curves correspond to the mean of the max correlation coefficients of four control cross-correlations (\pm standard deviation in grey). **d:** Normalized spiking activity of metathoracic depressor MN pools is plotted against normalized spiking activity of ipsilateral mesothoracic depressor MN pools, before pilocarpine application in the prothoracic ganglion. Data of overall three preparations are plotted on top of each other. Data are highly concentrated at the axes and sparsely distributed in the center of the plot. No clear clusters can be observed. **e:** Normalized spiking activity of metathoracic depressor MN pools is plotted against normalized spiking activity of ipsilateral mesothoracic depressor MN pools, after pilocarpine application in the prothoracic ganglion. Distribution pattern is changed compared to (d).

Summary

To summarize, the activity of ipsilateral depressor MN pools in the interconnected meso- and metathoracic ganglia was weakly coupled (Fig. 19, b and c, Fig. 20, a and b). The percentage of windows showing significant cross-correlation of activity between ipsilateral meso- and metathoracic depressor MN pools was higher than the percentage of windows showing significant cross-correlation between activity of pro- and mesothoracic depressor MN pools (Fig. 25, a). Correlation of ipsilateral activity between depressor MN pools in the pro- and mesothoracic ganglia appears to be stronger in the thoracic ganglia chain. In contrast, intersegmental correlation of the activity between ipsilateral meso- and metathoracic depressor MN pools was lower when the prothoracic ganglion was attached (Fig. 25, a). Similar to what has been described above concerning the intrasegmental coordination, prothoracic input to the meso- and metathoracic ganglia increased variability of the pilocarpine-induced activity in depressor MN pools and resulted in lower correlation of intersegmental activity. Finally, cross-correlation of the ipsilateral activity between pro- and metathoracic depressor MN pools was apparently the weakest (Fig. 25, a, white bar). In conclusion, intersegmental CPG coupling in the complete thoracic nerve cord of the stick insect was assessed by phase analysis and cross-correlation and was found to be very weak in the interconnected meso- and metathoracic ganglia, and almost absent in all other cases. The resulting centrally-generated intersegmental pattern of coordinated activity in the deafferented thoracic nerve cord does not resemble any of the leg coordination patterns that are observed in behavior (Fig. 25, b).

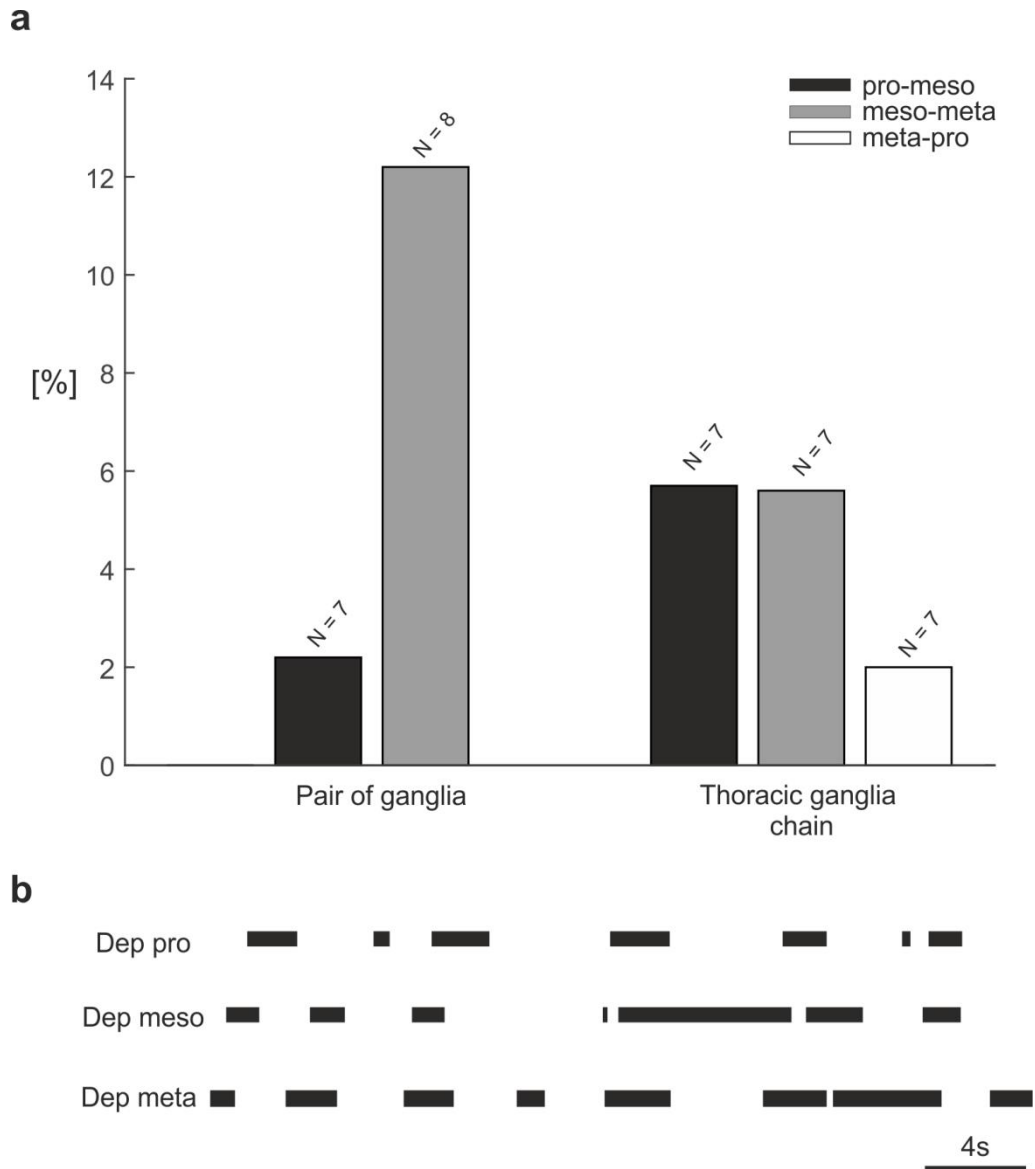


Figure 25: Results summary concerning the cross-correlation of activity between ipsilateral depressor MN pools. a: The percentage of windows that showed significantly correlated activity in the total number of preparations (N) is depicted on the x-axis. Generally, intersegmental activity of ipsilateral depressor MN pools is more correlated in the interconnected meso- and metathoracic ganglia. Intersegmental activity of ipsilateral pro- and mesothoracic depressor MN pools is more correlated in the complete thoracic ganglia chain, whereas intersegmental activity of ipsilateral depressor MN pools is in the interconnected meso- and metathoracic ganglia is negatively affected when prothoracic ganglion is attached. **b:** Coordination pattern between ipsilateral depressor MN pools of the complete thoracic ganglia chain. Black bars correspond to the depressor burst length. This coordination pattern does not resemble any of the coordination patterns observed in behavior.

III. Neuronal mechanisms underlying intra and intersegmental CPG coordination

Intrasegmental coordination of depressor MN activity after posterior midline section in the isolated mesothoracic ganglion

Contralateral coordination of depressor MN activity in the isolated mesothoracic ganglion was analyzed, after performing a midline section. The section started caudal from the midline trachea, and along the ganglionic midline throughout the posterior half of the ganglion. In accordance with Büschges and colleagues (1995), who first showed that pilocarpine could induce rhythmic MN activity in single hemiganglia after midline section in the stick insect mesothoracic ganglion, a reliable rhythm could be induced in eight out-of eleven preparations after posterior midline section. A systematic cycle-to-cycle coupling of activity between contralateral depressor MNs has never been observed (Fig. 26, a). In three out of eight preparations, contralateral activity of depressor MNs was not significantly correlated throughout the recording (fig. 26, b). However, significant correlation coefficients were reported for 8% of the windows in all eight preparations and for 37.5% of the windows in a preparation (Fig. 27, a and b), indicating that there may still be interdependence between contralateral CPGs that drive depressor MN activity. Nevertheless, the overall phase difference distribution did not significantly deviate from the uniform distribution at the 0.001 level for any of the three preparations tested (Table 8, Fig. 26, c and Fig. 27, c). The mean direction was 357° (95% CI: 315° to 39°) with angular deviation 72.3° . Although the statistical hypothesis for mean direction towards 0° could not be rejected for two out of three preparations at the 5% level, the rather short r-vector lengths and the high angular deviation imply that there is no detectable contralateral coupling between the CPGs driving the depressor MN pools. The distribution of pooled phase differences deviated from the uniform distribution at the 0.01 level ($p = 0.007$). However, it did not show a significant tendency towards 0° (Table 8), similar to what has been observed in the intact ganglion. The mean direction was 328° (95% CI: 299° to 357°) with angular deviation 75.3° and the r-vector was 0.14. Only 30% of the cycles showed a phase difference within the interval of 315° to 45° ($0^\circ \pm 45^\circ$), whereas the same percentage was 44% in the intact isolated mesothoracic ganglion.

Finally, plotting the spiking activity of contralateral depressor MN pools against each other did not result in data clusters or any sort of a pattern that would imply consistent coordination throughout the recording (Fig. 26, e) with only one exception (Fig. 27, d). Plotting of the pooled spiking activity also showed no clear clusters (Fig. 26, f). Taken together, on the one hand the weak correlation of activity between contralateral depressor MNs in some preparations indicates that activity interdependence persists after sectioning of the posterior dorsal commissures. On the other hand, there is no evidence for contralateral activity coupling. Thus, it may be concluded that the posterior commissures play an important role in contralateral CPG coupling in the mesothoracic ganglion.

Table 8: Phase analysis of the activity between contralateral depressor MNs of the isolated mesothoracic ganglion, after transection along the posterior ganglionic midline.

Rec.	Cycles	Circ_mean (90%C.I.) [°]	Circ_Std [°]	r-vector	P-value	h0°	h180°
1	198	344.5 (311.3 , 17.8)	73.4	0.18	0.02	0	1
2	101	356.8 (314.7 , 38.9)	72.3	0.20	0.04	0	1
3	133	258.3 (209, 307.8)	74.3	0.16	0.08	1	1
Pool	432	328.3 (299.4 , 357.2)	75.3	0.14	0.007	1	1

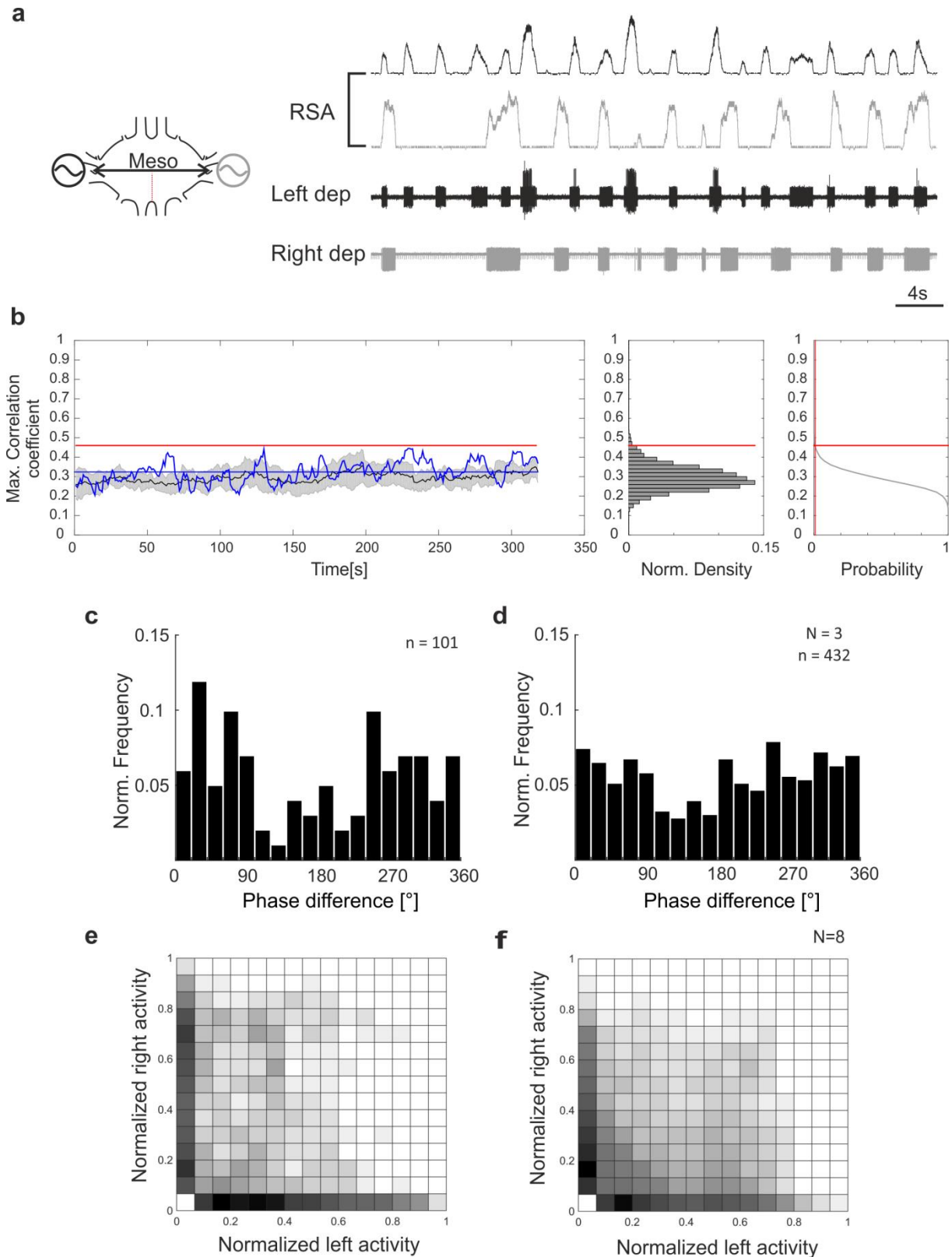


Figure 26: Coordination analysis between intrasegmental activity of depressor MN pools in the isolated mesothoracic ganglion after sectioning along the posterior ganglionic midline. a: Extracellular recording of the left and right depressor MN activity after application of 5 mM pilocarpine. Contralateral bursts do not form any recurrent pattern of activity and bursting frequency differs between the two depressor MN pools. **b:** Activity of contralateral depressor MNs is not significantly correlated throughout the recording. Black curves correspond to the mean of the max correlation coefficients of 14 control cross-correlations (\pm standard deviation in grey). **c:** The distribution of phase differences between the cycles of contralateral mesothoracic depressor MN pools does not significantly differ from the uniform distribution at the 99.9% level ($p = 0.04$). It has a

circular mean of 356.8 (95% CI: 314.7 to 38.9) and the r-vector length is 0.2. **d:** The distribution of the pooled phase differences does not significantly differ from the uniform distribution at the 99.9% level ($p = 0.007$) and does not show a significant direction towards 0° ($\alpha = 0.05$). **e:** Normalized spiking activity of the right mesothoracic depressor MN pools is plotted against normalized spiking activity of the contralateral depressor MN pools. Data are randomly distributed at the axes and towards the center of the plot. **f:** Normalized spiking activity of the right mesothoracic depressor MN pools is plotted against normalized spiking activity of the contralateral depressor MN pools. Data of overall eight preparations are plotted on top of each other. There is no clear cluster of data.

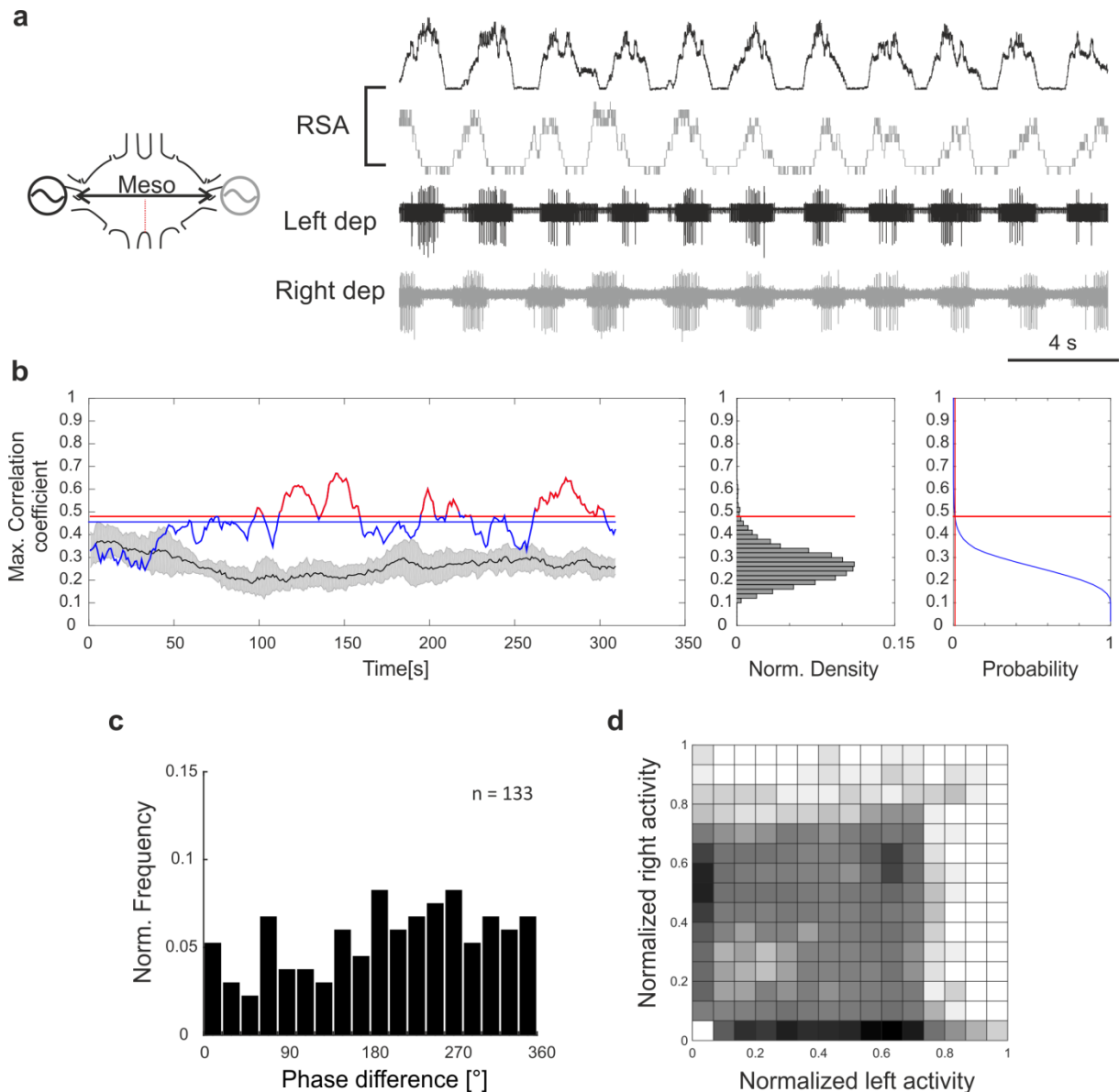


Figure 27: Coordination analysis between intrasegmental activity of depressor MN pools in the isolated mesothoracic ganglion after sectioning along the posterior ganglionic midline. a: Extracellular recording of the left and right depressor MN activity after application of 5 mM pilocarpine. Activity of contralateral depressors appears to drift throughout the recording. **b:** Activity of contralateral depressor MNs is significantly correlated in 37.5% of the windows throughout the recording. Black curves correspond to the mean of the max correlation coefficients of 14 control cross-correlations (\pm standard deviation in grey). **c:** The distribution of phase differences between the cycles of contralateral mesothoracic depressor MN pools does not significantly differ from the uniform distribution at the 99.9% level ($p = 0.08$). **d:** Normalized spiking activity of the right mesothoracic depressor MN pools is plotted against normalized spiking activity of the contralateral depressor MN pools. Data are clustered at the axes and also form a cluster in the center of the plot at almost the same level of normalized activity (0.6).

Intra- and intersegmental coordination of depressor MN activity after sectioning of one connective nerve in the interconnected meso- and metathoracic ganglia

To test whether signals transmitted through only one connective between the meso- and metathoracic ganglia are sufficient for inter- and intrasegmental coordination, one of the connectives was cut and then pilocarpine was applied to activate the CPGs. Raw recording data indicated in-phase bursting activity between contralateral depressor MNs of the metathoracic ganglion after transection of the left connective, similar to the previously reported in-phase activity in the intact interconnected meso- and metathoracic ganglia (Fig. 28, a and Fig. 29). However, these data showed high variability in temporal burst characteristics throughout the recording as well as among different preparations. The cycle could not be reliably defined in most of the recordings; therefore data were analyzed by cross-correlation.

Cross-correlation of activity between intersegmental depressor MN pools recorded ipsilateral to the transected connective resulted in no detectable correlation in five out of ten preparations. In the rest of the recordings, activity was found to be significantly correlated only in a very low percentage of windows, which did not exceed 3% (Fig. 28, b). Contralateral to the transected connective, intersegmental activity was found to be significantly correlated in a higher proportion of windows throughout the recording (Fig. 28, c). However, in a total number of seven recordings, activity of meso- and metathoracic depressor MN pools ipsilateral to the intact connective was significantly correlated in only 3.4% of the windows. In contrast, activity of contralateral depressor MN pools in the meso- and metathoracic ganglia was to a larger extent correlated. Activity of contralateral mesothoracic depressor MN pools in the mesothoracic ganglion was significantly correlated in 30.8% and in the metathoracic in 13% of the windows (Fig. 28, d and e). Pooled data showed significant correlation of activity between contralateral depressor MN pools in 12.2% and 14.5% of the windows of the meso- (N = 6) and metathoracic ganglion (N = 9), respectively. Moreover, the mean of maximum correlation coefficients was higher in the cross-correlation of intrasegmental compared to the intersegmental depressor MN activity (compare blue horizontal lines in Fig. 28, c-e). Thus,

interdependence of intersegmental activity between depressor MN pools of the meso- and metathoracic ganglia was apparently reduced, after transection of the ipsilateral or contralateral connective, whereas interdependence of intrasegmental activity between contralateral depressor MN pools within the meso- or metathoracic ganglion was affected to a lesser extent.

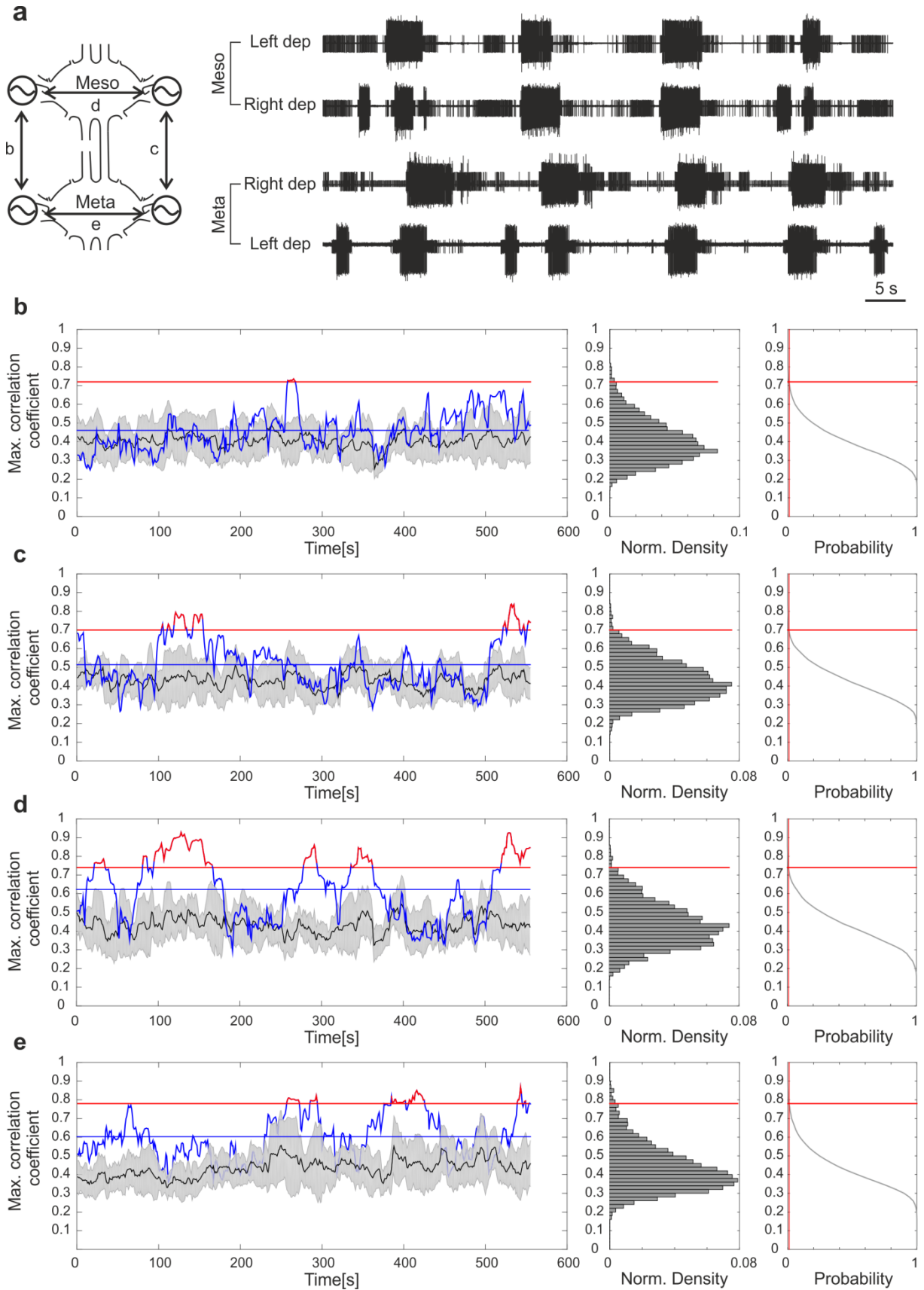


Figure 28: Cross-correlation analysis of the activity between ipsilateral and contralateral depressor MN pools in the interconnected meso- and metathoracic ganglia after sectioning of one connective. a: Extracellular recording of the activity of all depressor MN pools in the interconnected meso- and metathoracic ganglia after sectioning of the left connective.

b: Ipsilateral left activity (side of the cut) is significantly correlated in only 1.8% of the windows throughout the recording. Black curves correspond to the mean of the max correlation coefficients of 18 control cross-correlations (\pm standard deviation in grey). **c:** Ipsilateral right activity is significantly correlated in 11.2% of the windows throughout the recording. Black curves correspond to the mean of the max correlation coefficients of 12 control cross-correlations (\pm standard deviation in grey). **d:** Contralateral mesothoracic activity is significantly correlated in 30.8% of the windows throughout the recording. Black curves correspond to the mean of the max correlation coefficients of 10 control cross-correlations (\pm standard deviation in grey). **e:** Contralateral metathoracic activity is significantly correlated in 13% of the windows throughout the recording. Black curves correspond to the mean of the max correlation coefficients of 16 control cross-correlations (\pm standard deviation in grey).

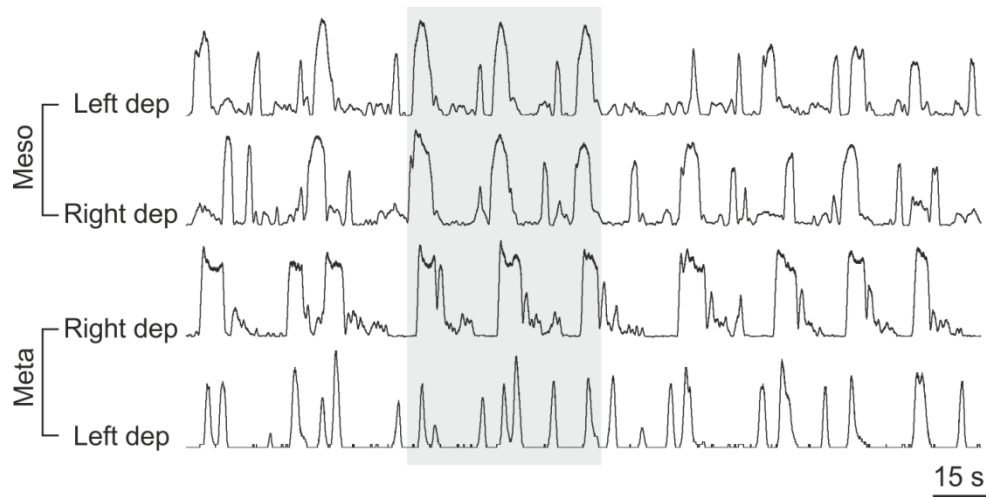


Figure 29: Activity of ipsilateral and contralateral depressor MNs in the interconnected meso- and metathoracic ganglia after sectioning of the left connective. This is the same recording as in Fig. 28. Signal was rectified and smoothed ($\tau = 0.3$). In spite of one connective being cut, inter- and intrasegmental coordination of depressor MN activity is still evident.

However, plotting the spike activity of the metathoracic depressor MNs against the spiking activity of the mesothoracic depressor MNs, both recorded ipsilateral or contralateral to the transected connective, resulted in distinct clusters at the axes (Fig. 30, a and b, between 0.6 and 0.8) and the center of the plot (Fig. 30, a). These plots indicated that activity was altered in both sides compared to the intact preparations (Fig. 20, c and d), and there was a higher tendency for asynchronous spiking between the meso- and metathoracic depressor MN pools contralateral to the cut. Data clusters were also observed after plotting the activity of the contralateral depressor MN pools against each other in the meso- or metathoracic ganglia. The mesothoracic clusters were less pronounced (Fig. 30 c and d), whereas contralateral metathoracic depressor MN pools had a tendency to be synchronously active (Fig. 30, d). In conclusion, intersegmental and intrasegmental CPG coordination was affected by transection of one of the connective nerves. However, these data imply that one

connective is enough to preserve at least contralateral CPG coordination in the metathoracic ganglion.

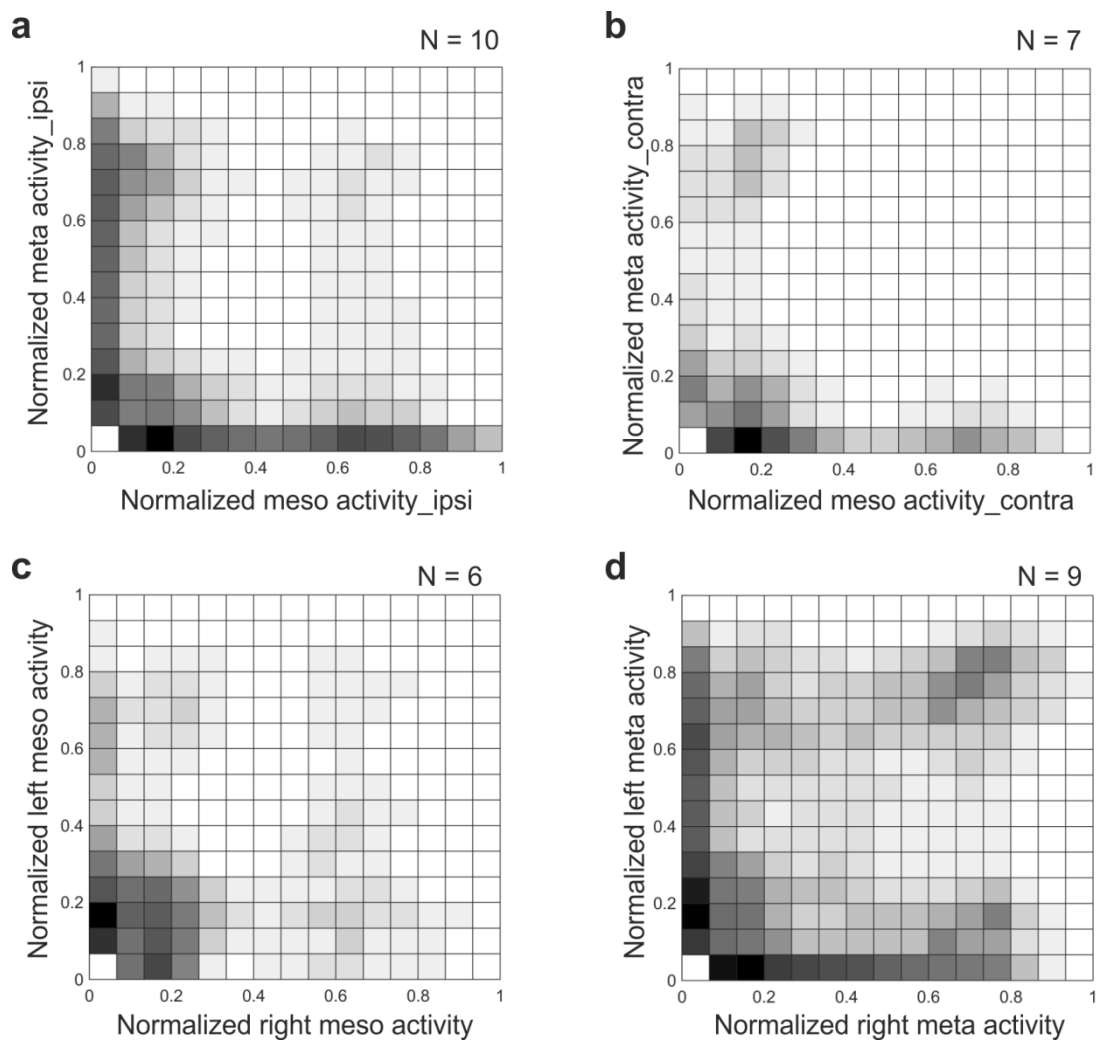


Figure 30: Coordination analysis of spiking activity between ipsilateral or contralateral depressor MNs of the meso- and metathoracic ganglia after sectioning of one connective. **a:** Normalized spiking activity of the metathoracic depressor MN pools is plotted against normalized spiking activity of the ipsilateral mesothoracic depressor MN pools, after cutting the ipsilateral connective. Data of overall ten preparations are plotted on top of each other. Data are clustered at the axes and also form a cluster in the center of the plot at normalized activity 0.6 to 0.8. **b:** Normalized spiking activity of the metathoracic depressor MN pools is plotted against normalized spiking activity of the ipsilateral mesothoracic depressor MN pools, after cutting the contralateral connective. Data of overall seven preparations are plotted on top of each other. Data are clustered close to the axes. **c:** Normalized spiking activity of the mesothoracic depressor MN pools is plotted against normalized spiking activity of the contralateral depressor MN pools. Data of overall six preparations are plotted on top of each other. Data are clustered at the axes and also form a cluster in the center of the plot at normalized activity 0.6. **d:** Normalized spiking activity of the metathoracic depressor MN pools is plotted against normalized spiking activity of the contralateral depressor MN pools. Data of overall nine preparations are plotted on top of each other. Data are clustered at the axes and also form a cluster in the center of the plot at normalized activity 0.6 to 0.8.

Intracellular recordings of the fast and slow depressor motor neuron activity

After having identified that activity between contralateral depressor MNs is weakly coupled in the deafferented thoracic ganglia, potential direct interactions between contralateral depressor MNs were investigated, and MN membrane potential modulations were analyzed in relation to the cycle of the contralateral CPG. Extracellular recordings of the activity of contralateral depressor MNs were combined with right-side intracellular recordings from either the SDTr or the FDTr, in the isolated mesothoracic ganglion (Fig. 31, a, and Fig. 32, a). In all six FDTr and SDTr recordings, there was no membrane potential modulation of the intracellular trace correlated to the onset of the contralateral depressor cycle (Fig. 31, b1 and Fig. 32, b1). As a control, membrane potential was modulated in-phase with the ipsilateral depressor cycle onset (Fig. 31, b2 and Fig. 32, b2). Thus, there is no direct influence between contralateral depressor MNs. In line with these results, current injection of up to 7 nA in a depressor MN did not entrain the pilocarpine-induced rhythm of the contralateral depressor MN activity. Moreover, the input resistance of the FDTr showed no alteration correlated with the left depressor cycle (Fig. 31, c, compare the two first stimulations). Taken together, there is apparently no direct influence of the CTr-joint CPG on the contralateral depressor MN.

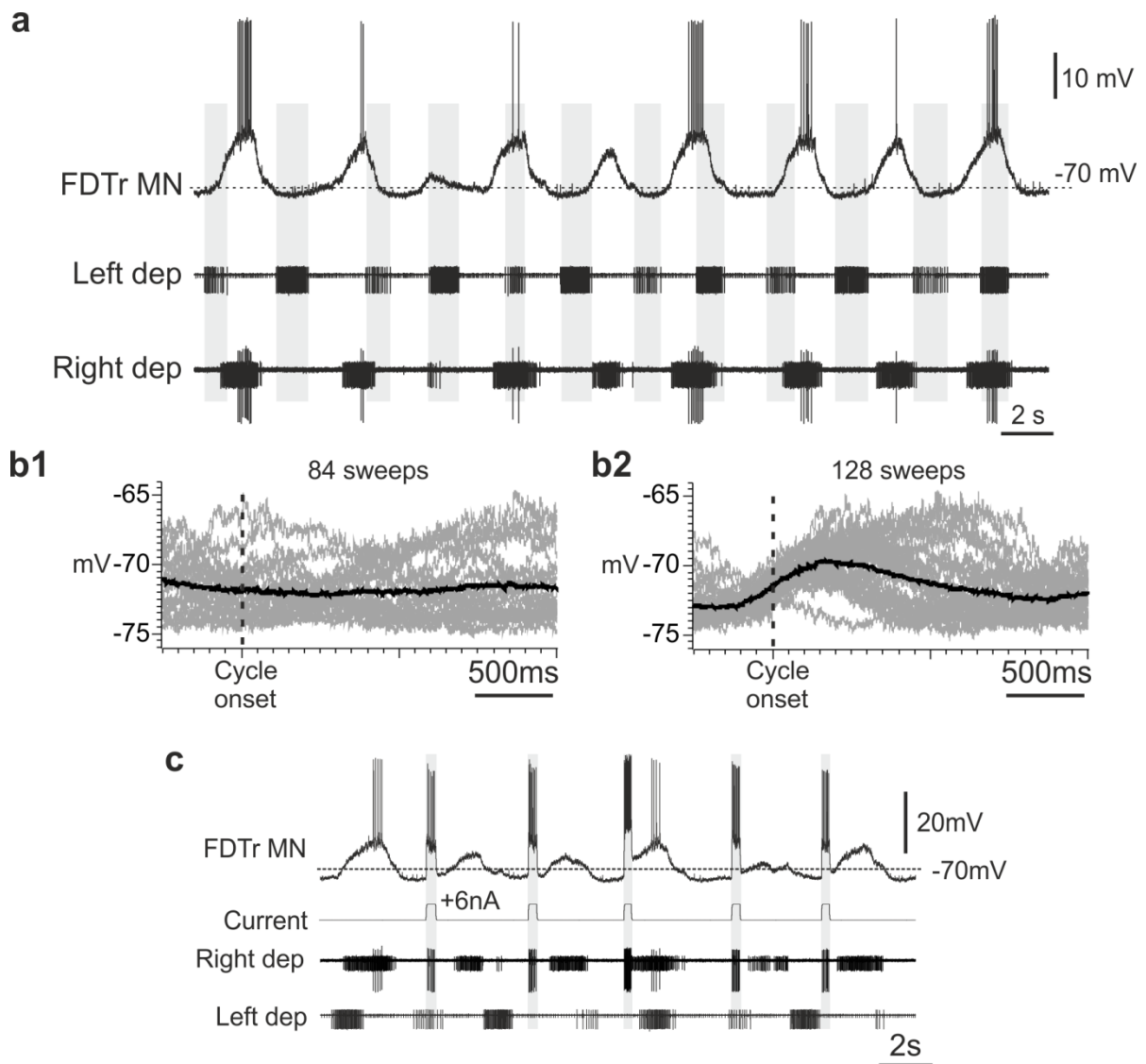


Figure 31: Intracellular recording of the fast depressor MN of the isolated mesothoracic ganglion. **a:** Activity of the fast depressor MN (FDTTr MN) was recorded with a intracellular sharp electrode from the right hemisegment and extracellular activity of contralateral depressor MN pools was monitored in the isolated mesothoracic ganglion. Rhythmic activity was induced by application of 0.1 mM pilocarpine in saline. FDTTr membrane potential is not modulated in-phase with the contralateral depressor (Left dep) burst onset (gray bars). **b1:** Overdraws of the intracellular trace (sweeps in grey) for 84 subsequent cycles, aligned according to the contralateral-left depressor cycle onset. The FDTTr was not spiking at its resting membrane potential during this analysis. The average trace (in black) shows no modulation of membrane potential in-phase with the contralateral cycle onset. **b2:** Overdraws of the intracellular trace (sweeps in grey) for 128 subsequent cycles, aligned according to the ipsilateral-right depressor cycle onset. The FDTTr was not spiking at its resting membrane potential during this analysis. The average trace (in black) shows a depolarization of membrane potential in-phase with the ipsilateral cycle onset. **c:** FDTTr does not influence contralateral depressor activity and does not entrain the contralateral rhythm, after injection of depolarizing current pulses of 6 nA.

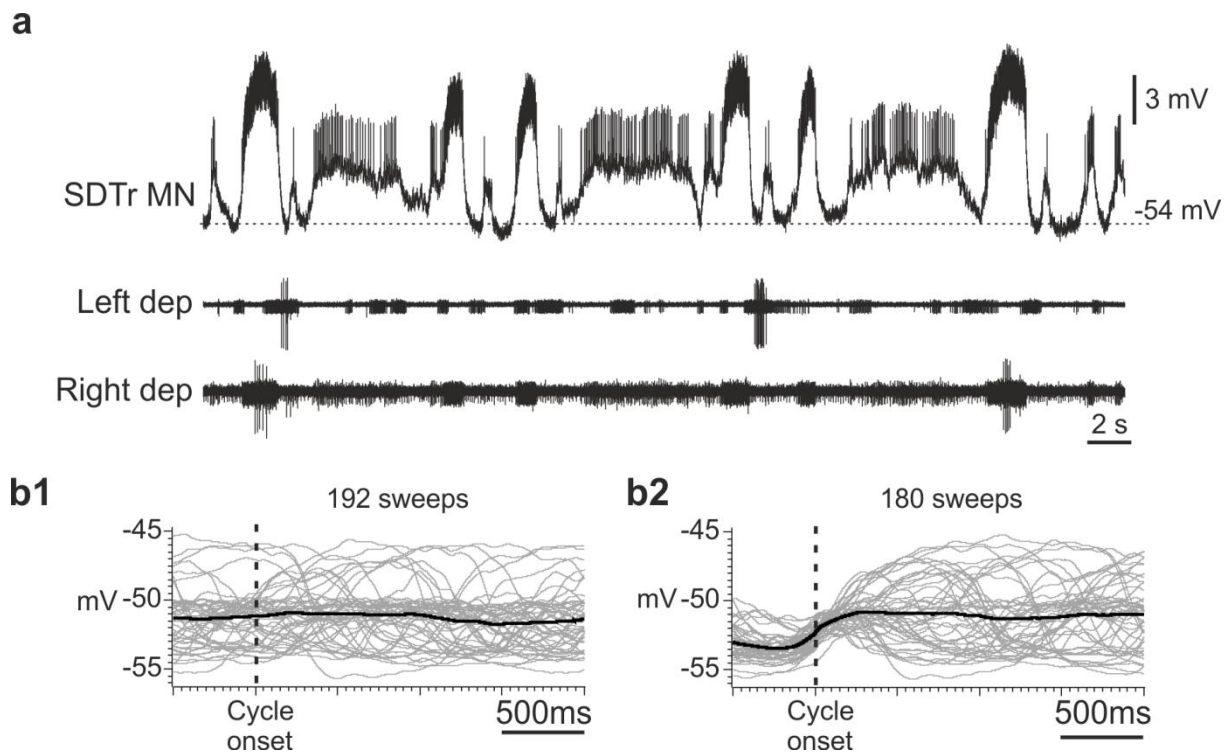


Figure 32: Intracellular recording of the slow depressor MN of the isolated mesothoracic ganglion. **a:** Activity of the slow depressor MN (SDTr MN) was recorded with a intracellular sharp electrode from the right hemisegment and extracellular activity of contralateral depressor MN pools was monitored in the isolated mesothoracic ganglion. Rhythmic activity was induced by application of 0.1 mM pilocarpine in saline. **b1:** Overdraws of the intracellular trace (sweeps in grey) for 192 subsequent cycles, aligned according to the contralateral-left depressor cycle onset. For this analysis, the SDTr waveform was filtered to cut out spikes. The average trace (in black) shows no modulation of membrane potential in-phase with the contralateral cycle onset. **b2:** Overdraws of the intracellular trace (sweeps in grey) for 180 subsequent cycles, aligned according to the ipsilateral-right depressor cycle onset. The average trace (in black) shows a depolarization of membrane potential in-phase with the ipsilateral cycle onset. For this analysis, the SDTr waveform was filtered to cut out spikes.

IV. Influence of QX 314 on motor neuron activity

Within the framework of this thesis, the intrinsic properties of MNs underlying the generation of membrane potential oscillations during rhythmic motor activity were analyzed. Calcium (Ca^{2+}) imaging of specific regions corresponding to dendritic areas of retractor MNs retrogradely filled with the Ca^{2+} indicator Oregon Green 488 BAPTA-1 dextran, resulted in Ca^{2+} oscillations after pilocarpine application in a semi-intact stick insect preparation (J. Goldammer, PhD thesis, UoC, 2013). Interestingly, Ca^{2+} transients highly correlated with MN activity and persisted in the absence of spikes, after backfilling the neurons with the non-selective blocker of voltage-activated Na^+ channels QX 314. However, the effect of QX 314 on MN membrane potential oscillations and whether they persist was not known. To test this, intracellular MN activity was recorded by means of sharp electrodes and QX314 was injected in MNs.

In a typical experiment, shown in Fig. 33, a and b, initial injection of depolarizing current pulses induced spike activity in the retractor MN, also visible in the extracellular recording trace. Based on the relatively negative resting membrane potential of -74 mV, this presumably is a fast retractor MN. Within three minutes, pilocarpine application resulted in alternating bursting between retractor and protractor MNs, and the membrane potential of the retractor MN gradually depolarized and started oscillating (Fig. 33, a). Membrane potential of retractor MNs depolarized by 5 mV in average ($N = 7$) after pilocarpine application. Within four minutes after QX 314 injection by applying 2 nA positive holding current, spikes were not generated anymore, whereas membrane potential oscillations persisted (Fig. 33, b). Interestingly, the amplitude of the oscillations slightly decreased after current injection. In seven preparations tested, injection of QX 314 caused a gradual decrease in spike amplitude and spike number, and spikes were blocked in 12 minutes on average. In control experiments, current injection of 2 to 4 nA did not affect retractor spiking for 19 minutes in average ($N = 3$). Therefore, QX 314 injection successfully blocked spike activity in retractor MNs, whereas membrane potential oscillations were apparently not affected.

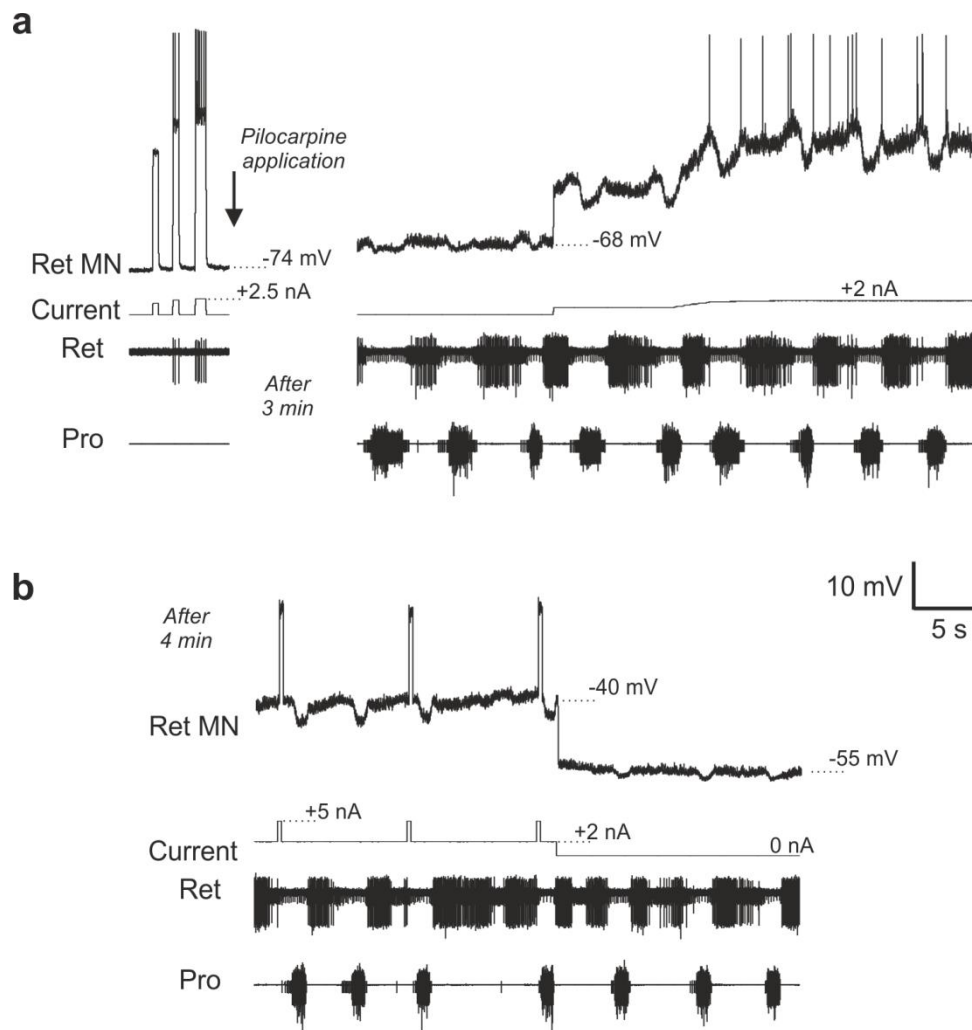


Figure 33: Effects of intracellular injection of QX 314 on retractor MN activity. a: Intracellular recording of the activity of a retractor MN (Ret MN) combined with extracellular recording of the ipsilateral retractor (Ret) and protractor (Pro) MN pool activity. Sharp electrodes were filled with QX 314, a lidocaine derivative, and rhythmic activity was induced by application of the 0.2 mM pilocarpine. Retractor MN spikes are visible upon depolarization in the extracellular recording trace Ret. Three minutes after pilocarpine application, the membrane potential of the Ret MN is depolarized and starts oscillating. Ret and Pro are active in alternation. QX 314 is released in the neuron by injecting holding current of 2 nA. **b:** The same recording as in (a) after four minutes. Spikes are blocked, as they cannot be elicited with current injection, whereas membrane potential oscillations persist. Thus, pilocarpine-evoked membrane potential oscillations in stick insect retractor MNs do not depend on voltage-gated sodium channels.

Discussion

In this thesis, the synchronization, phase coupling, and cross-correlation of activity between contralateral and ipsilateral depressor MN pools of the deafferented thoracic ganglia were investigated. These parameters were used as a proxy for the intra- and intersegmental coupling among CTr-joint CPGs driving the depressor muscle of *C. morosus*. In summary, contralateral CTr-joint CPGs showed a tendency for in-phase activity in the isolated mesothoracic ganglion (Fig. 9, a), in the isolated metathoracic ganglion a tendency for anti-phase activity (Fig. 9, b), and in the isolated prothoracic ganglion there was no evidence for coordinated cycle-to-cycle activity (Fig. 15, a1 and a2). Intrasegmental coordination was modified in the interconnected ganglia, with a higher likelihood for in-phase activity of contralateral CTr-joint CPGs in both the meso- and metathoracic ganglia (Fig. 10, a and b), and longer intervals of correlated activity between contralateral depressor MNs in the prothoracic ganglion (Fig. 18, black bars).

Moreover, intersegmental activity between ipsilateral CTr-joint CPGs in the interconnected meso- and metathoracic ganglia was coupled almost in-phase (Fig. 20, a). Intersegmental CPG coordination was modified in the interconnected meso- and metathoracic ganglia when the prothoracic ganglion was attached, as intervals of significantly correlated activity between ipsilateral depressor MNs corresponded to a lower percentage of the analyzed data (Fig. 25, grey bars). In contrast, ipsilateral depressor MN activity of the pro- and mesothoracic ganglia was slightly more correlated when all thoracic ganglia were interconnected (Fig. 25, black bars).

Furthermore, contralateral phase coupling in the isolated mesothoracic ganglion was affected after sectioning the posterior commissures (Fig. 26, d). Intra- and intersegmental CPG coordination was only partially impaired in the interconnected meso- and metathoracic ganglia when one connective was cut (Fig. 28, a, Fig. 29, and Fig. 30). Finally, intracellular depressor MNs showed no modulation correlated to the contralateral CTr-joint CPG cycle, and contralateral CPG rhythm was not affected by MN stimulation (Fig. 31 and Fig. 32).

Taken together, findings of this thesis reveal weak coupling among CTr-joint CPGs driving the depressor MN pools in an insect preparation lacking phasic sensory input. However, the centrally-generated intra- and intersegmental phase relationships between leg MN pools do not resemble those observed in muscle activity patterns of a behaving stick insect. Therefore, central CPG coupling alone is insufficient to bring about leg coordination during walking.

Results of a side-project revealed that action potentials of protractor MNs were inhibited, whereas membrane potential oscillations persisted after blocking voltage-activated Na⁺ channels, by intracellular injection of QX 314. This indicates that MN oscillations are not based on spike-related ionic mechanisms.

In the following section, the methods used in this thesis and their limitations will be discussed. The results and conclusions presented above will be reviewed in the light of both older and more recent publications, as well as in comparison to other animal preparations. In parallel, the possible implications of the results along with future prospects will be examined. Some of the issues and ideas discussed below have already been published in the discussion section of a previous publication (Mantziaris et al., 2017).

Variability in pilocarpine-induced activity and analysis of CPG coupling

According to the findings of the present thesis, pilocarpine-induced depressor MN activity in all thoracic ganglia showed non-stationary cycle period throughout the recording, thereby causing decelerations or accelerations in phase development, i.e. decrease and increase in frequency, respectively. Moreover, apart from recordings concerning the interconnected meso- and metathoracic ganglia, in which activity of contra- and ipsilateral depressor MN pools was coordinated in-phase for few consecutive cycles, patterns of coordinated MN activity were not regularly repeated throughout the recording. All the above taken into consideration, CPG-driven motor activity has apparently been highly variable.

There are many factors that could account for the observed irregularity. These factors are only partially known and largely unexplored; hence they are generally denoted as “noise”. There are many potential sources of noise in neural systems (Faisal et al., 2008). In order to function, neurons require that numerous biophysical and biochemical processes take place, such as opening and closing of membrane channels, diffusion of certain molecules (e.g. receptor agonists) and ions, binding of neurotransmitters, fusion or release of synaptic vesicles etc. Such cellular processes are based on small molecules, which are prone to thermodynamic changes. Thus, numerous stochastic processes result in random fluctuations of neural activity, therefore generating noise.

Another source of the variability observed may be related to the methods applied for the purposes of this thesis. CPG activity was assessed by recording the activity of the respective MN pools after bath-application of pilocarpine. Certain concerns have been raised as to this method of drug application with regard to pilocarpine diffusion in the ganglia and the unspecific stimulation of all mAChRs, irrespectively of their location.

Insect ganglia are equipped with a peripheral sheath, the perineurium, which consists of glial cells and functions as a diffusion barrier, similarly to the blood-brain barrier in vertebrates (Treherne and Schofield, 1981; Schofield and Treherne, 1984). In desheathed mesothoracic ganglia of the stick insect, namely ganglia whose perineurium has been mechanically or enzymatically impaired, the pilocarpine concentration that is needed to induce activity in MN pools is about ten times lower compared to that required for intact ganglia (see Materials and Methods). This suggests that pilocarpine diffusion is indeed impeded by the perineurium. There are no comparative data regarding the diffusion rate of pilocarpine in the ganglia of the stick insect. It could be that perineurium consistency differs among thoracic ganglia, resulting in variable pilocarpine diffusion rates in each ganglion and, in turn, asymmetric activation of the respective CPGs.

Furthermore, the mechanisms beneath pilocarpine actions are not completely understood. According to a review article by Trimmer (1993), presynaptic and postsynaptic

mAChRs are pharmacologically distinct and present different physiological actions in insects. On the one hand, presynaptic mAChRs are found in sensory terminals and have inhibitory action as they act against ACh release from the terminals. Postsynaptic mAChRs, on the other hand, have a depolarizing effect on MNs and interneurons (INs) (Trimmer, 1995). Particularly in the stick insect, muscarinic agonists applied to isolated MN somata did not elicit any current, suggesting that pilocarpine may act at the premotor neural networks (Oliveira et al., 2010). Finally, the preparation used here was deafferented by cutting or crushing all lateral nerves of the ganglia under investigation. However, sensory terminals, where mAChRs are presumably located, may still be functional after deafferentation. Thus, variability in pilocarpine-induced activity may also be related to unspecific stimulation of both the pre- and the postsynaptic mAChRs at the same time, due to pilocarpine bath-application.

Noise and variability in pilocarpine-induced activity has implications concerning the analysis of coupling between CPGs. Neuronal activity may be dominated by high levels of noise. Unbounded noise destroys synchronization in such a way that neither phase nor frequency coupling conditions can be fulfilled anymore (Pikovsky et al., 2001). This is exemplified here by the data concerning the isolated and interconnected prothoracic ganglion. Conversely, at low-level noise conditions, the phase difference between two oscillators fluctuates around a mean value. In this context, according to Pikovsky and colleagues (2001), it is trivial to define synchronization and coupling among CPGs as perfect entrainment between the respective oscillatory frequencies. Thus, it is essential to loosen the requirement for exact coincidence of frequencies, so that CPGs can be considered synchronized and phase-coupled when their oscillatory frequencies nearly adjust within some range of detuning (Tass et al., 1998; Pikovsky et al., 2001; Kralemann et al., 2008).

In this thesis, in recordings showing regular rhythmicity and well-defined cycle periods, it was possible to extract the phase dynamics of each activity and determine potential phase coupling, based on the phase difference distribution (Tass et al., 1998). In coupled activity, the phase difference distribution will show a peak at a certain angle, which, in the statistical sense, corresponds to the phase difference value that would be observed in the absence of

noise (Pikovsky et al. 2001, p.84). Nevertheless, this method could not be applied in highly noisy recordings of irregular activity. Therefore, spiking activity of the one trace was plotted against the activity of the other to test for recurrent patterns of activity, and cross-correlation was applied to analyze the interdependence of activity throughout the recording (See Fig. 2 and Fig. 3). Importantly, correlation of activity between two oscillators does not adequately imply synchronization and phase coupling (Tass et al., 1998), as also exemplified by Fig. 27. Conversely, activity between two phase-coupled oscillators is not necessarily strongly correlated, as the spiking dynamics may substantially differ. To conclude, weak CPG coupling could only be demonstrated with confidence in the meso- and metathoracic ganglia.

Finally, it is important here to note that investigating the mechanisms of pilocarpine actions was not within the scope of the current thesis. In fact, pilocarpine was only used here as a tool to induce oscillatory CPG activity, and indirectly assess CPG interactions by analyzing the phase and interdependence of MN activity in the free-running, unperturbed system. In the future, it would be interesting to perturb CPGs, at different phases of the oscillatory cycle, and search for modulation or synchronization of the adjacent ipsilateral or contralateral CPG motor output. This could be done externally by stimulating leg sensory organs that are known to have access on CPGs (Ludwar et al., 2005a; Akay et al., 2007; Borgmann et al., 2009) or by intracellular stimulation of INs that are known to reset centrally generated MN activity. A good candidate for such an experiment would be the non-spiking IN I4 that excites or inhibits the depressor MN pools when depolarized or hyperpolarized respectively (Büschges, 1995). Alternatively, meta-analysis of recordings that show random perturbations or gaps in the centrally-generated MN activity (Fig. 6, a), might be used to decipher whether contralateral or ipsilateral activity is consistently coupled.

Contralateral CPG coordination in isolated thoracic ganglia

Front, middle, and hind legs of *C. morosus* are apparently similar and do not show any particular specialization, unlike legs of other insects, e.g. the locust. Nevertheless, kinematics

differ among legs during straight walking and turning (Gruhn et al., 2009), and torques about homologous joints also vary across different legs (Dallmann et al., 2016). Moreover, the musculature is dissimilar among legs (Godlewska-Hammel et al., 2017). Therefore, front, middle and hind legs are functionally and morphologically distinct.

To further elaborate on this, front legs in stick insects appear to be more autonomous compared to the middle and hind legs, as they often perform additional steps or searching movements during walking on a flat surface (Cruse, 1976; Grabowska et al., 2012). Also, when they step, front legs contribute less compared to the other legs to the propulsion of the animal and support only 20% of its body weight (Dallmann et al., 2016). Moreover, front legs have been found to perform retargeting movements, according to the position of the last antennal contact on the substrate (Schütz et al., 2011). During curve-walking, front legs play a key role by pulling and pushing the animal into the turn, whereas the hind leg on the inside of the turn functions as a pivot and shows limited movement (Gruhn et al., 2009). Nevertheless, middle and hind legs are the main supporters of the animal's weight (Dallmann et al., 2016). The center of body-mass in *C. morosus* is estimated to be located between the hind-leg coxae; therefore, joint torques about the CTr joint of the hind legs are critical for the animal's propulsion (Dallmann et al., 2016). Finally, the proportion of slow muscle fibers in the retractor and depressor muscles increases from the front to the hind leg (Godlewska-Hammel et al., 2017). All the above taken into consideration, neuronal connectivity may also diverge among the front-, middle-, and hind-leg networks, to better meet the requirements pertaining to the distinct role of each leg during walking of *C. morosus*.

In line with these considerations, results in this thesis revealed that contralateral coordination varied among CPGs driving the front-, middle-, and hind-leg depressor MN pools of *C. morosus*. The flexibility and autonomy observed in the front legs of the stick insect may be related to the almost absent coordination between activity of contralateral depressor MN pools observed here, as a result of weak interaction between the underlying CPGs. In the absence of central coupling, prothoracic CPGs in the stick insect might be more sensitive to leg sensory input and descending information from the antennae. In fact, front

leg movements were found to be more strongly coordinated compared to the middle and hind legs in stick insects that were not deprived of sensory input (Cruse and Saxler, 1980; Dean, 1989). Therefore, central neural interactions may be adjusted in accordance with the afferent input, to support the special functions of the legs during behavior. In the isolated prothoracic ganglion of the hawk moth, levator MNs were in-phase coordinated with contralateral depressor MNs (Johnston and Levine, 2002), whereas in the locust, prothoracic contralateral depressor MN pools showed a tendency for in-phase activity in the isolated ganglion (Knebel et al., 2016).

In regard to the isolated meso- and metathoracic ganglia of the stick insect, contralateral CPGs driving the depressor MN pools were found to be weakly coupled, presenting a higher tendency for in- and anti-phase activity respectively. A similar tendency for in-phase activity has previously been reported concerning the contralateral protractor MN pools in the isolated mesothoracic ganglion of the stick insect (Büschges et al., 1995). In contrast to these results, in both the isolated meso- and metathoracic ganglia of the locust, pilocarpine application resulted in highly variable patterns of activity, with a tendency for anti-phase coordination between contralateral levator MN pools (Ryckebusch and Laurent, 1993, 1994). However, a recent study showed that contralateral depressor MNs were mainly active in- and anti-phase in the isolated meso- and metathoracic ganglia of the locust, respectively (Knebel et al., 2016), identically to the results of the current thesis. Thus, MN pools are active in alternation only in the isolated metathoracic ganglion.

Although it is not common, in-phase depression of contralateral legs has been observed in behaving stick insects (Wendler, 1965; Graham, 1985; Cruse and Knauth, 1989). In addition, in-phase contralateral forces were generated by two stationary middle legs that were restricted on the ground, during walking of the rest of the legs on a slippery surface (Cruse and Saxler, 1980). Hence, middle legs can move in-phase when uncoupled from the rest of the legs. The in-phase central coupling of activity observed in this thesis for the isolated mesothoracic ganglion may thus mirror leg coordination observed during behavior, when contralateral legs of one segment autonomously move in-phase. Finally,

behavioral experiments on stick insects after transection of the connectives (Dean, 1989), or upon removal of mechanical coupling between the legs, during walking on a slippery surface (Cruse and Knauth, 1989), resulted in impaired alternation of the middle legs. Therefore, central in-phase coupling may represent a default coordination pattern of the isolated mesothoracic segment, which can be modified by local and intersegmental sensory information to generate walking-relevant coordination patterns.

In contrast to the mesothoracic depressor MN pools, contralateral depressor MNs of the isolated metathoracic ganglion showed a tendency for anti-phase activity, similar to the contralateral muscle activity during walking. In line with this finding, out-of-phase contralateral forces were generated by two stationary hind legs, restricted on the ground, during walking of the rest of the legs on a slippery surface (Cruse and Saxler, 1980). Nevertheless, the exact reasons why inherent contralateral coupling in this ganglion differs when compared to coupling in the mesothoracic ganglion are not known. It could be related to the fact that this ganglion is fused with the first abdominal ganglion. Notably, in the preparation procedure followed for the purposes of this thesis, the second abdominal ganglion was also left attached to the metathoracic ganglion. Thus, intersegmental ascending information may contribute to contralateral coordination in the isolated metathoracic ganglion. However, as similar coordination was observed in the isolated metathoracic ganglion of the locust (Knebel et al., 2016), anti-phase activity is probably related to inherent connectivity of the metathoracic neural circuitry and not to the interconnection to the abdominal ganglia.

Influence of central intersegmental pathways on contralateral CPG coordination

In this thesis, activity of contralateral prothoracic depressor MN pools was correlated for a longer time throughout the recording and out-of-phase spiking patterns became evident when the prothoracic ganglion was attached to one or both of the other thoracic ganglia. Activity of contralateral depressor MN pools in both the interconnected meso- and

metathoracic ganglia was coordinated strictly in-phase. However, when the prothoracic ganglion was attached, contralateral coordination in the meso- and metathoracic ganglia was affected and activity became less correlated throughout the recording. This detrimental effect of intersegmental descending information from the prothoracic segment on contralateral coordination of posterior segments has not been reported for other insects and is a novel finding of this thesis. In the locust, contralateral depressor MN pools had a tendency for in-phase coordination in all interconnected ganglia, when pilocarpine was applied on the whole thoracic nerve cord, and for out-of-phase coordination, when pilocarpine was applied on the metathoracic ganglion only (Knebel et al., 2016). Thus, in both the stick insect and the locust, intersegmental information exchange among ganglia has an influence on intrasegmental coordination. In contrast, cutting the connectives between the interconnected pro- and pterothoracic ganglia, i.e. the fused meso- and metathoracic ganglia, only slightly affected contralateral phase relationships in the hawk moth (Johnston and Levine, 2002). Johnston and Levine concluded that intersegmental signals affect MN burst duration, resulting in increased variability after the connectives were cut, and not the phasing of the respective CPGs.

In the locust, cutting one connective between the pro- and mesothoracic ganglia impaired prothoracic activity ipsilateral to the cut, whereas activity of all other depressor MNs was not altered (Knebel et al., 2016). In contrast, information transfer through only one of the connectives is sufficient to maintain activity and contralateral coordination in the meso- and metathoracic ganglia of the stick insect (this thesis). Pilocarpine-induced activity was highly variable and did not allow for phase analysis. However, cross-correlation analysis and plotting of spiking activity revealed weak interdependence of activity between contralateral depressor MN pools in the interconnected, with a single connective, meso- and metathoracic ganglia. Interestingly, despite being weaker, contralateral middle- and hind-leg coordination during walking was maintained after cutting one of the connectives between the meso- and metathoracic ganglia of the stick insect (Dean, 1989). The same intersegmental neural pathways that affect central contralateral coordination in the deafferented ganglia may be

utilized by leg sensory organs to transmit coordinating information, thereby modifying the existing centrally-generated pattern.

Neural mechanisms underlying intrasegmental CPG coordination

In the mesothoracic ganglion of the stick insect there are six dorsal commissures (DCI to DCVI), a supramedian commissure (SMC), and three commissures that are more ventrally located (VCI, VCII and the posterior ventral commissure (PVC)) (Kittmann et al., 1991). The dorsal commissures contain large-, medium- and small size-fibers, whereas the ventral commissures contain mainly medium- and small-size fibers. Some of these fibers presumably play an important role in contralateral coordination. A total section along the midline of the mesothoracic ganglion did not affect pilocarpine-induced MN activity (Büschges et al., 1995). Midline sections performed in experiments presented here supposedly caused a lesion of commissures DCIV to DCVI, the SMC and the PVC, all located posteriorly to the midline trachea, in the caudal half of the ganglion. In accordance with Büschges and colleagues (1995), pilocarpine-induced activity was apparently not affected. However, activity of contralateral depressor MNs was not phase-coupled or correlated after lesioning the posterior commissures. Thus, coupling between autonomous CPGs in each mesothoracic hemisegment of the stick insect is impaired after partial midline section.

Similarly to the stick insect, mammals have autonomous CPGs in each hemisegment of the spinal cord. This network structure is also known as an autonomous half-center oscillator, a network that relies on mutually inhibitory connections to generate oscillatory activity. Partial lesioning along the spinal cord midline in neonatal rats had no major effect on oscillatory locomotor-like bursting activity and contralateral activity remained coupled after bath-application of pharmacological agents to activate CPGs (Kjaerulff and Kiehn, 1996). Moreover, in rat nerve cords, unilateral ventral root activity could be pharmacologically induced (Kjaerulff and Kiehn, 1997). In spinal cords of neonatal mice, stimulation of

glutamatergic networks was sufficient to independently induce flexor- and extensor-like activity in each hemisegment, pointing towards autonomous half-center organization of the underlying CPGs (Hägglund et al., 2013). Finally, contralateral coordination in rats and mice is mediated by distributed networks of both excitatory and inhibitory commissural INs (Kjaerulff and Kiehn, 1996, 1997; Talpalar et al., 2013), with the excitatory neurons being recruited at higher fictive locomotion frequencies in mice (Talpalar et al., 2013). Thus, reciprocal connections in mammals play a role in coordination rather than in rhythm generation.

In the lamprey, oscillatory motor activity could still be recorded from the ventral roots of the longitudinally-split spinal cord (Cangiano and Grillner, 2003). Interestingly, contralateral coordination between MNs innervating the fin muscles and ventral root activity persisted after partial hemisection, highlighting the importance of descending pathways in intrasegmental coordination (Mentel et al., 2008). Autonomous half-centers have also been reported for the *Xenopus* tadpole (Arshavsky Yul et al., 1993). However, in a recent study contralateral locomotor activity could not be generated in response to descending input, in a lamprey preparation after rostral midline lesion followed by spinal transection (Messina et al., 2017). In addition, rapid unilateral inhibition in the tadpole resulted in depression of reciprocal inhibition and cessation of activity on the contralateral hemisegment as well (Moult et al., 2013). In summary, in the lamprey and the tadpole, reciprocal connections not only contribute to contralateral CPG coordination, but may also be important for rhythm generation.

Invertebrates also show variability in CPG organization and contralateral organization. The swimming CPG of the sea slug *Dendronotus iris* is a special case as it consists of only two types of INs in each hemisegment (Sakurai and Katz, 2016). Heterologous, contralateral INs are electrically and synaptically connected, and homologous INs mutually inhibit their contralateral counterparts, thus comprising a twisted, interdependent half-center. Contralateral swimming CPGs in the leech also appear to function as a unit (Friesen and Hocker, 2001). In contrast, in the locust and the crayfish, alternating activity in flight MNs and

swimmeret MNs could be generated even in single, isolated hemisegments (Wolf et al., 1988; Murchison et al., 1993). Finally, the in-phase contralateral coordination between power- and return-stroke activity was retained in isolated abdominal ganglia of the crayfish (Murchison et al., 1993). Taken together, the mechanisms underlying contralateral coupling are far from being fully understood. However, it appears that there are organisms in which both the left- and right-side motor networks are necessary for activity and comprise an interdependent half-center, whereas in others the two half-centers can be autonomous.

In the swimmeret system of the crayfish, evidence supports that specific return-stroke MNs in contralateral hemisegments are electrically-coupled both with each other, as well as with their ipsilateral CPGs (Dr. Carmen Smarandache-Wellmann, personal communication). This would practically mean that MNs, could feed locomotor-relevant information back to the system of the contralateral leg, directly affecting contralateral coordination. MNs, which until recently have been considered as passive elements responsible for muscle activation, appear to have emerging properties and to play an active role in coordination and motor control. So far as that is concerned, gap junctions have been found to electrically connect MNs with the V2a INs in the spinal cord of the adult zebra fish (Song et al., 2016a). The V2a INs are excitatory and capable of the consecutive recruitment of slow, intermediate and fast MNs, therefore controlling the speed of locomotion in zebra fish (Ampatzis et al., 2014). Indeed, Song and colleagues (2016a) showed that frequency of fictive swimming was decreased when MNs were optogenetically hyperpolarized.

The present thesis suggests that in the stick insect MNs have no influence on the centrally-generated rhythm after pilocarpine application. Stimulation of a depressor MN did not entrain pilocarpine-induced depressor MN activity of the ipsi- or contralateral hemisegments, and the membrane potential of a depressor MN was not modulated in phase with the contralateral MN rhythm. Therefore, contralateral depressor MNs are connected neither directly with each other, nor with the contralateral CPG networks. In conclusion, contralateral coordination is possibly organized at the premotor level, is mediated via commissural INs, and is largely based on sensory input. In accordance with this hypothesis,

premotor non-spiking INs were found to process sensory signals from the contralateral fCO (Stein et al., 2006).

Intersegmental CPG coordination and the underlying mechanisms

In this thesis, activity in depressor MN pools, driven by CTr-joint CPGs of the interconnected meso- and metathoracic ganglia was weakly coupled almost in-phase with a mean phase lag of 10°. Intersegmental CPG coordination and MN activity became highly variable when the prothoracic ganglion was attached, and no recurrent patterns of activity could be observed. A tendency for in-phase intersegmental activity of MN pools has been reported earlier for the crayfish (Sillar et al., 1987) and the stick insect (Büschges et al., 1995). Similarly, in the thoracic ganglia chain of the locust, intersegmental depressor MN activity also tended to be in-phase (Knebel et al., 2016). However, older data have suggested coupling between ipsilateral levator and depressor MN activity in adjacent ganglia of the locust (Ryckebusch and Laurent, 1994). In the hawk moth, depressor MN pools were synchronously active in the ipsilateral front and hind leg, and the contralateral middle leg, an activity pattern that resembled the tripod coordination (Johnston and Levine, 2002). Finally, similar intersegmental coordination patterns were recorded in the interconnected meso- and metathoracic ganglia of the cockroach thoracic nerve cord with the sub-esophageal ganglion (SEG) attached to it (Fuchs et al., 2011; David et al., 2016). Thus, in thoracic ganglia of the stick insect, the locust and the crayfish, centrally-generated motor patterns revealed a weak tendency for in-phase intersegmental activity among CPGs.

The in-phase motor patterns induced by pilocarpine inevitably challenge the notion that fictive walking patterns exist in insects at all. Zill (1986), with elegant experiments on decapitated cockroaches, proposed that centrally-generated patterns in semi-intact preparations resemble righting movements, rather than walking (Zill, 1986). Generally, pilocarpine-induced activity is very irregular and patterns of coordinated motor activity, often designated as fictive walking, do not persist throughout the recording (Ryckebusch and

Laurent, 1993; Fuchs et al., 2011; David et al., 2016). The most regular and the only complete fictive walking pattern has been recorded in the thoracic nerve cord of the hawk moth and corresponds to a tripod coordination pattern (Johnston and Levine, 2002). However, such a walking pattern is hardly ever observed in hawk moths (Johnston and Levine, 1996a). In contrast, nerve cords of insects at the larvae stage show fictive locomotor patterns, which, despite being slower, correspond exactly to the crawling patterns observed in the living animals (Johnston and Levine, 1996b; Pulver et al., 2015). Thus, irrespective of whether coordination patterns recorded in deafferented insect preparations can be characterized as fictive walking or not, sensory input appears to be necessary for walking pattern generation in adult insects. To this end, the current thesis provides further evidence on the hypothesis raised by Borgmann and colleagues (2009) and extends it: Motor activity is weakly coupled because of intersegmental sensory or central input, and shows a default coordination pattern, until local sensory input operates to override this weak coordinating influence resulting in the generation of a walking-relevant motor output.

Concerning stick insects and crayfish, it has been shown that movement of adjacent legs is coupled to ensure coordination, i.e. interactions between ipsilateral legs are supposed to prevent synchronous swing movement of neighboring legs (Cruse, 1990). Nevertheless, stick insects walking on a flat surface may often walk in irregular coordination patterns, and simultaneous swing of two ipsilateral adjacent legs has been observed (Grabowska et al., 2012). Therefore, the centrally generated in-phase coordination patterns may represent the neural activity correlates of certain behavioral expressions.

According to the fifth “Cruse rule”, an increase in load on one leg, due to stumbling for instance, results in co-contraction and prolongation of the stance phase in other legs, a mechanism that efficiently distributes the load among legs (Cruse, 1990; Dürr et al., 2004). Furthermore, proprioceptive stimuli resulted in in-phase intersegmental entrainment of MN activity in both the stick insect and the crayfish semi-intact preparations (Sillar et al., 1987; Borgmann et al., 2007, 2009). In fact, Trimmer suggested that pilocarpine-elicited motor responses could be primed or activated by persistent sensory stimuli, adequately strong to

release enough ACh for mAChR activation (Trimmer, 1995). All the above taken into consideration, it may be that pilocarpine, by acting on presynaptic sensory terminals and their postsynaptic targets, mimics the effects of persistent sensory stimulation and activates the very same proprioceptive intersegmental pathways that result in the observed coordinated activity.

Nevertheless, coordinating influences from a stepping front leg had only a weak modulatory effect on the MN activity of more distal segmental and joint CPGs (Borgmann et al., 2009, 2011). Moreover, in contrast to a study by Knebel and colleagues (2017), pilocarpine application in only one ganglion did not elicit motor activity in adjacent, untreated ganglia (Ludwar et al., 2005, this thesis). Hence, central intersegmental coupling between CPGs appears to be very weak in the stick insect. Considering the contribution of local sensory input in stepping generation (Büschges et al., 2008), and in intersegmental coordination (Borgmann et al., 2009), local sensory signals from the legs essentially contribute to walking pattern generation in the stick insect. In line with this, it has been observed in both cockroaches and stick insects that unloading in one leg precedes stance onset of an ipsilateral posterior leg (Zill et al., 2009; Dallmann et al., 2017). Thus, the neural mechanisms underlying intersegmental CPG coupling in the stick insect are still not known. However, the neural mechanisms of load transfer among legs in combination with biomechanics have an emerging role in the understanding of insect locomotion.

To date, the neural mechanisms underlying intersegmental CPG coupling have been described in great detail only for the swimmeret system of the crayfish. Ascending and descending coordinating neurons (ASC and DSC) of each segmental CPG extend axons that project to all other segmental CPGs of the abdominal nerve cord (Mulloney and Smarandache-Wellmann, 2012). There they synapse onto a commissural IN (ComInt1) that integrates the excitatory synaptic potentials of the coordinating axons and transmits the signal to the local CPG. Coordination in this system is based on a gradient of synaptic strength, as coordinating axons from neighboring ganglia cause larger excitatory postsynaptic deflections of the ComInt1 membrane potential (Smarandache et al., 2009). In

the lamprey (Grillner, 2003), excitatory INs that generate locomotor activity in each segment have long axons extending towards rostral and caudal segments. The rostral segments are active at a higher rate and lead in terms of phase, thereby entraining the caudal segments. Thus, again it is an excitation gradient that underlies intersegmental coordination. In mammals (Frigon, 2017), CPGs are coupled via propriospinal neurons that make crossed projections throughout the spinal cord and are important for cervicolumbar coordination. In contrast to the lamprey, here an ascending excitatory influence from the lumbar to the cervical CPGs appears to be stronger. Finally, long descending propriospinal neurons appear to play a role in speed-dependent, contralateral coordination of the hind limbs. Thus, a distributed network of propriospinal, ascending and descending neurons controls cervicolumbar coordination and probably mediates gait transitions.

Insects generally walk forward by sequential movement of ipsilateral legs always from back to the front on each side of the body i.e. protraction of a hind leg is followed by protraction of the ipsilateral middle leg and subsequently the front leg, after which this cycle restarts. This may be paralleled by the strong ascending influence from the lumbar to the cervical spinal networks in mammals, and comes in contrast with forward swimming in the lamprey, in which anterior-to-posterior undulations are observed. In this thesis, a systematic posterior-to-anterior propagation of MN activity was not observed in the deafferented thoracic nerve cord. In contrast, a stronger descending influence was observed, as the metathoracic contralateral coordination adapted to the in-phase contralateral coordination of the mesothoracic ganglion, when the two were interconnected. Moreover, the in-phase intersegmental coordination between the meso- and metathoracic ganglia was often impaired when the prothoracic ganglion was attached. Consistently with this result, the endogenous oscillation frequency of the prothoracic MN pools was twice as high compared to the frequency in meso- and metathoracic ganglia. Therefore, it appears that neural networks of the isolated thoracic nerve cord are not sufficient to generate a gradient of excitation with anterior direction. Intriguingly, it has previously been shown that prothoracic activity was boosted and entrained by sensory input from a walking hind leg (Grabowska, 2014). This

ascending sensory influence had been predicted in advance by mathematical modeling and appears to be necessary for switching between coordination patterns in the stick insect (Daun and Tóth, 2011; Tóth and Daun-Gruhn, 2016).

Speed-dependence of intersegmental coordination patterns

Cockroaches (Blattodea), locusts (Orthoptera), and stick insects (Phasmatodea) all have a common ancestor; they all belong to the monophyletic superorder of Polyneoptera (Ishiwata et al., 2011; Misof et al., 2014; Song et al., 2016b). They diverged during evolution from other insects such as the hawk moth (Lepidoptera) and the fruit fly (Diptera). Even within Polyneoptera, there are profound differences in walking behavior. Cockroaches are adapted to fast walking on flat surfaces at speeds ranging from 1 to 20 body lengths per second (BLs^{-1}) (Bender et al., 2011), and they mostly use a stable tripod coordination pattern (Ayali et al., 2015). Although locusts' hind legs are specialized for jumping, they can walk with their legs being coordinated in a highly variable tripod pattern, and at walking speeds up to 3 BLs^{-1} (calculated according to Burns, 1973). Hawk moths walking on an inclined surface show highly variable and unclear coordination patterns (Johnston and Levine, 1996a), while fruit flies express a continuum of different coordination patterns that depend on the walking speed ranging between 2 and 16 BLs^{-1} , with a higher likelihood for a tripod pattern the higher the speed (Wosnitza et al., 2013). Finally, adult stick insects walk at speeds up to 1 BLs^{-1} on flat surfaces presenting a higher tendency for tetrapod than tripod coordination. Collectively, irrespective of their evolutionary origin, insects express different coordination patterns that appear to depend on their walking speed and enable them to efficiently move within a certain environmental niche. A walking coordination pattern resembling the tripod pattern is more likely to be observed at faster walking speeds and neurophysiological and behavioral data highlight the importance of central coupling mechanisms in fast-walking animals.

Similar differences in coordination of motor activity between fast- and slow-walking animals have also been observed in deafferented insect preparations. Centrally-generated

motor patterns of the cockroach and the hawk moth resembled the tripod walking pattern (Johnston and Levine, 2002; Knebel et al., 2016), whereas in the stick insect and locust they did not (Büschges et al., 1995; Ayali et al., 2015; Knebel et al., 2016; Mantziaris et al., 2017). Cockroaches and moths show relatively short cycle periods during walking (Johnston and Levine, 1996a; Couzin-Fuchs et al., 2015) compared to locusts and stick insects (Burns, 1973; Graham, 1985). All the above taken into consideration, there may be potential differences in the relative contribution of central and peripheral neural mechanisms of CPG coupling and coordination between slow- and fast-walking insects, i.e. coordination in slow-walking animals may be largely based on sensory input. In accordance with this premise, cockroaches have been observed to rapidly recover from leg-movement perturbations during running (Couzin-Fuchs et al., 2015). Finally, stronger CPG central coupling at high walking speeds could explain the entrainment of a leg stump and the increase in coordination strength that are both observed in fast-walking fruit flies (Berendes et al., 2016).

Motor neuron activity and the role of Ca^{2+}

In *C. morosus*, membrane potential of leg MNs upon activation shows a tonic depolarization that is shaped by phasic inhibitory and excitatory input from the CPG and sensory organs respectively (Büschges, 1998; Büschges et al., 2004; Ludwar et al., 2005b; Westmark et al., 2009). Pilocarpine-induced Ca^{2+} oscillations were recorded in dendritic areas of retractor MNs that were retrogradely filled with a Ca^{2+} -sensitive dye (Goldammer, 2013). Importantly, these Ca^{2+} oscillations strongly correlated with the activity of the backfilled MNs. To investigate, the mechanisms resulting in correlation between MN activity and $[Ca^{2+}]_i$, Goldammer (2013) retrogradely filled retractor MNs with both the Ca^{2+} -sensitive dye and the non-selective Na^+ -channel blocker QX 314, in order to impair action potential generation. Ca^{2+} oscillations were apparently not affected by QX 314, therefore suggesting that Ca^{2+} oscillations are not related to a spike-dependent mechanism. However, what could not be tested in the extracellular MN recording of those experiments is whether MN

oscillations persisted in QX 314-loaded MNs. All the above taken into consideration, in case that MN oscillations persist, this would be indirect proof of relation to Ca^{2+} oscillations. In fact, in MNs retrogradely filled with the Ca^{2+} - specific chelator BAPTA, the amplitude of the tonic depolarization was reduced by $44 \pm 21\%$, indicating that MN tonic depolarization depends on intracellular $[\text{Ca}^{2+}]_i$ (Westmark et al., 2009).

In this thesis, intracellular administration of QX 314 into retractor MNs blocked action potentials, whereas pilocarpine-induced membrane potential oscillations persisted. Thus, considering that both low- and high-voltage-activated Ca^{2+} channels have been found in insect MNs (Ryglewski et al., 2012), it may be that Ca^{2+} oscillations are based on the opening of the former rather than the latter. Nevertheless, ligand-gated channels could also play a role in $[\text{Ca}^{2+}]_i$ increase. In accordance with these results, Baden and Hedwig (2009) observed $[\text{Ca}^{2+}]_i$ elevations even during spike failure. Moreover, hyperpolarization of slow extensor MNs combined with stimulation of descending axons also resulted in increased $[\text{Ca}^{2+}]_i$, suggesting that ligand-gated channels may contribute to this (Baden and Hedwig, 2009). So far as that is concerned, Ca^{2+} imaging in dissociated MN somata of *C. morosus* revealed that about 18% of the ACh-induced current was carried by Ca^{2+} (Oliveira et al., 2010). Assuming that the same channels found in MN somata can also be expressed in dendritic areas would provide indirect evidence of a ligand-gated mechanism of Ca^{2+} entrance in the cell. Finally, the decrease in the oscillation amplitude of the membrane potential observed in recordings performed after current injection may be due to the blockage of voltage-dependent Na^+ channels by QX 314, an assumption congruent with observations concerning MNs in the lamprey (Hu et al., 2002).

References

Akay T, Bässler U, Gerharz P, Büschges A. The role of sensory signals from the insect coxa-trochanteral joint in controlling motor activity of the femur-tibia joint. *J Neurophysiol* 85: 594–604, 2001.

Akay T, Haehn S, Schmitz J, Büschges A. Signals from load sensors underlie interjoint coordination during stepping movements of the stick insect leg. *J Neurophysiol* 92: 42–51, 2004.

Akay T, Ludwar BC, Göritz ML, Schmitz J, Büschges A. Segment specificity of load signal processing depends on walking direction in the stick insect leg muscle control system. *J Neurosci* 27: 3285–94, 2007.

Alexander RM. Optimization and gaits in the locomotion of vertebrates. *Physiol Rev* 69: 1199–227, 1989.

Ampatzis K, Song J, Ausborn J, El Manira A. Separate microcircuit modules of distinct v2a interneurons and motoneurons control the speed of locomotion. *Neuron* 83: 934–43, 2014.

Arshavsky Yul, Orlovsky GN, Panchin YuV, Roberts A, Soffe SR. Neuronal control of swimming locomotion: analysis of the pteropod mollusc *Clione* and embryos of the amphibian *Xenopus*. *Trends Neurosci* 16: 227–33, 1993.

Ausborn J, Stein W, Wolf H. Frequency control of motor patterning by negative sensory feedback. *J Neurosci* 27: 9319–28, 2007.

Ayali A, Borgmann A, Büschges A, Couzin-Fuchs E, Daun-Gruhn S, Holmes P. The comparative investigation of the stick insect and cockroach models in the study of insect locomotion. *Curr Opin Insect Sci* 12: 1–10, 2015.

Baden T, Hedwig B. Dynamics of free intracellular Ca²⁺ during synaptic and spike activity of cricket tibial motoneurons. *Eur J Neurosci* 29: 1357–68, 2009.

Bässler U, Büschges A. Pattern generation for stick insect walking movements--

multisensory control of a locomotor program. *Brain Res Brain Res Rev* 27: 65–88, 1998.

Bässler U, Wegner U. Motor output of the denervated thoracic ventral nerve cord in the stick insect *Carausius morosus*. *J Exp Biol* 105: 127–145, 1983.

Beliez L, Barrière G, Bertrand SS, Cazalets J-R. Origin of thoracic spinal network activity during locomotor-like activity in the neonatal rat. *J Neurosci* 35: 6117–30, 2015.

Bender JA, Simpson EM, Tietz BR, Daltorio KA, Quinn RD, Ritzmann RE. Kinematic and behavioral evidence for a distinction between trotting and ambling gaits in the cockroach *Blaberus discoidalis*. *J Exp Biol* 214: 2057–2064, 2011.

Berendes V, Zill SN, Büschges A, Bockemühl T. Speed-dependent interplay between local pattern-generating activity and sensory signals during walking in *Drosophila*. *J Exp Biol* 219: 3781–3793, 2016.

Berens P. CircStat: A MATLAB Toolbox for Circular Statistics. *J Stat Softw* 31, 2009.

Borgmann A, Hooper SL, Büschges A. Sensory feedback induced by front-leg stepping entrains the activity of central pattern generators in caudal segments of the stick insect walking system. *J Neurosci* 29: 2972–83, 2009.

Borgmann A, Scharstein H, Büschges A. Intersegmental coordination: influence of a single walking leg on the neighboring segments in the stick insect walking system. *J Neurophysiol* 98: 1685–96, 2007.

Borgmann A, Toth TI, Gruhn M, Daun-Gruhn S, Büschges A. Dominance of local sensory signals over inter-segmental effects in a motor system: experiments. *Biol Cybern* 105: 399–411, 2011.

Brown TG. The Intrinsic Factors in the Act of Progression in the Mammal. *Proc R Soc B Biol Sci* 84: 308–319, 1911.

Burns MD. The Control of Walking in Orthoptera: I. Leg Movements in Normal Walking. *J Exp Biol* 58: 45–58, 1973.

Büschges A. Nonspiking Pathways in a Joint-control Loop of the Stick Insect *Carausius*

Morosus. *J Exp Biol* 151: 133 LP-160, 1990.

Büschges A. Role of local nonspiking interneurons in the generation of rhythmic motor activity in the stick insect. *J Neurobiol* 27: 488–512, 1995.

Büschges A. Inhibitory synaptic drive patterns motoneuronal activity in rhythmic preparations of isolated thoracic ganglia in the stick insect. *Brain Res* 783: 262–71, 1998.

Büschges A, Akay T, Gabriel JP, Schmidt J. Organizing network action for locomotion: insights from studying insect walking. *Brain Res Rev* 57: 162–71, 2008.

Büschges A, Borgmann A. Network modularity: back to the future in motor control. *Curr Biol* 23: R936-8, 2013.

Büschges A, Ludwar BC, Bucher D, Schmidt J, DiCaprio RA. Synaptic drive contributing to rhythmic activation of motoneurons in the deafferented stick insect walking system. *Eur J Neurosci* 19: 1856–1862, 2004.

Büschges A, Schmitz J, Bässler U. Rhythmic patterns in the thoracic nerve cord of the stick insect induced by pilocarpine. *J Exp Biol* 198: 435–56, 1995.

Buzsáki G, Draguhn A. Neuronal oscillations in cortical networks. *Science* 304: 1926–9, 2004.

Cangiano L, Grillner S. Fast and slow locomotor burst generation in the hemispinal cord of the lamprey. *J Neurophysiol* 89: 2931–42, 2003.

Chrachri A, Clarac F. Fictive locomotion in the fourth thoracic ganglion of the crayfish, *Procambarus clarkii*. *J Neurosci* 10: 707–19, 1990.

Connors BW, Prince DA. Effects of local anesthetic QX-314 on the membrane properties of hippocampal pyramidal neurons. *J Pharmacol Exp Ther* 220: 476 LP-481, 1982.

Couzin-Fuchs E, Kiemel T, Gal O, Ayali A, Holmes P. Intersegmental coupling and recovery from perturbations in freely running cockroaches. *J Exp Biol* 218: 285–97, 2015.

Cruse H. The function of the legs in the free walking stick insect, *Carausius morosus*. *J Comp*

Physiol ? A 112: 235–262, 1976.

Cruse H. What mechanisms coordinate leg movement in walking arthropods? *TINS* 13: 15–21, 1990.

Cruse H, Knauth A. Coupling mechanisms between the contralateral legs of a walking insect (*Carausius morosus*). *J exp Biol* 144: 199–213, 1989.

Cruse H, Saxler G. Oscillations of Force in the Standing Legs of a Walking Insect (*Carausius morosus*). *Biol Cybern* 36: 159–163, 1980.

Dallmann CJ, Dürr V, Schmitz J. Joint torques in a freely walking insect reveal distinct functions of leg joints in propulsion and posture control. *Proceedings Biol Sci* 283: 20151708, 2016.

Dallmann CJ, Hoinville T, Dürr V, Schmitz J. A load-based mechanism for inter-leg coordination in insects. *Proceedings Biol Sci* 284, 2017.

Daun S, Tóth TI. An inter-segmental network model and its use in elucidating gait-switches in the stick insect. *J Comput Neurosci* 31: 43–60, 2011.

David I, Holmes P, Ayali A. Endogenous rhythm and pattern-generating circuit interactions in cockroach motor centres. *Biol Open* 5: 1229–40, 2016.

Dean J. Leg Coordination in the Stick Insect *Carausius Morosus*: Effects of Cutting Thoracic Connectives. *J Exp Biol* 145: 103–131, 1989.

Delcomyn F. Neural basis of rhythmic behavior in animals. *Science* 210: 492–8, 1980.

Dürr V, Schmitz J, Cruse H. Behaviour-based modelling of hexapod locomotion: linking biology and technical application. *Arthropod Struct Dev* 33: 237–50, 2004.

Faisal a A, Selen LPJ, Wolpert DM. Noise in the nervous system. *Nat Rev Neurosci* 9: 292–303, 2008.

Foth E, Bässler U. Leg movements of stick insects walking with five legs on a treadmill and with one leg on a motor-driven belt. II. Leg coordination when step-frequencies differ

from leg to leg. *Biol Cybern* 51: 319–24, 1985.

Friesen WO, Hocker CG. Functional analyses of the leech swim oscillator. *J Neurophysiol* 86: 824–35, 2001.

Frigon A. The neural control of interlimb coordination during mammalian locomotion. *J Neurophysiol* 117: 2224–2241, 2017.

Fuchs E, Holmes P, David I, Ayali A. Proprioceptive feedback reinforces centrally generated stepping patterns in the cockroach. *J Exp Biol* 215: 1884–91, 2012.

Fuchs E, Holmes P, Kiemel T, Ayali A. Intersegmental coordination of cockroach locomotion: adaptive control of centrally coupled pattern generator circuits. *Front Neural Circuits* 4: 125, 2011.

Getting AP. Emerging Principles Governing the Operation of Neural Networks. *Annu Rev Neurosci* 12: 185–204, 1989.

Godlewska-Hammel E, Büschges A, Gruhn M. Fiber-type distribution in insect leg muscles parallels similarities and differences in the functional role of insect walking legs. *J Comp Physiol A Neuroethol Sens Neural Behav Physiol* 203: 773–790, 2017.

Goldammer J. Morphology of antennal hair field afferents, descending interneurons and mesothoracic motoneurons, and in situ calcium imaging of retrogradely labeled retractor coxae neurons in the stick insect. PhD Thesis, Universität zu Köln 2013.

Goldammer J, Büschges A, Schmidt J. Motoneurons, DUM cells, and sensory neurons in an insect thoracic ganglion: a tracing study in the stick insect *Carausius morosus*. *J Comp Neurol* 520: 230–57, 2012.

Grabowska M. Theoretical and experimental investigations of intra- and inter-segmental control networks and their application to locomotion of insects and crustaceans. PhD Thesis, Universität zu Köln 2014.

Grabowska M, Godlewska E, Schmidt J, Daun-Gruhn S. Quadrupedal gaits in hexapod animals - inter-leg coordination in free-walking adult stick insects. *J Exp Biol* 215: 4255–66,

2012.

Graham D. Influence of Coxa-Thorax Joint Receptors on Retractor Motor Output During Walking in *Carausius-Morosus*. *J Exp Biol* 114: 131–139, 1985.

Grillner S. The motor infrastructure: from ion channels to neuronal networks. *Nat Rev Neurosci* 4: 573–86, 2003.

Grillner S, Markram H, De Schutter E, Silberberg G, LeBeau FEN. Microcircuits in action--from CPGs to neocortex. *Trends Neurosci* 28: 525–33, 2005.

Grillner S, Zangger P. How detailed is the central pattern generation for locomotion? *Brain Res* 88: 367–71, 1975.

Grillner S, Zangger P. On the central generation of locomotion in the low spinal cat. *Exp brain Res* 34: 241–61, 1979.

Gruhn M, Zehl L, Büschges A. Straight walking and turning on a slippery surface. *J Exp Biol* 212: 194–209, 2009.

Hägglund M, Dougherty KJ, Borgius L, Itohara S, Iwasato T, Kiehn O. Optogenetic dissection reveals multiple rhythmogenic modules underlying locomotion. *Proc Natl Acad Sci U S A* 110: 11589–94, 2013.

Hess D, Büschges a. Role of proprioceptive signals from an insect femur-tibia joint in patterning motoneuronal activity of an adjacent leg joint. *J Neurophysiol* 81: 1856–65, 1999.

Hill A, Masino M, Calabrese R. Intersegmental coordination of rhythmic motor patterns. *J Neurophysiol* 90: 531–8, 2003.

Hoyt DF, Taylor CR. Gait and the energetics of locomotion in horses. *Nature* 292: 239–240, 1981.

Hu G, Biró Z, Hill RH, Grillner S. Intracellular QX-314 causes depression of membrane potential oscillations in lamprey spinal neurons during fictive locomotion. *J Neurophysiol* 87: 2676–83, 2002.

- Hughes GM.** The co-ordination of insect movements. *J Exp Biol* 29: 267–285, 1952.
- Ishiwata K, Sasaki G, Ogawa J, Miyata T, Su ZH.** Phylogenetic relationships among insect orders based on three nuclear protein-coding gene sequences. *Mol Phylogenet Evol* 58: 169–180, 2011.
- Johnston RM, Levine RB.** Locomotory behavior in the hawkmoth *Manduca sexta*: kinematic and electromyographic analyses of the thoracic legs in larvae and adults. *J Exp Biol* 199: 759–774, 1996a.
- Johnston RM, Levine RB.** Crawling motor patterns induced by pilocarpine in isolated larval nerve cords of *Manduca sexta*. *J Neurophysiol* 76: 3178–95, 1996b.
- Johnston RM, Levine RB.** Thoracic leg motoneurons in the isolated CNS of adult *Manduca* produce patterned activity in response to pilocarpine, which is distinct from that produced in larvae. *Invert Neurosci* 4: 175–92, 2002.
- Katz PS, Hooper SL.** Invertebrate Central Pattern Generators. In: *Invertebrate Neurobiology*, edited by Norrth G, Greenspan RJ. Cold Spring Harbor, New York: Cold Spring Harbor Laboratory Press, 2007.
- Kittmann R, Dean J, Schmitz J.** An atlas of the thoracic ganglia in the stick insect, *Carausius morosus*. *Phil Trans R Soc Lond B* 331: 101–121, 1991.
- Kjaerulff O, Kiehn O.** Distribution of networks generating and coordinating locomotor activity in the neonatal rat spinal cord in vitro: a lesion study. *J Neurosci* 16: 5777–94, 1996.
- Kjaerulff O, Kiehn O.** Crossed rhythmic synaptic input to motoneurons during selective activation of the contralateral spinal locomotor network. *J Neurosci* 17: 9433–47, 1997.
- Knebel D, Ayali A, Pflüger H-J, Rillich J.** Rigidity and Flexibility: The Central Basis of Inter-Leg Coordination in the Locust. *Front Neural Circuits* 10: 112, 2016.
- Kralemann B, Cimponeriu L, Rosenblum M, Pikovsky A, Mrowka R.** Phase dynamics of coupled oscillators reconstructed from data. *Phys Rev E* 77: 66205, 2008.

- Ludwar BC, Göritz ML, Schmidt J.** Intersegmental coordination of walking movements in stick insects. *J Neurophysiol* 93: 1255–65, 2005a.
- Ludwar BC, Westmark S, Büschges A, Schmidt J.** Modulation of membrane potential in mesothoracic moto- and interneurons during stick insect front-leg walking. *J Neurophysiol* 94: 2772–84, 2005b.
- Mantziaris C, Bockemühl T, Holmes P, Borgmann A, Daun S, Büschges A.** Intra- and intersegmental influences among central pattern generating networks in the walking system of the stick insect. *J Neurophysiol* 118: 2296–2310, 2017.
- Marder E.** Developmental biology: senseless motion. *Nature* 416: 131–2, 2002.
- Marder E, Bucher D.** Central pattern generators and the control of rhythmic movements. *Curr Biol* 11: R986-96, 2001.
- Marder E, Calabrese RL.** Principles of rhythmic motor pattern generation. *Physiol Rev* 76: 687–717, 1996.
- Mendes CS, Bartos I, Akay T, Márka S, Mann RS.** Quantification of gait parameters in freely walking wild type and sensory deprived *Drosophila melanogaster*. *Elife* 2: e00231, 2013.
- Mentel T, Cangiano L, Grillner S, Büschges A.** Neuronal substrates for state-dependent changes in coordination between motoneuron pools during fictive locomotion in the lamprey spinal cord. *J Neurosci* 28: 868–79, 2008.
- Messina JA, St Paul A, Hargis S, Thompson WE, McClellan AD.** Elimination of Left-Right Reciprocal Coupling in the Adult Lamprey Spinal Cord Abolishes the Generation of Locomotor Activity. *Front Neural Circuits* 11: 89, 2017.
- Misof B, Liu S, Meusemann K, Peters RS, et al. E.** Phylogenomics resolves the timing and pattern of insect evolution. *Science* (80-) 346: 763–767, 2014.
- Moult PR, Cottrell GA, Li W-C.** Fast silencing reveals a lost role for reciprocal inhibition in locomotion. *Neuron* 77: 129–40, 2013.

- Mulloney B, Smarandache-Wellmann C.** Neurobiology of the crustacean swimmeret system. *Prog Neurobiol* 96: 242–267, 2012.
- Murchison D, Chrachri A, Mulloney B.** A separate local pattern-generating circuit controls the movements of each swimmeret in crayfish. *J Neurophysiol* 70: 2620–31, 1993.
- Oliveira EE, Pippow A, Salgado VL, Büschges A, Schmidt J, Kloppenburg P.** Cholinergic currents in leg motoneurons of *Carausius morosus*. *J Neurophysiol* 103: 2770–82, 2010.
- Pearson KG.** Central programming and reflex control of walking in the cockroach. *J Exp Biol* 56: 173–193, 1972.
- Pearson KG.** Common principles of motor control in vertebrates and invertebrates. *Annu Rev Neurosci* 16: 265–97, 1993.
- Pearson KG, Iles JF.** Discharge patterns of coxal levator and depressor motoneurons of the cockroach, *Periplaneta americana*. *J Exp Biol* 52: 139–65, 1970.
- Pikovsky A, Rosenblum M, Kurths J.** *Synchronization A universal concept in nonlinear sciences*. New York: Cambridge University Press, 2001.
- Pulver SR, Bayley TG, Taylor AL, Berni J, Bate M, Hedwig B.** Imaging fictive locomotor patterns in larval *Drosophila*. *J Neurophysiol* 114: 2564–77, 2015.
- Rosenbaum P, Wosnitza A, Büschges A, Gruhn M.** Activity patterns and timing of muscle activity in the forward walking and backward walking stick insect *Carausius morosus*. *J Neurophysiol* 104: 1681–95, 2010.
- Ryckebusch S, Laurent G.** Rhythmic patterns evoked in locust leg motor neurons by the muscarinic agonist pilocarpine. *J Neurophysiol* 69: 1583–95, 1993.
- Ryckebusch S, Laurent G.** Interactions between segmental leg central pattern generators during fictive rhythms in the locust. *J Neurophysiol* 72: 2771–85, 1994.
- Ryglewski S, Lance K, Levine RB, Duch C.** Ca(v)2 channels mediate low and high voltage-

activated calcium currents in *Drosophila* motoneurons. *J Physiol* 590: 809–25, 2012.

Sadeh B, Szczepanski SM, Knight RT. Oscillations and Behavior. In: *Cognitive Electrophysiology of Attention*. Elsevier, p. 268–281.

Sakurai A, Katz PS. The central pattern generator underlying swimming in *Dendronotus* iris: a simple half-center network oscillator with a twist. *J Neurophysiol* 116: 1728–1742, 2016.

Schilling M, Hoinville T, Schmitz J, Cruse H. Walknet, a bio-inspired controller for hexapod walking. *Biol Cybern* 107: 397–419, 2013.

Schmidt J, Fischer H, Büschges A. Pattern generation for walking and searching movements of a stick insect leg. II. Control of motoneuronal activity. *J Neurophysiol* 85: 354–61, 2001.

Schmitz J, Büschges A, Delcomyn F. An improved electrode design for en passant recording from small nerves. *Comp Biochem Physiol A Comp Physiol* 91: 769–72, 1988.

Schofield PK, Treherne JE. Localization of the blood-brain barrier of an insect: Electrical model and analysis. *J Exp Biol* 109: 319–331, 1984.

Schütz C, Dürr V, Schutz C, Durr V. Active tactile exploration for adaptive locomotion in the stick insect. *Philos Trans R Soc Lond B Biol Sci* 366: 2996–3005, 2011.

Selverston AI, Moulins M. Oscillatory neural networks. *Annu Rev Physiol* 47: 29–48, 1985.

Sherrington CS. Further observations on the production of reflex stepping by combination of reflex excitation with reflex inhibition. *J Physiol* 47: 196–214, 1913.

Sillar KT, Skorupski P. Central input to primary afferent neurons in crayfish, *Pacifastacus leniusculus*, is correlated with rhythmic motor output of thoracic ganglia. *J Neurophysiol* 55: 678–88, 1986.

Sillar TK, Clarac F, Bush MB. Intersegmental Coordination of Central Neural Oscillators for Rhythmic Movements of the Walking Legs in Crayfish, *Pacifastacus Leniusculus*. *J Exp Biol* 131: 245 LP-264, 1987.

Singer W. Neuronal oscillations: unavoidable and useful? *Eur J Neurosci* 140: 874–888, 2018.

Smarandache C, Hall WM, Mulloney B. Coordination of rhythmic motor activity by gradients of synaptic strength in a neural circuit that couples modular neural oscillators. *J Neurosci* 29: 9351–60, 2009.

Smith JC, Abdala APL, Borgmann A, Rybak IA, Paton JFR. Brainstem respiratory networks: Building blocks and microcircuits. *Trends Neurosci* 36: 152–162, 2013.

Smith JC, Greer JJ, Liu GS, Feldman JL. Neural mechanisms generating respiratory pattern in mammalian brain stem-spinal cord in vitro. I. Spatiotemporal patterns of motor and medullary neuron activity. *J Neurophysiol* 64: 1149–69, 1990.

Song J, Ampatzis K, Björnfors ER, El Manira A. Motor neurons control locomotor circuit function retrogradely via gap junctions. *Nature* 529: 399–402, 2016a.

Song N, Li H, Song F, Cai W. Molecular phylogeny of Polyneoptera (Insecta) inferred from expanded mitogenomic data. *Sci Rep* 6: 36175, 2016b.

Stein PSG. Central pattern generators in the turtle spinal cord: selection among the forms of motor behaviors. *J Neurophysiol* 119: 422–440, 2018.

Stein W, Büschges A, Bässler U. Intersegmental transfer of sensory signals in the stick insect leg muscle control system. *J Neurobiol* 66: 1253–69, 2006.

Talpalar AE, Bouvier J, Borgius L, Fortin G, Pierani A, Kiehn O. Dual-mode operation of neuronal networks involved in left-right alternation. *Nature* 500: 85–8, 2013.

Tass P, Rosenblum MG, Weule J, Kurths J, Pikovsky a., Volkmann J, Schnitzler a., Freund H-J. Detection of n:m Phase Locking from Noisy Data: Application to Magnetoencephalography. *Phys Rev Lett* 81: 3291–3294, 1998.

Tóth TI, Daun-Gruhn S. A three-leg model producing tetrapod and tripod coordination patterns of ipsilateral legs in the stick insect. *J Neurophysiol* 115: 887–906, 2016.

- Treherne JE, Schofield PK.** Mechanisms of ionic homeostasis in the central nervous system of an insect. *J Exp Biol* 95: 61–73, 1981.
- Trimmer BA.** Current excitement from insect muscarinic receptors. *Trends Neurosci* 18: 104–11, 1995.
- Tuthill JC, Wilson RI.** Mechanosensation and Adaptive Motor Control in Insects. *Curr Biol* 26: R1022–R1038, 2016.
- Wendler G.** The Coordination of Walking Movements in Arthropods. *Symp Soc exp Biol* 20: 229–49, 1965.
- Westmark S, Oliveira EE, Schmidt J.** Pharmacological analysis of tonic activity in motoneurons during stick insect walking. *J Neurophysiol* 102: 1049–61, 2009.
- Whelan PJ.** Control of Locomotion in the Decerebrate Cat. @ *Pergamon Prog Neurobiol* 49: 481–515, 1996.
- Wilson DM.** Insect walking. *Annu Rev Entomol* 11: 103–22, 1966.
- Wolf H, Ronacher B, Reichert H.** Patterned synaptic drive to locust flight motoneurons after hemisection of thoracic ganglia. *J Comp Physiol A* 163: 761–769, 1988.
- Wosnitza A, Bockemühl T, Dübbert M, Scholz H, Büschges A.** Inter-leg coordination in the control of walking speed in *Drosophila*. *J Exp Biol* 216: 480–91, 2013.
- Zill SN.** A model of pattern generation of cockroach walking reconsidered. *J Neurobiol* 17: 317–28, 1986.
- Zill SN, Chaudhry S, Büschges A, Schmitz J.** Force feedback reinforces muscle synergies in insect legs. *Arthropod Struct Dev* 44: 541–53, 2015.
- Zill SN, Keller BR, Duke ER.** Sensory signals of unloading in one leg follow stance onset in another leg: transfer of load and emergent coordination in cockroach walking. *J Neurophysiol* 101: 2297–304, 2009.
- Zill SN, Neff D, Chaudhry S, Exter A, Schmitz J, Büschges A.** Effects of force detecting

sense organs on muscle synergies are correlated with their response properties. *Arthropod Struct Dev* 46: 564–578, 2017.

Acknowledgments

To my family and friends, because what I am is the reflection of their expectations. Thank you all!

I wish to express my sincere gratitude to my advisor Prof. Dr. Ansgar Büschges for the continuous support of my Ph.D. study, for his enthusiasm, motivation and immense knowledge.

Besides my advisor, I would like to thank all those who co-supervised me and helped me throughout my studies: The rest of my thesis committee, Dr. Carmen Smarandache-Wellmann and Dr. Arnd von Twickel for their insightful comments; Dr. Anke Borgmann for her support throughout the first year of my Ph.D.; Dr. Till Bockemühl for his guidance and his crucial contribution to my project; Dr. Joachim Schmidt for always answering my questions, and Dr. Matthias Gruhn for his encouragement, as well as for entrusting me the supervision of the ERG lab course; Dr. Silvia Daun, Dr. Christoph Guschlbauer, and Dr. Nicholas Szczecinski for the excellent collaboration and stimulating discussions.

Special thanks to Hans-Peter Bollhagen, Sima Seyed-Nejadi, Sherylane Seeliger, Michael Dübber, Jan Sydow and Tobias Schulze. Without their precious support it would not be possible to conduct this research.

My sincere thanks go to my fellow students of the Büschges, Wellmann and Daun groups. I am very grateful for the friendly environment I have experienced in the office thanks to Dr. Volker Berendes, Dr. Eva Berg, Dr. Jens Goldammer, Dr. Philipp Rosenbaum, Alexander Chockley, Gesa Dinges, Anna Dino, and Corinna Rosch.

The use of English in the Introduction and Discussion was edited by my dear friend Thomai Gamagari. Dr. Till Bockemühl, Dr. Katerina Vlantis, Dr. Matthias Gruhn and Hans-Peter Bollhagen also read and corrected parts of the thesis. Many thanks!

Last but not least, a very special gratitude goes out to the office assistants of the Institute for Zoology, and the coordinators of the GSfBS and RTG-NCA | GRK 1960 programs at the University of Cologne for organizing my studies and for funding.

This study was supported by the joint BMBF/NSF-CRCNS Project to A. Büschges and S. Daun (01GQ1412) entitled “Central pattern generators and reflexive feedback in insect locomotion: a cross-species study.”

Appendix

RESEARCH ARTICLE | *Control of Movement*

Intra- and intersegmental influences among central pattern generating networks in the walking system of the stick insect

Charalampos Mantziaris,¹ Till Bockemühl,¹ Philip Holmes,² Anke Borgmann,¹ Silvia Daun,^{1,3} and Ansgar Büschges¹

¹Department of Animal Physiology, Zoological Institute, Biocenter, University of Cologne, Cologne, Germany; ²Department of Mechanical and Aerospace Engineering, Program in Applied and Computational Mathematics and Princeton Neuroscience Institute, Princeton University, Princeton, New Jersey; and ³Institute of Neuroscience and Medicine (INM-3), Forschungszentrum Jülich, Jülich, Germany

Submitted 2 May 2017; accepted in final form 17 July 2017

Mantziaris C, Bockemühl T, Holmes P, Borgmann A, Daun S, Büschges A. Intra- and intersegmental influences among central pattern generating networks in the walking system of the stick insect. *J Neurophysiol* 118: 2296–2310, 2017. First published July 19, 2017; doi:10.1152/jn.00321.2017.—To efficiently move around, animals need to coordinate their limbs. Proper, context-dependent coupling among the neural networks underlying leg movement is necessary for generating intersegmental coordination. In the slow-walking stick insect, local sensory information is very important for shaping coordination. However, central coupling mechanisms among segmental central pattern generators (CPGs) may also contribute to this. Here, we analyzed the interactions between contralateral networks that drive the depressor trochanteris muscle of the legs in both isolated and interconnected deafferented thoracic ganglia of the stick insect on application of pilocarpine, a muscarinic acetylcholine receptor agonist. Our results show that depressor CPG activity is only weakly coupled between all segments. Intrasegmental phase relationships differ between the three isolated ganglia, and they are modified and stabilized when ganglia are interconnected. However, the coordination patterns that emerge do not resemble those observed during walking. Our findings are in line with recent studies and highlight the influence of sensory input on coordination in slowly walking insects. Finally, as a direct interaction between depressor CPG networks and contralateral motoneurons could not be observed, we hypothesize that coupling is based on interactions at the level of CPG interneurons.

NEW & NOTEWORTHY Maintaining functional interleg coordination is vitally important as animals locomote through changing environments. The relative importance of central mechanisms vs. sensory feedback in this process is not well understood. We analyzed coordination among the neural networks generating leg movements in stick insect preparations lacking phasic sensory feedback. Under these conditions, the networks governing different legs were only weakly coupled. In stick insect, central connections alone are thus insufficient to produce the leg coordination observed behaviorally.

motor control; locomotion; pilocarpine; coordination; phase coupling

ANIMALS MOVE VIA COORDINATED action of their trunk muscles and appendages: body segments and fins for swimming, wings

Address for reprint requests and other correspondence: A. Büschges, Dept. of Neurobiology/Animal Physiology, Biocenter, University of Cologne, Room 1.610, Zülpicher Straße 47b, 50674 Cologne, Germany (e-mail: ansгар.bueschges@uni-koeln.de).

for flying, and legs for walking. Irrespective of the mode of locomotion, underlying rhythmic motor activity is generated by specialized neural networks located anatomically close to the muscles they control (for overview, see Orlovsky et al. 1999). Central pattern generators (CPGs), neural circuits that can generate rhythmic motor activity in the absence of phasic input, are core elements of these networks (Katz and Hooper 2007; Marder and Bucher 2001; Marder and Calabrese 1996; Smith et al. 2013). Proper intra- and intersegmental coupling between CPGs is essential for limb coordination and adaptive motor control.

Insects generate different interleg coordination patterns during walking, depending on their behavioral task and locomotion speed (Bender et al. 2011; Cruse 1990; Grabowska et al. 2012; Mendes et al. 2013; Wendler 1964; Wosnitza et al. 2013). The number of legs simultaneously in swing phase increases with walking speed, allowing insects to express a continuum of walking patterns ranging from “wave gait” at low speeds (Graham 1985; Hughes 1952; Wosnitza et al. 2013) to tetrapod and tripod coordination patterns at higher speeds (Berendes et al. 2016; Hughes 1952; Mendes et al. 2013; Wilson 1966; Wosnitza et al. 2013). Thus there is great flexibility in intersegmental phase relationships between oscillatory neural networks that control leg movement, and these phase relationships vary between high and low walking speeds. However, information on the underlying mechanisms and the relative contribution of central and peripheral signaling in CPG coupling and interlimb coordination in insects remains highly elusive.

To induce centrally generated fictive motor activity in insects, the muscarinic acetylcholine receptor agonist pilocarpine has been commonly applied to deafferented invertebrate nerve cord preparations. Pharmacologically induced motor activity in the locust (Ryckebusch and Laurent 1993, 1994), the hawk moth (Johnston and Levine 2002), and the cockroach (Fuchs et al. 2011, 2012) have revealed approximately constant phase relationships between motor outputs of different segmental CPGs that closely resemble those observed in a tripod coordination pattern. In line with these studies, David et al. (2016) have recently proposed a connectivity model that attempts to account for this fictive tripod-like coordination, thereby em-

phasizing the importance of central connectivity in coordination. In contrast, a recent study reported a tendency for in-phase activity between homologous motoneuron (MN) pools in the isolated and deafferented thoracic nerve cord of the locust (Knebel et al. 2017). This activity pattern did not resemble any of the known walking interleg coordination patterns in insects. Some indications for in-phase intersegmental coordination between homologous MNs have been published for the stick insect as well (Büschges et al. 1995). This discrepancy between species highlights potential differences in intersegmental information transfer between CPGs in the walking system of fast- and slow-walking animals and indicates the need to unravel the role of central connections in interleg coordination.

In the present study, we used the stick insect *Carausius morosus*, an exceptional animal model to study coordination as it is a nocturnal, slow-walking insect that inhabits highly variable environments, shows only minor functional differences between legs, and its locomotor behavior has been thoroughly investigated (Cruse 1990; Grabowska et al. 2012; Graham 1985; Wendler 1966). Its central nervous system (CNS) shares neuroanatomical and morphological characteristics with other invertebrate and vertebrate CNSs (Smarandache-Wellmann 2016). The MN pools driving the muscles of each leg joint are independently controlled by individual CPGs, located in the respective hemisegment of the ventral thoracic nerve cord (Bässler and Wegner 1983; Büschges et al. 1995). The mechanisms underlying the neural control of single-leg stepping in the stick insect have been extensively studied (Bässler and Wegner 1983; Büschges et al. 2008; Graham 1985), and the role of sensory feedback signals in intersegmental coordination has been well established (Borgmann et al. 2007, 2009; Cruse 1990; Cruse and Knauth 1989). However, the potential role of central neural interactions in interleg coordination during walking and the underlying neural mechanisms have never been addressed.

For the first time here, we applied a comprehensive phase analysis of pharmacologically induced, long-term rhythmicity in the stick insect. We show that, in the absence of sensory input, segmental CPGs controlling the movement of homologous muscles of the stick insect are only weakly phase coupled. We report intersegmental phase relationships that cannot account for the generation of any of the known interleg coordination patterns observed in the stick insect. Furthermore, we found no direct influence of CPGs on contralateral MN activity that would account for the weak interactions we observed. Thus we conclude that the weak central CPG interactions observed in the stick insect may add to the flexibility these animals need for interleg coordination when they move through their heterogeneous natural habitat.

MATERIALS AND METHODS

Animals

We used adult female stick insects of the species *Carausius morosus*. The animals were bred in-house in our colony and maintained at 22–24°C at ~60% humidity and under a 12:12-h light-dark cycle. The following experimental procedures comply with the German National and State Regulations for Animal Welfare and Animal Experiments.

Preparation

The experimental setup was based on established procedures (Büschges et al. 1995). CPG activity was assessed by recording rhythmic MN activity in the isolated and deafferented thoracic nerve cord after bath application of 5–7 mM of pilocarpine (Büschges et al. 1995). This concentration ensured activation and stable rhythmicity of MN pools in all segmental ganglia, a prerequisite for the subsequent analysis (Büschges et al. 1995). CPG coordination was analyzed within each deafferented thoracic ganglion (intra-segmental) while isolated (connective nerves were cut anteriorly and posteriorly to the ganglion) or connected to other thoracic ganglia of the isolated and deafferented thoracic nerve cord. To prevent peripheral sensory input from influencing the motor activity, we either pinched or cut all lateral nerves at the ganglia of interest.

Electrophysiological Recordings

Previous investigations (Büschges 1995; Büschges et al. 1995) have shown that pilocarpine-induced rhythmic activity in levator and depressor trochanteris MN pools consistently alternates, thus allowing us to monitor rhythmicity in these MN pools by exclusively recording and analyzing the activity of the depressor MNs. We focused on the coxa-trochanter (CTr) joint, because the activity of the muscles controlling movement of the CTr joint defines the stance and swing phases of each leg's stepping cycle, irrespective of the walking direction and orientation of locomotion (Rosenbaum et al. 2010). Moreover, there are only two excitatory MNs innervating the depressor trochanteris muscle in each hemisegment, a slow (SDTr) and a fast (FDTr) MN, a fact that increased the accuracy of our analysis. Lastly, there is a plethora of publications focusing on MN and muscle activity with regards to the same joint in other preparations (Johnston and Levine 2002; Knebel et al. 2017; Ryckebusch and Laurent 1994).

To record depressor MN activity, extracellular hook electrodes (Schmitz et al. 1988) were placed on the lateral nerve C2 of the *nervus cruris* (Graham 1985), which carries the axons that innervate the depressor trochanteris muscle (Bässler and Wegner 1983; Goldammer et al. 2012). Signals were preamplified by an isolated low-noise preamplifier (100-fold; model PA101; Electronics workshop, Zoological Institute, University of Cologne). The signal was further amplified 10-fold and high- and low-pass filtered (high pass: 200 Hz, low pass: 3 kHz) using a standard four-channel amplifier/signal conditioner (model MA102, Electronics workshop, Zoological Institute, University of Cologne). The signal was digitized and recorded at a sampling rate of 12 kHz, using the Micro 1401-3 analog-to-digital converter (Cambridge Electronic Design, Cambridge, UK) and Spike2 software (Cambridge Electronic Design).

Intracellular recordings were performed according to established procedures (Büschges 1998) in bridge mode (intracellular amplifier SEC-10L, NPI Electronic, Tamm, Germany) using electrodes with resistances ranging from 15 to 35 M Ω . Glass microfilaments were pulled using a Sutter Micropuller (P-1000, Sutter Instruments, Novato, CA) and filled with 3 M KAc/0.1 M KCl or 5% neurobiotin in 3 M KAc/0.1 M KCl.

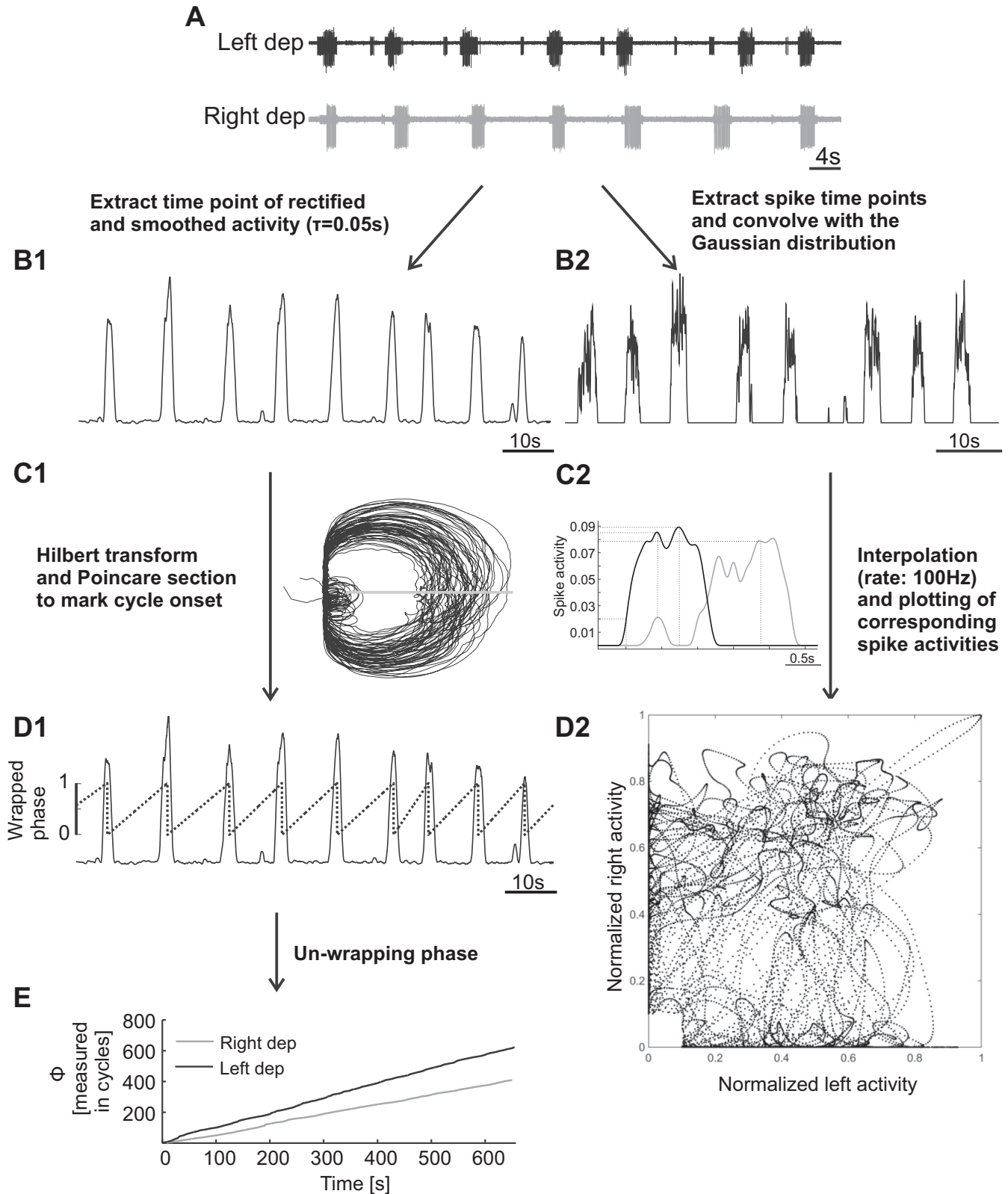
Data Analysis

Phase analysis of rhythmic activity in the meso- and metathoracic ganglia. To investigate potential interactions between meso- and metathoracic CPGs that drive the trochanteral MN pools in the absence of sensory input, we chose and adapted time series analysis methods widely used in electrodiagnostic medicine and functional neuroimaging techniques to suit our requirements for analyzing non-stationary extracellularly recorded rhythmic motor activity (Kralemann et al. 2008; Pikovsky et al. 2001; Tass et al. 1998).

A representative recording of contralateral depressor nerve activity in the isolated mesothoracic ganglion after application of 5 mM

pilocarpine serves to demonstrate the method used (Fig. 1A). First, we removed direct current offset and then rectified and smoothed each extracellular waveform signal with a time constant of 0.05 s (Fig. 1B1). Then waveforms were resampled to a rate of 100 Hz, and data were extracted as a time series. The real data sequence was then transformed to a discrete-time analytic signal according to the formula

$x = xr + i \times xi$ (xr is the real part corresponding to the original data, and xi is the imaginary part containing the Hilbert transform). The resulting signal (Fig. 1C1) has the same amplitude and frequency content as the original sequence and includes phase information that depends on the phase of the original data. The Poincaré section (Fig. 1C1, shaded horizontal line) was used to mark cycle onsets and



determine the instantaneous, wrapped phase, increasing from 0 to 1 for each cycle (Fig. 1D1). Finally, we unwrapped the phase and let it continuously grow from one cycle to the next (cumulative phase), and we plotted this infinite phase over the recording time (Fig. 1E, shaded curve). In parallel, all of the above steps were applied for the contralateral nerve recording, and its infinite phase development was also plotted (Fig. 1E, solid curve). Subtracting the two curves yields the phase difference of the two rhythms (see Fig. 2B2). Furthermore, we calculated the phase difference between the two rhythmic signals and plotted the angle distribution on the unit circle. For this, the rhythmic activity that had more cycles was used as a reference, and the relative phase of the cycle onset of the contralateral nerve rhythm was calculated throughout the recording. The angles extracted were binned, and the number of events in each bin was normalized to the sum of the events. We also calculated the percentage of the cycles showing a phase difference within the interval $0 \pm 45^\circ$ or $180 \pm 45^\circ$, as an indicator of the tendency for in- and antiphase activity, respectively.

Synchronization analysis of contralateral rhythmic motor activity in the prothoracic ganglion. In the isolated prothoracic ganglion, pilocarpine-induced motor activity was more variable than in the two other thoracic ganglia. It often consisted of periods of regular bursting in both depressor MNs (i.e., the SDTr and the FDTr). These periods intermingled with intervals of long SDTr bursts. The discrete analytic signal did not show clear loops. Consequently, the Poincaré section often resulted in errors such as double cycle onsets, rendering the determination of cycle onset unreliable. Thus the aforementioned phase analysis method could not be applied.

To investigate synchronization between contralateral networks in the prothoracic ganglion, we followed a different approach. We first marked all spike events in the recordings and extracted the corresponding time series at a sample rate of 1,000 Hz. Then data were smoothed by convolving the spike time series with a Gaussian function (Fig. 1B2). Lastly, we resampled both resultant time series to 100 Hz (Fig. 1C2) and plotted the normalized activity of each data trace against the other (Fig. 1D2). In case of synchronous activity, spike events will occur at a similar time, and high normalized activity in one recording trace will correspond to high activity in the other (Fig. 1D2; data points clustered at the center of the plot). Conversely, out-of-phase events will result in data accumulation along the axes (Fig. 1D2, data points close to the x - and y -axes of the plot). Completely random data corresponding to uncoordinated nerve activity are expected to cluster around the origin. Lastly, we binned our data in a 15×15 grid and generated two-dimensional probability distributions (see Figs. 6 and 7 in RESULTS). To increase contrast, we excluded from the analysis all data that correspond to single or double spikes with normalized activity up to 0.1 and result from noise in the nervous system. For the same reason, the map scale was adjusted and applies to all figures (it is therefore shown only once on Fig. 6B2).

Statistical Analysis

We used the MATLAB toolbox CircStat (Berens 2009) for statistical analysis of circular data. We calculated the mean phase difference with 95% confidence interval (CI) estimation for the population and the angular deviation from the mean direction. To measure the

spread around the mean, we estimated the resultant vector length (r -vector). Circular uniformity was tested using the “omnibus test” (circ_ostest function, CircStat toolbox). Finally, we used a test similar to the one-sample t -test on a linear scale (circ_mtest function, CircStat toolbox) to examine whether the mean angle of our data is equal to a specified direction.

RESULTS

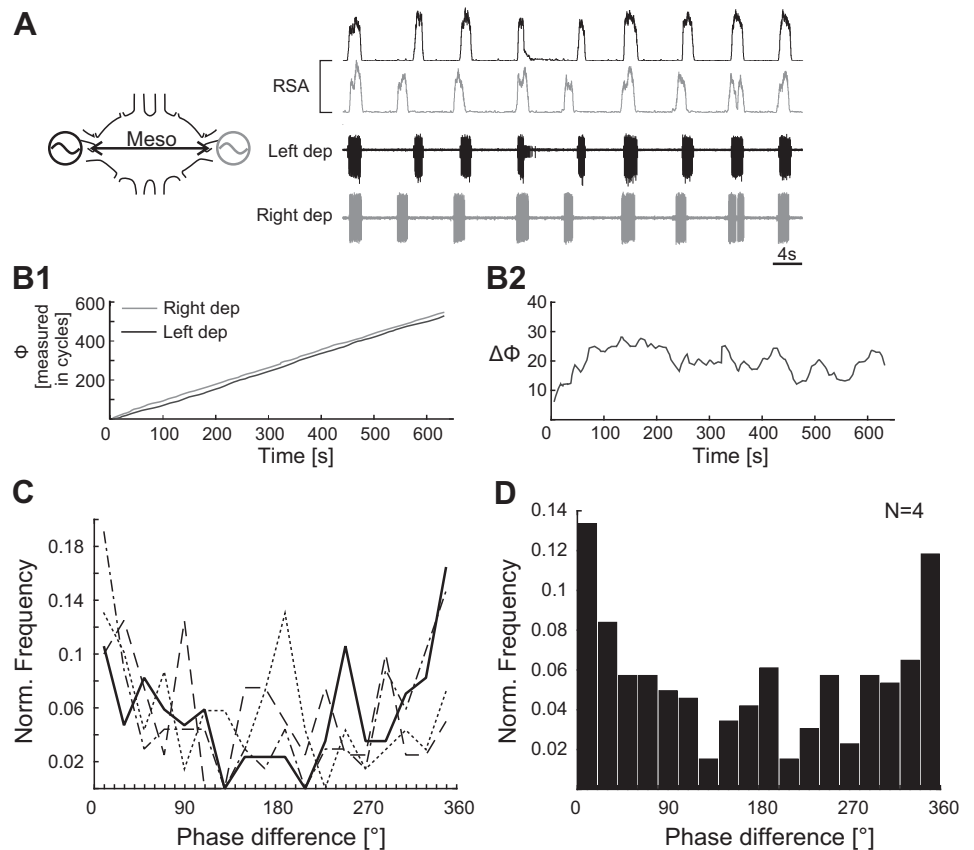
Coordination Between Contralateral Depressor Activity in the Isolated Mesothoracic Ganglion

To determine whether depressor MN pools on both sides of the mesothoracic segment are centrally coupled, we analyzed the coordination between rhythmically active depressor MNs ($N = 4$). For this, we recorded depressor MN activity from both sides of the completely isolated and deafferented mesothoracic ganglion following pilocarpine application. We calculated the mean cycle period of each depressor rhythmic activity, and the average mean cycle period of the four preparations was 4.6 ± 1.4 s. As reported previously for MN pools of the thoraco-coxal joint (Büschges et al. 1995), we did not observe systematic cycle-to-cycle coupling between left and right depressor MN activity. However, we detected periods in which bursting activity appeared to be almost synchronous (Fig. 2A, solid and shaded traces). To systematically analyze the relationship between rhythmic motor activity on both sides of the mesothoracic ganglion and its development over time, we first plotted the infinite phase of each motor nerve trace individually (Fig. 2B1). This phase analysis demonstrated an almost linear phase increase and parallel phase development for both depressor MNs, as indicated by the slopes of the two phase curves. Stable relationships between the frequencies of the two rhythms would be a prerequisite for synchronization. To test whether any frequency locking existed, we then computed the instantaneous frequency of each MN trace. The overall frequency ratio was irregular and fluctuated close to 1, suggesting that the frequencies were similar (data not shown). The activity of the two depressor MN pools retained a nearly constant phase difference with each other, as was also exemplified by the unsteady phase difference curve (Fig. 2B2). The above results are indicative of weak coupling between contralateral depressor MNs.

Nevertheless, the overall phase difference distribution, calculated throughout >600 s of recording, showed distinct peaks (Fig. 2C, solid line). The data showed statistically significant deviation from circular uniformity ($P < 0.001$). The mean direction was 352° (95% CI: 328 to 15°) with an angular deviation of 64.5° and an r -vector of 0.37. In this recording, about one-half of the cycles (48%) showed a phase difference within the interval of 315 to 45° ($0 \pm 45^\circ$). These values are indicative of synchronized activity and suggest weak in-phase

Fig. 1. Two methods for the analysis of synchronization between contralateral depressor MN activities. *A*: extracellular recording of contralateral mesothoracic C2 nerves innervating the left and right depressor (dep) muscles of the stick insect. Rhythmic activity was induced by application of 5 mM pilocarpine in saline. *B1*: each recording trace (only one is shown here) was rectified and smoothed with a time constant (τ) of 0.05 s. *C1*: each trace was resampled at a rate of 100 Hz and underwent Hilbert transform to automatically mark cycle onsets using the Poincaré section and estimate the wrapped phase. *D1*: wrapped phase defined on the circle from 0 to 1. *E*: infinite (cumulative) phase (Φ) of each nerve. *B2*: time series of spike events were extracted at a sampling rate of 1,000 Hz, and data were smoothed after convolution with the Gaussian distribution (only one trace is shown). *C2*: contralateral spike activity was compared after applying interpolation to introduce corresponding values every 10 ms in both time series. In asynchronous bursting, high-spike activity in one nerve corresponds to low activity in the contralateral nerve. *D2*: plot of the normalized spike activity of each data trace against activity of the other. Synchronous activity results in data points close to the center of the plot. Asynchronous spike events result in data points close to the x - and y -axes of the plot.

Fig. 2. Phase analysis of the isolated mesothoracic (Meso) ganglion. **A**: extracellular recording of left (solid trace) and right (shaded trace) depressor (dep) MN activity in the isolated Meso ganglion. Rhythmic activity was induced by application of 5 mM pilocarpine in saline. Rectified and smoothed activity (RSA) allows direct comparison. **B1**: the infinite phase (Φ) of each nerve is plotted throughout the recording. Activity of contralateral MNs is not systematically coupled. **B2**: phase difference ($\Delta\Phi$) time course throughout the recording. **C**: overall $\Delta\Phi$ distributions for four different animal preparations plotted on top of each other. They show a tendency for in-phase activity. The solid line corresponds to the preparation analyzed in previous subfigures. **D**: normalized and pooled data from four different animal preparations show a clear peak at the start of the cycle. *N*, no. of animal preparations.



coupling between the underlying networks driving the depressor MNs on either side of the mesothoracic ganglion. Results obtained from three further preparations were consistent with these observations, showing distinct peaks around 0° (Fig. 2C, dashed lines). The statistical hypothesis for mean direction toward 0° could not be rejected in any preparation, implying that all distributions showed mean angles equal to 0° . The phase difference distribution after pooling the data from all four animals, corresponding to a total recording time of $\sim 2,400$ s, showed a preferred direction ($P < 0.001$) with a mean angle of 5° (95% CI: 347 to 22°) and a 69° angular deviation (Fig. 2D). The r-vector length was 0.28. However, only 44% of the cycles showed phase relationships of $0 \pm 45^\circ$, indicating that interactions between contralateral networks driving the depressor MNs are weak and allow for other phase relationships to develop as well (i.e., peaks at various angles in phase distributions). Taken together, these observations suggest that the CPGs generating rhythmic activity in depressor MNs on the left and right side of the isolated and deafferented mesothoracic ganglion are weakly coupled and show a tendency for in-phase relationship with each other.

Coordination Between Contralateral Depressor MN Activity in the Isolated Metathoracic Ganglion

Next, we applied the same approach to analyze the phase relationships between contralateral rhythmically active depressor MNs in the isolated metathoracic ganglion ($N = 4$). The mean of the mean cycle periods was 4.9 ± 1.37 s. Similar to the situation in the mesothoracic ganglion, we did not observe systematic cycle-to-cycle coupling between rhythmic activity in depressor MNs on either side of the metathoracic ganglion.

However, unlike the isolated mesothoracic ganglion preparation, contralateral depressor MN bursts in the isolated metathoracic ganglion were found to be antiphase for many cycles (Fig. 3A). Infinite phases of the two rhythmically active metathoracic depressor MN pools also developed linearly (Fig. 3B1). The corresponding phase curves had different slopes, indicating different phase development for each of the two MN rhythms. Although variable, their frequency ratio fluctuated around 1. This indicated similar, but not systematically coupled, frequencies (data not shown). Moreover, the phase difference between left and right depressor rhythms continuously shifted throughout the recording, showing only few and short intervals during which the two rhythms nearly retained a constant phase relationship (Fig. 3B2). This suggests that there is no strong and systematic coupling between the two sides. The phase distribution calculated for a 615-s recording period (Fig. 3C, solid line) highlighted a slight tendency for antiphase activity with a mean angle of 165° (95% CI: 138 to 192°), angular deviation of 66° , and r-vector length of 0.34. Here, 43% of the cycles had a phase difference of $180 \pm 45^\circ$. This distribution was the only one of the four that significantly deviated from the uniform distribution ($P < 0.001$). However, two other preparations also showed a tendency for out-of-phase activity between contralateral depressors (Fig. 3C, solid and dash-dotted lines). For all distributions, the statistical hypothesis for mean direction toward 180° could not be rejected. A clear phase preference close to the start of the cycle was observed in one preparation (Fig. 3C). Pooled data ($\sim 2,500$ s of total recording time) resulted in a more uniform phase difference distribution than that of the isolated mesothoracic ganglion, as indicated by the higher P value ($0.001 < P < 0.01$),

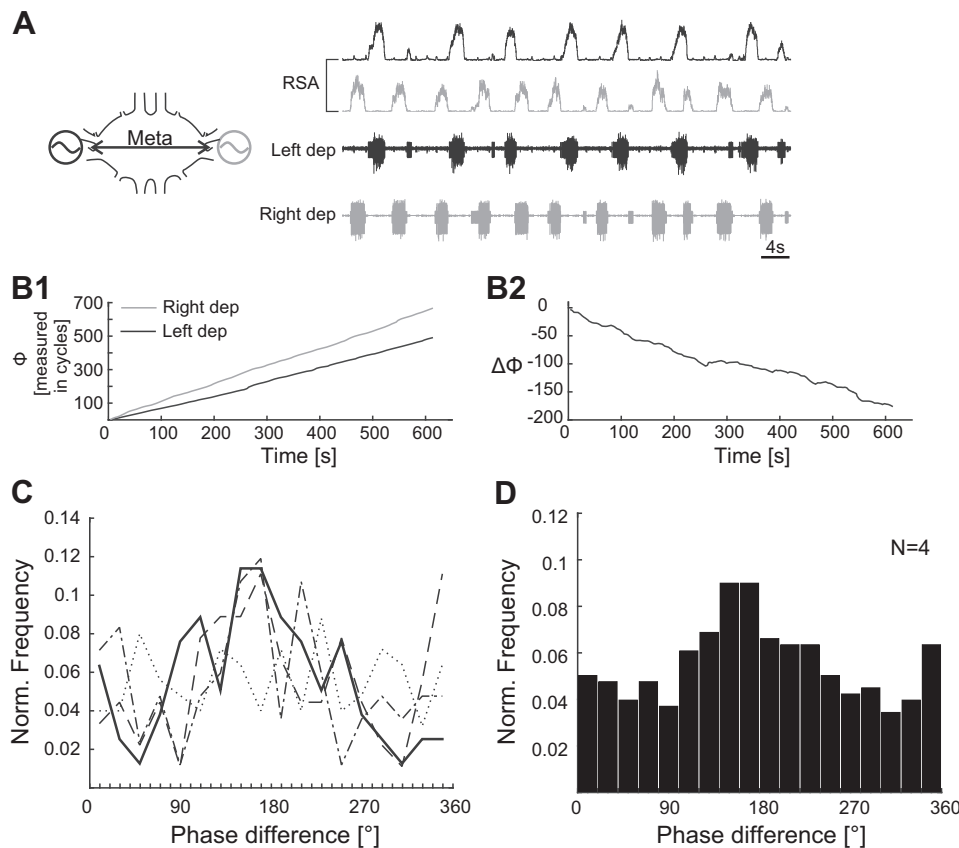


Fig. 3. Phase analysis of the isolated metathoracic (Meta) ganglion. *A*: extracellular recording of left (solid trace) and right (shaded trace) depressor (dep) MN activity in the isolated Meta ganglion. Rhythmic activity was induced by application of 5 mM pilocarpine in saline. Rectified and smoothed activity (RSA) allows direct comparison. *B1*: the infinite phase (Φ) of each nerve is plotted throughout the recording. Activity of contralateral MNs is not systematically coupled. *B2*: phase difference ($\Delta\Phi$) time course throughout the recording. *C*: overall $\Delta\Phi$ distributions for four different animal preparations plotted on top of each other. They show a tendency for out-of-phase activity. The solid line corresponds to the preparation analyzed in previous subfigures. *D*: normalized and pooled data from four different animal preparations shows a smooth peak at around 180° . *N*, no. of animal preparations.

with a mean direction of 166° (95% CI: 137.5 to 195°), 75° deviation, and an *r*-vector of 0.15 (Fig. 3*D*). Only 33% of the cycles of the pooled data showed clear antiphase activity, with phase differences between 135 and 225° ($180 \pm 45^\circ$).

Thus consistent with our results from the mesothoracic ganglion, weak coupling exists between rhythmic depressor MN activity on both sides of the isolated and deafferented metathoracic ganglion. However, phase relationships vary between preparations and do not consistently show a distinct direction, although a slight tendency for antiphase activity is present.

Intrasegmental Coordination of Depressor Activity Is Influenced by Intersegmental Signals

Next, we studied the influence of potential intersegmental signaling on left-right coordination in the meso- and metathoracic ganglia. To do this, we extracellularly recorded pilocarpine-induced activity in contralateral depressor MNs of the interconnected meso- and metathoracic ganglia, and we analyzed the phase relationships between contralateral CPG outputs. Interestingly, we observed a striking change in rhythmic activity in both ganglia, namely synchronous, in-phase bursting activity of all depressors for many consecutive cycles (Fig. 4*A*). This change is best exemplified by comparing Figs. 3*A* and 4*A*. Although these intervals of simultaneous bursting were often interrupted by gaps in activity or double bursts, coordination recovered within a few cycles (see asterisks in Fig. 4*A*). This indicates the existence of an underlying mechanism that induces weak coupling between depressor MNs in the meso- and metathoracic ganglia.

In the mesothoracic ganglion, phase analysis of the observed rhythmicity revealed long intervals during which the frequencies of contralateral CTr-joint CPGs were similar (data not shown). During such intervals, rhythmic activity was coupled and retained a constant phase difference between contralateral sides for >200 s (Fig. 4*B1*). Notably, such long periods of coupled activity have never been detected in isolated ganglia. The same holds for the metathoracic ganglion, although rhythmic activity on both contralateral sides was more variable, and intervals of coupled activity were shorter in duration compared with those of the interconnected mesothoracic ganglion (Fig. 4*B2*). These results suggest that intersegmental signals between both thoracic segments can increase contralateral coupling between depressor MNs in both ganglia and influence contralateral phase relationships.

We also calculated the overall phase difference distribution between contralateral depressor rhythms of both ganglia. All distributions of the mesothoracic ganglion ($N = 7$) and 8/10 metathoracic preparations significantly deviated from the null hypothesis of uniformity at the 95% level at least. They all showed clear peaks at or close to 0° (Fig. 4, *C1* and *C2*). Contralateral depressor rhythms in the interconnected mesothoracic ganglion recording shown in Fig. 4 had a mean phase difference of 0° (95% CI: 353 to 8°), an angular deviation of 34° , and an *r*-vector length of 0.83 . Contralateral depressor rhythms in the interconnected metathoracic ganglion had a mean phase difference of 23° (95% CI: 7.5 to 39°), with a deviation of 61° and an *r*-vector length of 0.44 . Pooled data extracted from 3,588 s of recording time showed that contralateral depressor MNs of the mesothoracic ganglion were strictly

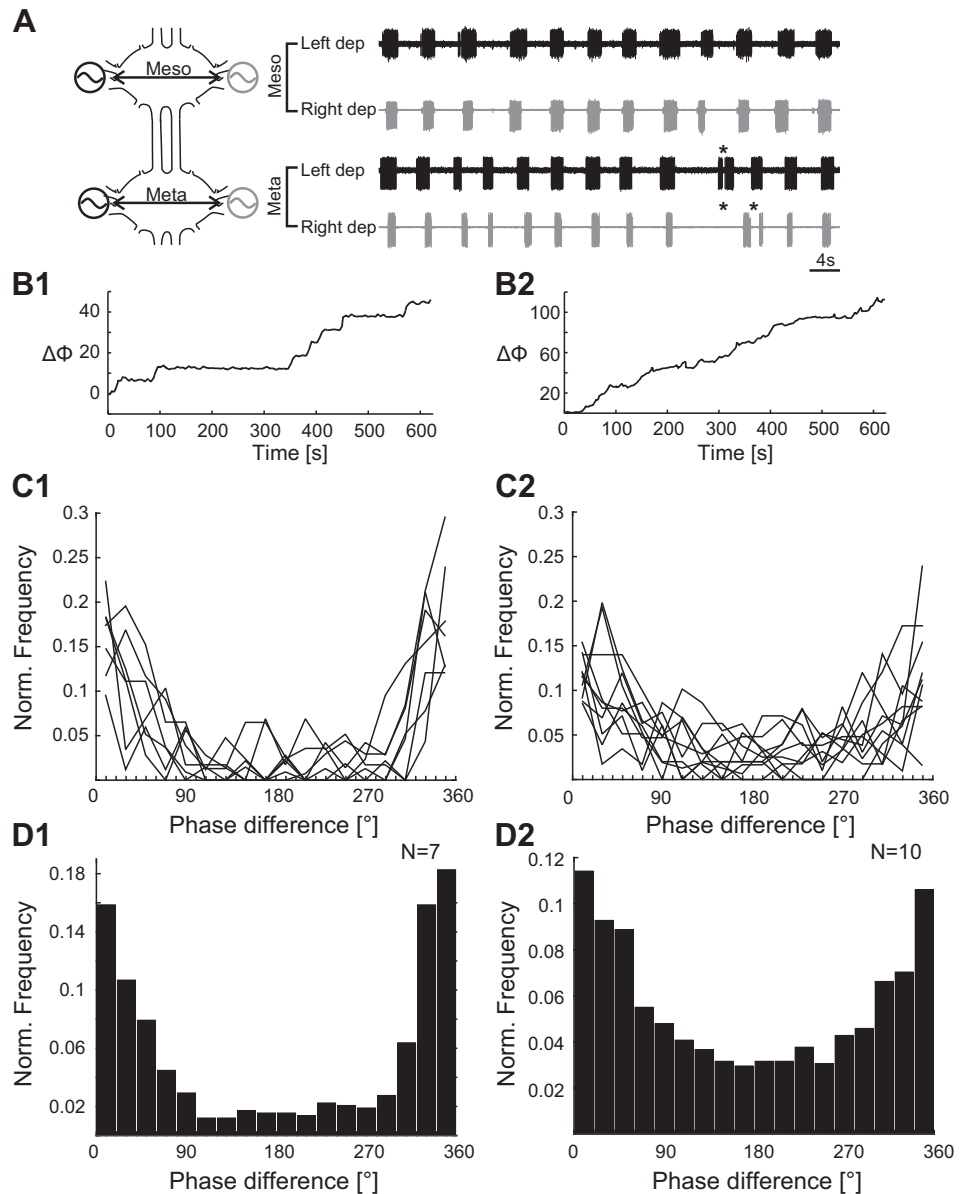


Fig. 4. Phase analysis of the interconnected meso- (Meso) and metathoracic (Meta) ganglia. *A*: extracellular recording of contralateral depressor (dep) MN activity in the interconnected Meso and Meta ganglia. Rhythmic activity was induced by application of 5 mM pilocarpine in saline. Simultaneous bursting activity of contralateral depressor MNs is observed in both ganglia. Approximately simultaneous bursting was often interrupted by gaps in activity or double bursts (asterisks). *B1*: the phase difference ($\Delta\Phi$) between contralateral rhythmic activity of the interconnected Meso ganglion shows very long recording intervals of coupled activity. *B2*: the $\Delta\Phi$ between contralateral rhythmic activity of the interconnected Meta ganglion fluctuate more, but also show long intervals of coupled activity. *C1* and *C2*: overall $\Delta\Phi$ distributions between contralateral activity of the interconnected Meso (*C1*) and Meta ganglion (*C2*) plotted on top of each other. All distributions in both ganglia (7 in *C1* and 10 in *C2*) show clear peaks at the start of the cycle. Intersegmental connection has an influence on contralateral coupling. *D1* and *D2*: distributions based on normalized and pooled data from 7 and 10 different animal preparations for the interconnected Meso (*D1*) and Meta ganglion (*D2*). There is a preference for in-phase activity between contralateral depressor motor outputs of both interconnected ganglia. *N*, no. of animal preparations.

in-phase with a mean angle of 360° (95% CI: 354.5 to 4.5°), an angular deviation of 52° , and an r-vector length of 0.59 (Fig. 4*D1*). More than one-half of the cycles (66%) had a phase difference of $0 \pm 45^\circ$, while the rest of the cycles showed phase differences distributed all around the unit circle. Pooled data from the interconnected metathoracic ganglion showed a mean angle of 10° (95% CI: 2 to 18°), an angular deviation of 67.4° , and an r-vector length of 0.31 . Here, 43% of the cycles showed phase differences within the interval of $0 \pm 45^\circ$.

Apparently, neural signals transmitted through the connectives that link the two ganglia stabilize contralateral phase relationships and/or restrict them to certain values. Moreover, intersegmental signals coming from the mesothoracic ganglion have a significant influence on coordination between rhythmic activity of contralateral depressor MNs in the metathoracic ganglion, leading to long intervals of in-phase activity (compare Figs. 3*B2* and 4*B2*). To substantiate this observation, we split the bath between the meso- and the metathoracic ganglia

and applied pilocarpine first to the metathoracic ganglion and, subsequently, to both ganglia ($N = 6$).

After activation of the metathoracic ganglion, the overall distributions of phase differences in six different preparations showed peaks at different angles throughout the cycle (Fig. 5*B1*). In two preparations, peaks were formed either at 180° , or between 0 and 90° and close to 270° , while distributions of all other preparations did not show such peaks. Interestingly, after subsequent activation of rhythmic activity in the mesothoracic ganglion, a tendency toward in-phase activity was apparent in four out of six preparations (Fig. 5*B2*). The phase distributions corresponding to these preparations showed a significant directedness toward 0° , whereas the hypothesis for mean direction toward 180° was rejected. Pooled data from 3,200 s of recording showed a uniform distribution ($P = 0.954$) and no distinct phase difference preference for contralateral metathoracic activity before activation of rhythmic activity in the mesothoracic ganglion, as indicated by a low r-vector length (0.01 ; Fig. 5*C1*). Following application of pilocarpine to the

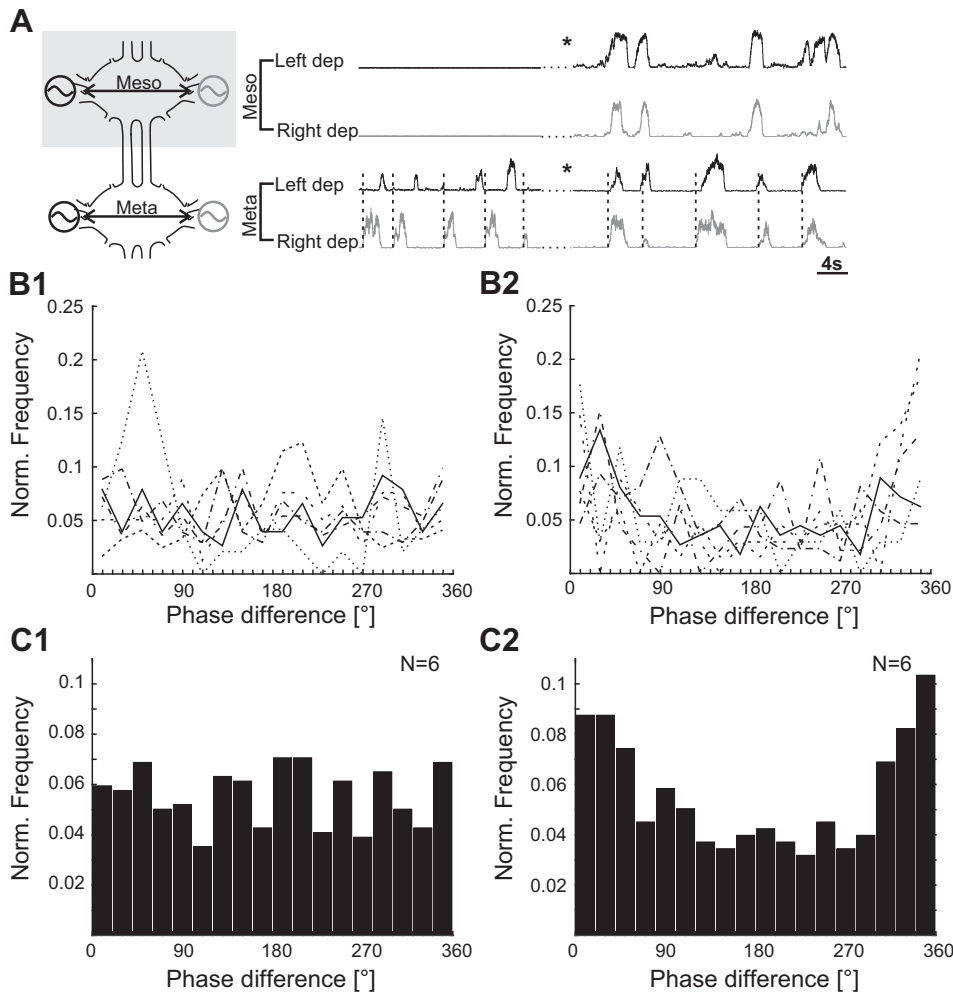


Fig. 5. Phase analysis of the interconnected metathoracic (Meta) ganglion before and after activation of the mesothoracic (Meso) networks. *A*: extracellular recording of contralateral depressor (dep) MN activity in the interconnected Meso and Meta ganglia. Rectified and smoothed activity (RSA) is shown to allow direct comparison. Bath was split with a silicone wall between the two ganglia. Rhythmic activity was induced by application of 5 mM pilocarpine, first on the Meta (left part of the recording) and subsequently on the Meso ganglion (right part). *B1*: overall phase difference ($\Delta\Phi$) distributions between contralateral activity of the interconnected Meta ganglion before pilocarpine application on the Meso ganglion. Distributions show no clear preference for any certain $\Delta\Phi$. *B2*: overall $\Delta\Phi$ distributions between contralateral activity of the interconnected Meta ganglion after pilocarpine application on the Meso ganglion. Intersegmental connection has an influence on contralateral coupling. *C1* and *C2*: distributions of the $\Delta\Phi$ between contralateral depressor MNs of the interconnected Meta ganglion, based on normalized and pooled data from six different split-bath preparations, before (*C1*) and after (*C2*) application of pilocarpine on the Meso ganglion. Distribution is uniform before (*C1*), whereas it shows a preference for in-phase activity after activation of Meso networks (*C2*). *N*, no. of animal preparations.

mesothoracic ganglion, the distribution of pooled data (2,600 s) formed a clear peak ($P < 0.001$) around the beginning of the cycle. These data showed a mean angle of 10° (95% CI: 352 to 27°), and the r-vector length was as high as 0.24, indicating higher tendency for in-phase activity (Fig. 5C2). Before the activation of the mesothoracic networks, only 26% of the cycles in the interconnected metathoracic ganglion had phase differences in the range of $0 \pm 45^\circ$, whereas this percentage was increased to 38% thereafter. These experiments support our previous conclusion that intersegmental neural signals operating between the two thoracic ganglia induce weak in-phase coupling of rhythmic activity in depressor MNs of both segments.

Coordination Between Contralateral Depressor MNs in the Isolated and Interconnected Prothoracic Ganglion

We first investigated coupling between contralateral depressor MNs in the isolated prothoracic ganglion. Here, the mean of the mean cycle periods of six different preparations was 1.79 ± 0.24 s. This is almost three times shorter than the mean cycle periods of the isolated meso- and metathoracic ganglia. In prothoracic recordings, intervals of activated bursts consisting of both the SDTr and FDTr units alternated with long SDTr bursts, and we observed no clear coordination pattern between contralateral sides (Fig. 6A). Indeed, recurrent patterns of synchronous bursting were detected in one preparation only,

which implied weak interaction between the networks that drive contralateral depressors of the prothorax (data not shown). Plotting spike activity of each depressor MN against its contralateral counterpart confirmed the above observations. Data were randomly distributed and did not show clear clusters (Fig. 6, *B1* and *B2*). Collectively, in five out of six preparations, we found no obvious coordination patterns between the contralateral sides, as pooled data of all preparations (3,900 s) showed no distinct pattern of activity (Fig. 6, *C1* and *C2*). Data in these two plots built up around zero, indicating a random distribution. Thus there exists no clear coordination between contralateral CTr-joint CPGs in the isolated prothoracic ganglion.

We next investigated whether intersegmental signals from the mesothoracic segment would affect left-right coordination of CTr-CPGs in the prothoracic ganglion. For this, we recorded contralateral depressor activity in the prothoracic ganglion, while it was connected to the mesothoracic ganglion after pilocarpine application to both ganglia (Fig. 7A). A comparison of the depressor MN activity of both ganglia showed no systematic coupling, although synchronous bursting intervals in both traces were intermingled with periods during which only slow depressor units were active. However, plotting the corresponding normalized activity of the two contralateral depressor MN pools of the prothoracic ganglion against each other revealed not only data points close to the two axes, but

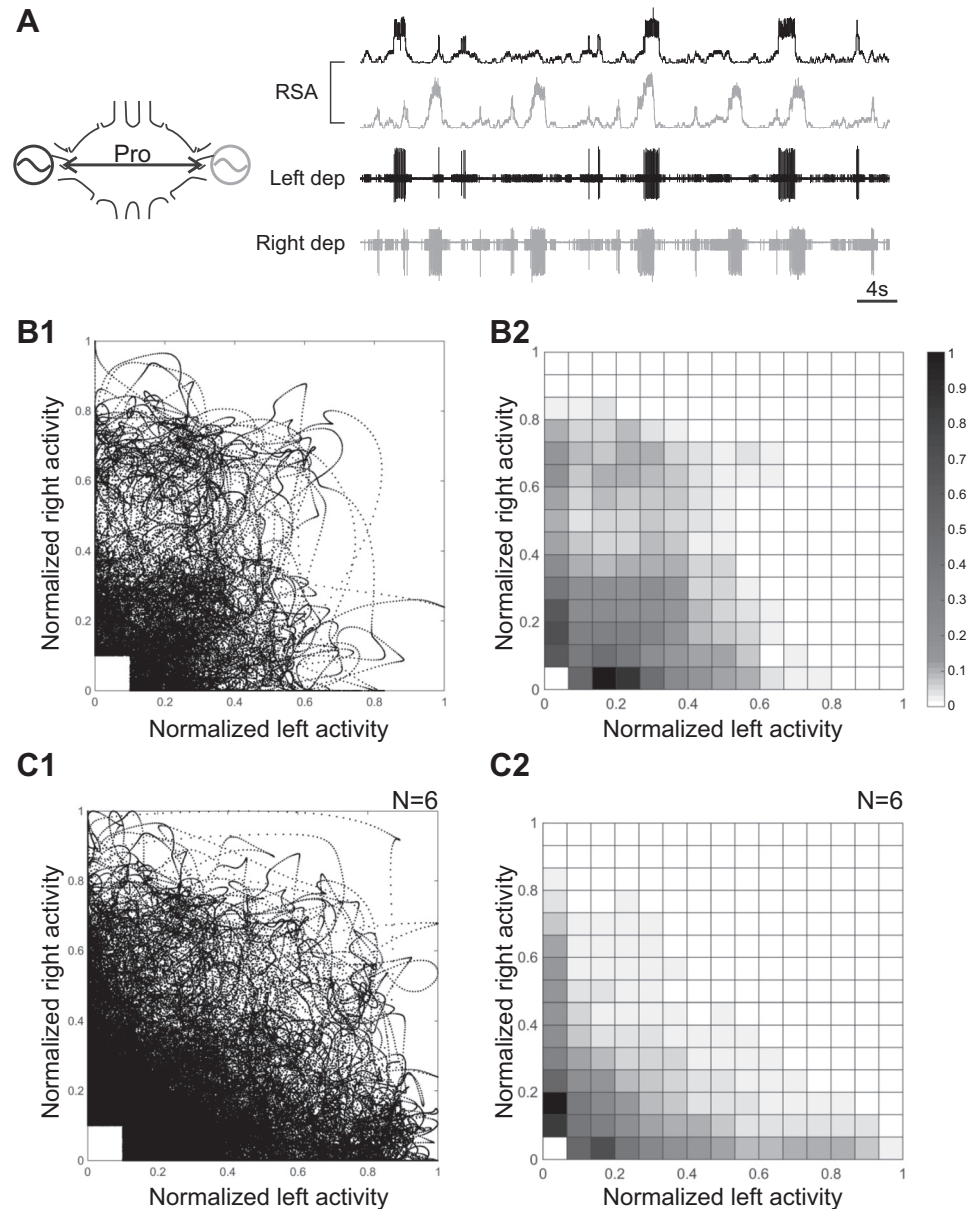


Fig. 6. Synchronization analysis of the isolated prothoracic (Pro) ganglion. *A*: extracellular recording of contralateral depressor (dep) MN activity in the isolated Pro ganglion. Rhythmic activity was induced by application of 5–7 mM pilocarpine in saline. RSA, rectified and smoothed activity. *B1*: spike activity of each nerve was smoothed, and corresponding spike activity values at a rate of 100 Hz throughout the recording were plotted against each other after being normalized to the maximum activity value. The plot shows a random distribution of data, indicating no clear coordination pattern between contralateral depressor MNs. *B2*: heat map based on the data shown in *B1*. *C1*: pooled data from six preparations. Data are randomly distributed, and thus MNs show no clear coordination. *C2*: heat map based on data shown in *C1*. *N*, no. of animal preparations.

also a higher frequency of data points in the center of the plot at similar levels (around 0.6) of normalized activity (Fig. 7, *B1* and *B2*). This clustering of data indicated a higher likelihood for synchronous spiking between the two depressor MN pools, implying that there is an intersegmental influence on contralateral coordination in the prothoracic ganglion. The same was true, when both caudal ganglia were connected to the prothoracic ganglion (data not shown). Similar synchronous activity was observed between contralateral depressor MNs of the mesothoracic ganglion, while being interconnected to the prothoracic ganglion (data not shown). Distinction between synchronous and asynchronous activity was still evident after pooling the data from all five preparations with a total recording length of ~3,400 s (Fig. 7*C1*). Comparison between the heat map in Fig. 7*C2* with the isolated ganglion (Fig. 6*C2*) clearly shows a lack of coordination in the isolated prothoracic ganglion and how activity was shaped and coordinated when it was interconnected. These results

suggest that coordination between contralateral depressor MN pools in the prothoracic ganglion is influenced by intersegmental signals from the mesothoracic ganglion, resulting in synchronization and coordination between contralateral prothoracic CTr-CPGs.

Influence of Contralateral Mesothoracic Depressor CPG Activity on Contralateral Depressor MNs

Having identified that CTr-joint CPG motor outputs are weakly coupled, we sought to investigate whether ipsilateral depressor MN activity is directly affected by input coming from the contralateral CPG, resulting in weak contralateral coupling. To do this, we tested the effect of MN activity from each side of the ganglion on MN activity in the contralateral side. We combined extracellular recordings of contralateral depressor MN activity with intracellular recordings from either the SDTr or the FDTr located on the right hemisegment of the isolated and deafferented mesothoracic ganglion. In six out of

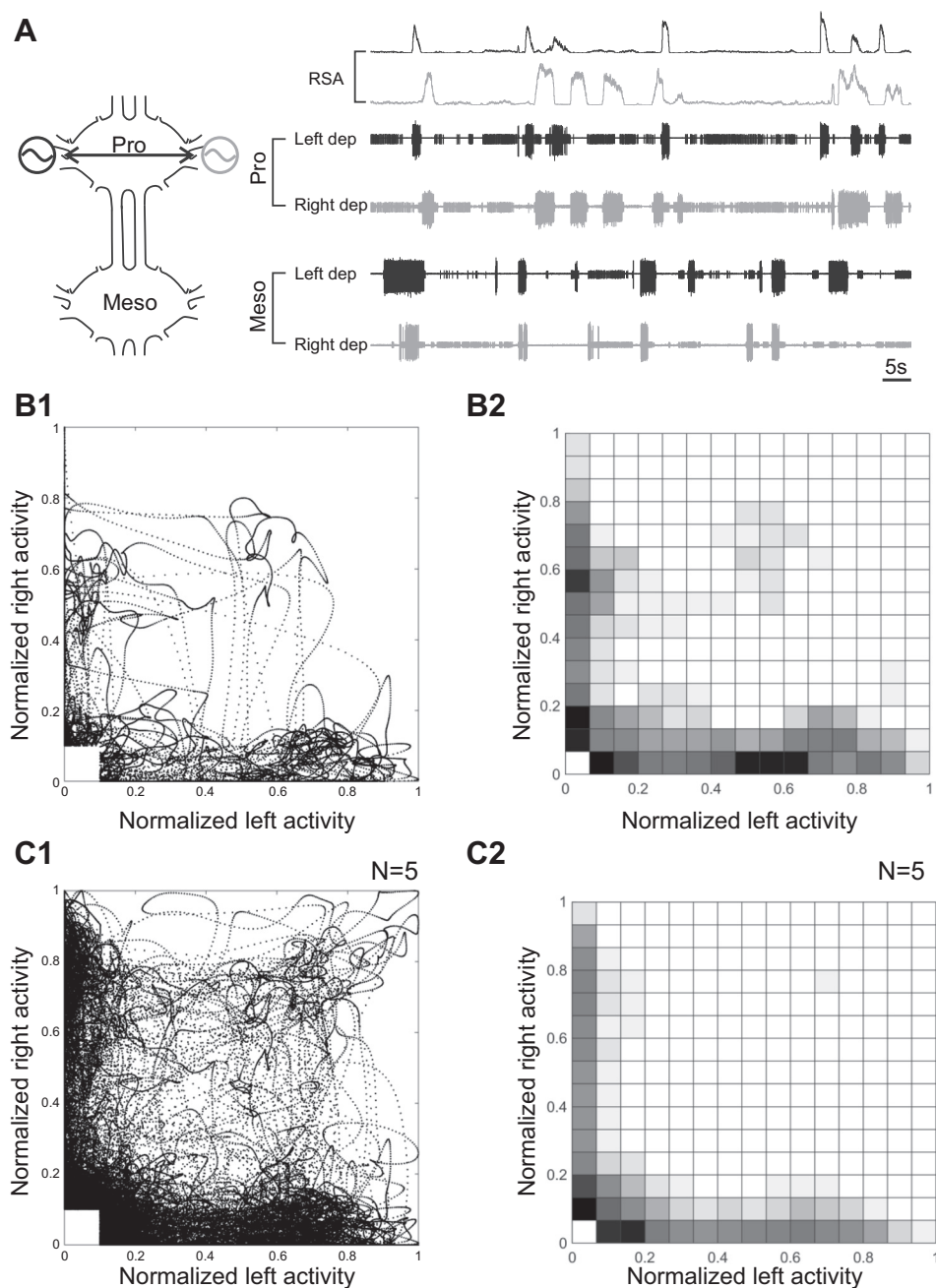


Fig. 7. Synchronization analysis of the interconnected prothoracic (Pro) ganglion. *A*: extracellular recording of contralateral depressor (dep) MN activity in the interconnected Pro and mesothoracic (Meso) ganglia. Rhythmic activity was induced by application of 5–7 mM pilocarpine in saline. RSA, rectified and smoothed activity of the left and right Pro depressor traces. Bursting intervals alternate with long slow unit activation periods. *B1*: normalized spike activity of one Pro depressor is plotted against the contralateral depressor activity. There are clear clusters of data points at around 0.6 close to the two axes (asynchronous activity) and at the center (synchronous activity) of the plot. *B2*: heat map based on the data shown in *B1*. Distinct data clusters indicate coordination of activity between the two MNs. *C1*: pooled data from five preparations. Data are clustered, indicating improved coordination between contralateral depressor MNs when Pro and Meso ganglia are connected. *C2*: heat map based on data shown in *C1*. *N*, no. of animal preparations.

six recordings, we detected no effect on the intracellular trace at the contralateral depressor cycle onset, indicating that there is no direct influence between contralateral depressor MNs (Fig. 8*A*). Superposition of the intracellular recording trace aligned to the cycle onset of either the contralateral (Fig. 8*Bi*) or the ipsilateral (Fig. 8*Bii*) depressor cycle confirmed that the FDTr receives no input related to the contralateral depressor activity. In agreement with these results, current injection of up to 7 nA in a depressor MN on one side had no influence on the rhythm of the contralateral depressor activity. The input resistance of the neuron showed no alteration correlated with the left depressor cycle (Fig. 8*C*). Therefore, based on activation patterns in the presence of pilocarpine, it is unlikely that there exists a direct influence of the CTr-joint CPG on the contralateral depressor MN.

DISCUSSION

In the present study, we analyzed intra- and intersegmental interactions between segmental CPGs of the depressor trochanteris MNs in all three isolated or interconnected thoracic ganglia of the stick insect. According to our data, there is no strong and persistent cycle-to-cycle coupling between contralateral sides of any of the three thoracic ganglia in the presence of pilocarpine. More particularly, we observed a tendency for certain phase differences in the isolated meso- and metathoracic ganglia (Figs. 2*D* and 3*D*) and no evidence for coordination in the isolated prothoracic ganglion (Fig. 6, *C1* and *C2*). However, when ganglia were connected, intrasegmental CPG coordination was modified, so that the likelihood for coordinated activity increased for all ganglia (Figs. 4, *D1* and *D2*, and 7). Finally, intracellular recordings of depressor

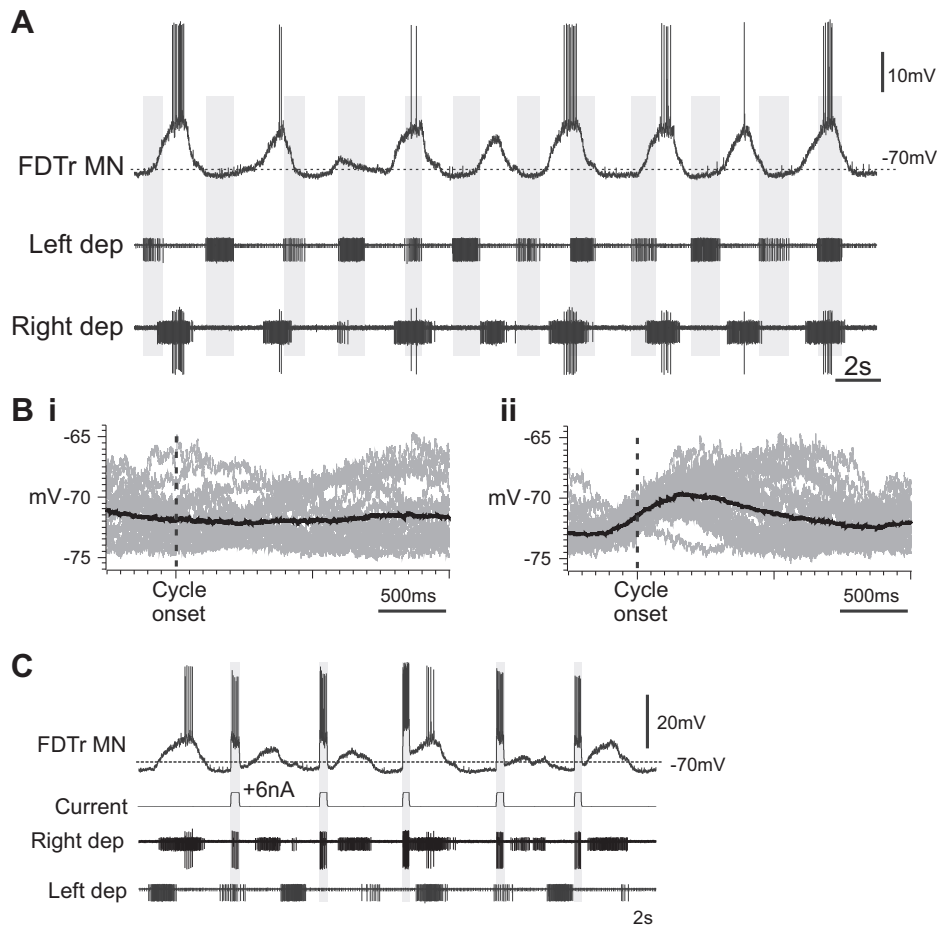


Fig. 8. Intracellular recording of the fast depressor (dep) MN of the isolated mesothoracic ganglion. *A*: intracellular recording of the fast depressor MN (FDTTr) from the right hemisegment, combined with extracellular recording of contralateral depressor MN activity in the isolated mesothoracic ganglion. Rhythmic activity was induced by application of 5 mM pilocarpine in saline. There was no FDTTr membrane potential modulation in phase with the contralateral depressor burst onset (shaded bars). *B*: superpositions of the intracellular trace aligned according to the contralateral-left (*i*) or the ipsilateral-right (*ii*) depressor cycle onset. For this analysis, an interval was chosen, during which the FDTTr was not spiking. No input in phase with the contralateral cycle onset could be observed in the FDTTr trace. *C*: rectangular depolarizing current pulses of 6 nA applied on FDTTr had no influence on contralateral depressor activity or rhythmicity.

MNs in the isolated mesothoracic ganglion showed no direct interaction between depressor CPG networks and contralateral MNs (Fig. 8). Our study highlights the presence of weak central intersegmental interactions between depressor MNs in the stick insect walking system, giving rise to synchronous segmental activity, a coordination pattern that is not observed in freely walking insects.

Coordination in Isolated Ganglia

We have shown that contralateral depressor rhythms are apparently not coordinated in the isolated prothoracic ganglion, whereas in the meso- and metathoracic ganglia they show a tendency for in-phase and antiphase activity, respectively.

Front, middle, and hind legs are structurally and functionally similar to each other, and they all actively contribute to walking on horizontal surfaces. Nevertheless, front legs have a special role, as they can perform additional steps or searching movements independently from other legs (Cruse 1976; Grabowska et al. 2012). Moreover, front legs in swing may perform retargeting movements that result in leg positioning at the height of the last antennal contact on the substrate (Schütz and Dürr 2011). Lastly, front legs have been shown to play only a minor role in propulsion and body weight support of *C. morosus* (Dallmann et al. 2016). Taken together, our findings suggest that the weak central influences between contralateral prothoracic depressor CPGs reported here make those networks more susceptible to sensory and descending input and add to the observed flexibility and autonomy of the front legs.

This conclusion agrees with behavioral data that show stronger coordination between the two front legs compared with all other legs in preparations that are not deprived of sensory input (Cruse and Saxler 1980; Dean 1989).

Our results suggest that central coupling interactions are more important for contralateral depressor coordination in the meso- and metathoracic ganglia. In accordance with the data of Knebel et al. (2017), we observed a tendency for in-phase depressor MN activity in the isolated mesothoracic ganglion. In freely behaving animals, in-phase depression of contralateral legs can be observed after synchronous elevation of legs in one segment (Cruse and Knauth 1989; Graham 1985; Wendler 1966). In addition, forces generated by two stationary middle legs on the ground oscillate in-phase, while all other legs walk on a slippery surface (Cruse and Saxler 1980). Thus mesothoracic legs can be synchronously active when they are uncoupled from the front and hind legs. Taken together, the central coupling interactions observed in our experiments result in a default in-phase coordination that could support synchronous middle-leg movements when these legs become uncoupled from the rest. Central in-phase coupling can then be modified by local and intersegmental sensory information to generate behaviorally relevant coordination. The importance of sensory input for coordination in the mesothoracic ganglion has been indicated by behavioral experiments after connective transection (Dean 1989) and in animals walking on a slippery surface (Cruse and Knauth 1989). These experiments show impaired and unclear con-

tralateral coordination between the two middle legs compared with the other two pairs of legs.

In line with data from the locust (Knebel et al. 2017), contralateral depressors of the isolated metathoracic ganglion in the stick insect show a tendency for antiphase activity, exactly as is expected from a freely behaving animal. Our findings are complemented by the previous observation that force oscillations of contralateral, standing hind legs are also out of phase when the other legs walk on a slippery surface (Cruse and Saxler 1980). Considering that hind legs are the closest to the center of mass of the animal, and hind leg depressor joint torques are critical for the animal's propulsion (Dallmann et al. 2016), we, therefore, believe that central coupling mechanisms in the isolated metathoracic ganglion are crucial for the animal's survival by being able to produce functional motor output when all other ganglia are decoupled and sensory information is absent.

Differences in intrasegmental coordination among thoracic ganglia may arise from segmental differences in excitability that could be related to differential expression of muscarinic acetylcholine receptors in each ganglion. At present, no data are available on this issue. Thus, under the assumption that there are no such differences in excitability among thoracic ganglia, we may currently conclude that differences in intrasegmental coordination originate in the different intrasegmental connectivities among the central neural networks that drive the CTr-CPGs of the front, middle, and hind legs of *C. morosus*.

Contribution of Central Intersegmental Pathways to Leg Coordination During Walking

The in-phase coordination patterns we observed in this study after activation of interconnected ganglia may, on initial consideration, appear counterintuitive for understanding walking behavior in the stick insect. It is a nonfunctional coordination pattern that does not resemble any of the walking patterns stick insects use. However, based on this in-phase default output of the deafferented system, we can now provide feasible explanations for previously published observations.

Behavioral studies regarding the influence between walking legs in the stick insect have resulted in seven different effects that legs can have on their immediate neighbors (either contralateral or rostral and caudal), known as the Cruse rules (Cruse 1990; Schilling et al. 2013). These rules are sufficient for generating stable and coordinated six-legged locomotion in computational models (Cruse 1990; Dürr et al. 2004; Schilling et al. 2013). According to *rule 5*, an increase in load in one of the legs will prolong the stance phases in other legs, thereby efficiently distributing load among them (Cruse 1990; Dürr et al. 2004). This intersegmental joint activation of MNs is reminiscent of the in-phase bursting episodes we observed in our experiments. Thus we hypothesize that the centrally generated in-phase coordination patterns result from the stochastic activation of sensory-related central pathways. Pilocarpine could potentially activate such pathways, as it binds to metabotropic acetylcholine receptors that are present on sensory terminals (Trimmer 1995).

In a previous study, the influence of one stepping front leg on MN activity in posterior segments was analyzed (Borgmann et al. 2009). This study showed that activity of the ipsilateral

middle and hind leg retractor MNs was entrained in phase with the front leg stepping cycle. However, it is not known whether distinct intersegmental sensory pathways mediate this influence or whether sensory signals are transmitted through specific central connections between CPGs. Here, we show that there are indeed central neural pathways capable of supporting intrasegmental in-phase coupling between CPGs. Interestingly, even signals from a quiescent mesothoracic ganglion seem to affect intrasegmental coordination in the metathoracic ganglion, since phase distributions of contralateral activity in the metathoracic segment, when connected to the quiescent mesothoracic ganglion, were uniform, differing from those of the completely isolated metathoracic ganglion that exhibited slight peaks at 180° (cf., Figs. 3 and 5). Thus, although we cannot exclude the existence of distinct sensory pathways, it is possible that pilocarpine activates sensory afferents that transmit their signals through central connections between CPGs and synchronize CPG activity. If this is true, then we provide further evidence for the hypothesis advanced by Borgmann et al. (2009), according to which an unloaded leg moves in synchrony with its neighboring leg until it receives load information that overrides this weak coordinating influence.

Comparison with Other Insect Walking Systems

Pilocarpine-induced fictive motor patterns in deafferented preparations of the cockroach, hawk moth, locust, and stick insect have been routinely analyzed to detect central interactions between CPGs (Büschges et al. 1995; David et al. 2016; Johnston and Levine 2002; Knebel et al. 2017; Ryckebusch and Laurent 1994). In some preparations, centrally generated coordination patterns were similar to those observed in freely behaving animals, whereas, in others, they substantially differed. This may be due to the relative contribution of central CPG coupling mechanisms for coordination. In addition, behavioral studies have provided input for our understanding of the influence sensory deprivation has on coordination and its dependence on walking speed (Berendes et al. 2016).

Pilocarpine application to the isolated and deafferented thoracic nerve cord of cockroaches results in generation of a tripod-like coordination pattern, similar to the pattern these insects show during actual walking (Fuchs et al. 2011). In a recent study, intersegmental phase relationships between depressor MNs were found to be in accordance with those observed in the walking cockroach (David et al. 2016). Moreover, in the isolated thoracic nerve cord of the hawk moth, pilocarpine elicited strictly alternating activity between contralateral depressor MNs in all segments, and intersegmental coordination resembled a tripod pattern (Johnston and Levine 2002). In contrast, depressor activity in all segments of the locust (Knebel et al. 2017) and the stick insect (in the present study) were found to be weakly coupled in phase, resulting in coordination patterns that have never been observed in behavioral experiments. This reveals that the contribution of central coupling mechanisms to CPG coordination differs among these insect species. Considering that cockroaches and moths show relatively short cycle periods during walking (Couzin-Fuchs et al. 2015; Johnston and Levine 1996) compared with locusts and stick insects (Burns 1973; Graham 1985), our current results support the notion that coordination in slow-walking insects is largely based on sensory input contributions, while

present evidence suggests that, in fast-walking insects, central CPG coupling plays an important role (Couzin-Fuchs et al. 2015; Fuchs et al. 2011). Thus it may be that central CPG connections in the stick insect provide the substrate on which sensory signals can act to shape the coordination pattern into a behaviorally relevant one (Borgmann et al. 2009). In addition, such a hypothesis would explain the entrainment of a leg stump and the subsequent increase in coordination strength observed at fast walking speeds in the fruit fly (Berendes et al. 2016) and the rapid recovery from perturbations during running in cockroaches (Couzin-Fuchs et al. 2015).

A recent study by Knebel et al. (2017) is particularly relevant to our results. In both their study and the present study, the three isolated thoracic ganglia showed different inherent contralateral phase relationships, and, interestingly, depressor MN pools of the isolated metathoracic ganglion showed a high tendency for antiphase activity. Furthermore, intersegmental coupling influenced contralateral phase relationships, especially in the metathoracic ganglion, and, similar to the data we present herein, depressor CPGs of all segments were synchronously active after pilocarpine application to the whole nerve cord. However, data from the present study point out the irregularity of pilocarpine-induced rhythmicity, as there was no consistent cycle-to-cycle coupling. Phase relationships were distributed all around the unit circle, and we only found tendencies for certain phase relationships. Moreover, in contrast to the study by Knebel et al. (2017), pharmacological activation of one ganglion in the present study never induced activity in neighboring, untreated ganglia (Ludwar et al. 2005). Therefore, we conclude that coupling interactions between CPGs in the stick insect are weak, and the deafferented system is characterized by the absence of strict cycle-to-cycle coupling. Given the important roles of local sensory feedback in the generation of stepping (Büschges et al. 2008) and in the coordination between neighboring legs (Borgmann et al. 2009), we propose that sensory signals from the legs serve as a primary source of neural information for generating functional intersegmental leg coordination patterns.

Neural Mechanisms Underlying Intrasegmental CPG Coordination

In vertebrates, there is detailed information on the neural mechanisms underlying intrasegmental coordination. In the mouse spinal cord, flexor extensor CPG activity can be independently induced in each hemisegment, showing that contralateral networks do not form a half-center (Häggglund et al. 2013). Left-right alternation in mice is not only achieved by direct and indirect contralateral MN inhibition via inhibitory and excitatory commissural interneurons, respectively (Butt and Kiehn 2003; Quinlan and Kiehn 2007), but also by excitatory neurons recruited at higher fictive locomotion frequencies (Talpalar et al. 2013). In the lamprey, although there are both excitatory and inhibitory commissural neurons (Biró et al. 2008), contralateral alternating activity is based on glycinergic inhibitory commissural neurons, and hemisegments become synchronously active when glycinergic transmission is blocked (Grillner 2003).

Presumably the simplest CPG organization is the one underlying swimming in the sea slug *Dendronotus iris* (Sakurai and Katz 2016). This CPG consists of only two types of

interneurons in each hemisegment that mutually inhibit their contralateral counterparts. Interestingly, the one interneuron type forms an excitatory and an electrical synapse with the contralateral heterologous interneuron, resulting in a twisted half-center CPG organization. In contrast, in the locust wing-beat system, hemisegmental networks in the mesothoracic ganglion are more independent, and rhythm generation in flight MNs appears not to exclusively depend on commissural pathways (Wolf et al. 1988). Moreover, deafferentation has almost no influence on contralateral coordination in this system. Thus coordination between autonomous local hemisegmental networks in the locust flight system is based on a central distributed network (Wolf et al. 1988). In the deafferented preparation of the stick insect, a cut along the midline of the meso- and metathoracic ganglia did not abolish pilocarpine-induced rhythmicity of the protractor and retractor MN pools (Büschges et al. 1995). Considering the intrasegmental influences observed regarding contralateral coordination in our experiments, we hypothesize that such a distributed coordinating network also applies to the stick insect system.

Information regarding intrasegmental coupling between contralateral networks in the stick insect is highly elusive. Here, intracellular recordings of depressor MNs on one side of the ganglion, combined with extracellular depressor MN recordings after pilocarpine application, showed that contralateral depressor MNs are directly connected neither with each other, nor with the contralateral CPG networks. Therefore, we expect weak coupling between them to be mediated via commissural interneurons that cross the midline and could potentially transfer coordinating signals between premotor networks of the two hemisegments. This is supported by reports of premotor nonspiking neurons that process sensory signals coming from the contralateral side (Stein et al. 2006). In the mesothoracic ganglion of the stick insect, there are six dorsal and five ventral commissural tracts (Kittmann et al. 1991). Intracellular recording and identification of neurons that send their axons through those tracts may unravel the neural networks underlying weak intrasegmental coupling.

Conclusion

The stick insect walking system is a highly modular system. There are distinct oscillatory networks controlling the activity of single leg joints that need to be efficiently coordinated during walking. We show here that CPGs interact centrally at the premotor level and form a distributed coordinating network that is unable to generate the coordinating patterns expressed *in vivo*. However, this default coordinating scheme is susceptible to intersegmental and local sensory signals that shape its inherent pattern to produce behaviorally relevant motor output. Our data further support the notion that sensory input is more important for establishing coordination in slow walking animals.

ACKNOWLEDGMENTS

We thank the following colleagues who contributed to this work: N. Rosjat for helpful suggestions on a previous draft of the manuscript; A. Chockley for editing it; and M. Dübbert, J. Sydow, and H.-P. Bollhagen for providing excellent technical assistance.

GRANTS

This study was supported by the joint Bundesministerium für Bildung und Forschung/National Science Foundation Collaborative Research in Computational Neuroscience Project to A. Büschges, S. Daun (01GQ1412), and P. Holmes (DMS-1430077), entitled “Central pattern generators and reflexive feedback in insect locomotion: a cross-species study.”

DISCLOSURES

No conflicts of interest, financial or otherwise, are declared by the authors.

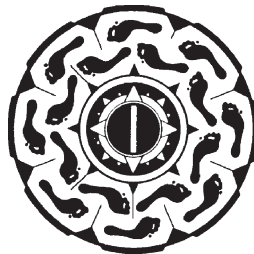
AUTHOR CONTRIBUTIONS

C.M., P.H., A. Borgmann, S.D., and A. Büschges conceived and designed research; C.M. performed experiments; C.M., T.B., and A. Büschges analyzed data; C.M., T.B., P.H., A. Borgmann, S.D., and A. Büschges interpreted results of experiments; C.M. prepared figures; C.M. and A. Büschges drafted manuscript; C.M., P.H., S.D., and A. Büschges edited and revised manuscript; C.M., T.B., P.H., A. Borgmann, S.D., and A. Büschges approved final version of manuscript.

REFERENCES

- Bässler U, Wegner U. Motor output of the denervated thoracic ventral nerve cord in the stick insect *Carausius morosus*. *J Exp Biol* 105: 127–145, 1983.
- Bender JA, Simpson EM, Tietz BR, Daltorio KA, Quinn RD, Ritzmann RE. Kinematic and behavioral evidence for a distinction between trotting and ambling gaits in the cockroach *Blaberus discoidalis*. *J Exp Biol* 214: 2057–2064, 2011. doi:10.1242/jeb.056481.
- Berendes V, Zill SN, Büschges A, Bockemühl T. Speed-dependent interplay between local pattern-generating activity and sensory signals during walking in *Drosophila*. *J Exp Biol* 219: 3781–3793, 2016. doi:10.1242/jeb.146720.
- Berens P. CircStat: a MATLAB toolbox for circular statistics. *J Stat Softw* 31: 1–21, 2009. doi:10.18637/jss.v031.i10.
- Biró Z, Hill RH, Grillner S. The activity of spinal commissural interneurons during fictive locomotion in the lamprey. *J Neurophysiol* 100: 716–722, 2008. doi:10.1152/jn.90206.2008.
- Borgmann A, Hooper SL, Büschges A. Sensory feedback induced by front-leg stepping entrains the activity of central pattern generators in caudal segments of the stick insect walking system. *J Neurosci* 29: 2972–2983, 2009. doi:10.1523/JNEUROSCI.3155-08.2009.
- Borgmann A, Scharstein H, Büschges A. Intersegmental coordination: influence of a single walking leg on the neighboring segments in the stick insect walking system. *J Neurophysiol* 98: 1685–1696, 2007. doi:10.1152/jn.00291.2007.
- Burns MD. The control of walking in *Orthoptera*. I. Leg movements in normal walking. *J Exp Biol* 58: 45–58, 1973.
- Büschges A. Role of local nonspiking interneurons in the generation of rhythmic motor activity in the stick insect. *J Neurobiol* 27: 488–512, 1995. doi:10.1002/neu.480270405.
- Büschges A. Inhibitory synaptic drive patterns motoneuronal activity in rhythmic preparations of isolated thoracic ganglia in the stick insect. *Brain Res* 783: 262–271, 1998. doi:10.1016/S0006-8993(97)01370-X.
- Büschges A, Akay T, Gabriel JP, Schmidt J. Organizing network action for locomotion: insights from studying insect walking. *Brain Res Rev* 57: 162–171, 2008. doi:10.1016/j.brainresrev.2007.06.028.
- Büschges A, Schmitz J, Bässler U. Rhythmic patterns in the thoracic nerve cord of the stick insect induced by pilocarpine. *J Exp Biol* 198: 435–456, 1995.
- Butt SJB, Kiehn O. Functional identification of interneurons responsible for left-right coordination of hindlimbs in mammals. *Neuron* 38: 953–963, 2003. doi:10.1016/S0896-6273(03)00353-2.
- Couzin-Fuchs E, Kiemel T, Gal O, Ayali A, Holmes P. Intersegmental coupling and recovery from perturbations in freely running cockroaches. *J Exp Biol* 218: 285–297, 2015. doi:10.1242/jeb.112805.
- Cruse H. The function of the legs in the free walking stick insect, *Carausius morosus*. *J Comp Physiol A Neuroethol Sens Neural Behav Physiol* 112: 235–262, 1976. doi:10.1007/BF00606541.
- Cruse H. What mechanisms coordinate leg movement in walking arthropods? *Trends Neurosci* 13: 15–21, 1990. doi:10.1016/0166-2236(90)90057-H.
- Cruse H, Knauth A. Coupling mechanisms between the contralateral legs of a walking insect (*Carausius morosus*). *J Exp Biol* 144: 199–213, 1989.
- Cruse H, Saxler G. Oscillations of force in the standing legs of a walking insect (*Carausius morosus*). *Biol Cybern* 36: 159–163, 1980. doi:10.1007/BF00365770.
- Dallmann CJ, Dürr V, Schmitz J. Joint torques in a freely walking insect reveal distinct functions of leg joints in propulsion and posture control. *Proc Biol Sci* 283: 20151708, 2016. doi:10.1098/rspb.2015.1708.
- David I, Holmes P, Ayali A. Endogenous rhythm and pattern-generating circuit interactions in cockroach motor centres. *Biol Open* 5: 1229–1240, 2016. doi:10.1242/bio.018705.
- Dean J. Leg coordination in the stick insect *Carausius morosus*: effects of cutting thoracic connectives. *J Exp Biol* 145: 103–131, 1989.
- Dürr V, Schmitz J, Cruse H. Behaviour-based modelling of hexapod locomotion: linking biology and technical application. *Arthropod Struct Dev* 33: 237–250, 2004. doi:10.1016/j.asd.2004.05.004.
- Fuchs E, Holmes P, David I, Ayali A. Proprioceptive feedback reinforces centrally generated stepping patterns in the cockroach. *J Exp Biol* 215: 1884–1891, 2012. doi:10.1242/jeb.067488.
- Fuchs E, Holmes P, Kiemel T, Ayali A. Intersegmental coordination of cockroach locomotion: adaptive control of centrally coupled pattern generator circuits. *Front Neural Circuits* 4: 125, 2011. doi:10.3389/fncir.2010.00125.
- Goldammer J, Büschges A, Schmidt J. Motoneurons, DUM cells, and sensory neurons in an insect thoracic ganglion: a tracing study in the stick insect *Carausius morosus*. *J Comp Neurol* 520: 230–257, 2012. doi:10.1002/cne.22676.
- Grabowska M, Godlewska E, Schmidt J, Daun-Gruhn S. Quadrupedal gaits in hexapod animals—inter-leg coordination in free-walking adult stick insects. *J Exp Biol* 215: 4255–4266, 2012. doi:10.1242/jeb.073643.
- Graham D. Influence of coxa-thorax joint receptors on retractor motor output during walking in *Carausius morosus*. *J Exp Biol* 114: 131–139, 1985.
- Grillner S. The motor infrastructure: from ion channels to neuronal networks. *Nat Rev Neurosci* 4: 573–586, 2003. doi:10.1038/nrn1137.
- Hägglund M, Dougherty KJ, Borgius L, Itohara S, Iwasato T, Kiehn O. Optogenetic dissection reveals multiple rhythmogenic modules underlying locomotion. *Proc Natl Acad Sci USA* 110: 11589–11594, 2013. doi:10.1073/pnas.1304365110.
- Hughes GM. The co-ordination of insect movements. *J Exp Biol* 29: 267–285, 1952.
- Johnston RM, Levine RB. Locomotory behavior in the hawkmoth *Manduca sexta*: kinematic and electromyographic analyses of the thoracic legs in larvae and adults. *J Exp Biol* 199: 759–774, 1996.
- Johnston RM, Levine RB. Thoracic leg motoneurons in the isolated CNS of adult *Manduca* produce patterned activity in response to pilocarpine, which is distinct from that produced in larvae. *Invert Neurosci* 4: 175–192, 2002. doi:10.1007/s10158-002-0019-4.
- Katz PS, Hooper SL. Invertebrate central pattern generators. In: *Invertebrate Neurobiology*, edited by Norrth G, Greenspan RJ. Cold Spring Harbor, NY: Cold Spring Harbor Laboratory Press, 2007.
- Kittmann R, Dean J, Schmitz J. An atlas of the thoracic ganglia in the stick insect, *Carausius morosus*. *Philos Trans R Soc Lond B Biol Sci* 331: 101–121, 1991. doi:10.1098/rstb.1991.0002.
- Knebel D, Ayali A, Pflüger HJ, Rillich J. Rigidity and flexibility: the central basis of inter-leg coordination in the locust. *Front Neural Circuits* 10: 112, 2017. doi:10.3389/fncir.2016.00112.
- Kralemann B, Cimponeriu L, Rosenblum M, Pikovsky A, Mrowka R. Phase dynamics of coupled oscillators reconstructed from data. *Phys Rev E Stat Nonlin Soft Matter Phys* 77: 066205, 2008. doi:10.1103/PhysRevE.77.066205.
- Ludwar BC, Göritz ML, Schmidt J. Intersegmental coordination of walking movements in stick insects. *J Neurophysiol* 93: 1255–1265, 2005. doi:10.1152/jn.00727.2004.
- Marder E, Bucher D. Central pattern generators and the control of rhythmic movements. *Curr Biol* 11: R986–R996, 2001. doi:10.1016/S0960-9822(01)00581-4.
- Marder E, Calabrese RL. Principles of rhythmic motor pattern generation. *Physiol Rev* 76: 687–717, 1996.
- Mendes CS, Bartos I, Akay T, Márka S, Mann RS. Quantification of gait parameters in freely walking wild type and sensory deprived *Drosophila melanogaster*. *Elife* 2: e00231, 2013. doi:10.7554/eLife.00231.
- Orlovsky GN, Deliagina TG, Grillner S. *Neuronal Control of Locomotion*. Oxford: Oxford University Press, 1999. doi:10.1093/acprof:oso/9780198524052.001.0001.

- Pikovsky A, Rosenblum M, Kurths J.** *Synchronization: A Universal Concept in Nonlinear Sciences*. New York: Cambridge University Press, 2001. doi:10.1017/CBO9780511755743.
- Quinlan KA, Kiehn O.** Segmental, synaptic actions of commissural interneurons in the mouse spinal cord. *J Neurosci* 27: 6521–6530, 2007. doi:10.1523/JNEUROSCI.1618-07.2007.
- Rosenbaum P, Wosnitza A, Büschges A, Gruhn M.** Activity patterns and timing of muscle activity in the forward walking and backward walking stick insect *Carausius morosus*. *J Neurophysiol* 104: 1681–1695, 2010. doi:10.1152/jn.00362.2010.
- Ryckebusch S, Laurent G.** Rhythmic patterns evoked in locust leg motor neurons by the muscarinic agonist pilocarpine. *J Neurophysiol* 69: 1583–1595, 1993.
- Ryckebusch S, Laurent G.** Interactions between segmental leg central pattern generators during fictive rhythms in the locust. *J Neurophysiol* 72: 2771–2785, 1994.
- Sakurai A, Katz PS.** The central pattern generator underlying swimming in *Dendronotus iris*: a simple half-center network oscillator with a twist. *J Neurophysiol* 116: 1728–1742, 2016. doi:10.1152/jn.00150.2016.
- Schilling M, Hoinville T, Schmitz J, Cruse H.** Walknet, a bio-inspired controller for hexapod walking. *Biol Cybern* 107: 397–419, 2013. doi:10.1007/s00422-013-0563-5.
- Schmitz J, Büschges A, Delcomyn F.** An improved electrode design for en passant recording from small nerves. *Comp Biochem Physiol A* 91: 769–772, 1988. doi:10.1016/0300-9629(88)90963-2.
- Schütz C, Dürr V.** Active tactile exploration for adaptive locomotion in the stick insect. *Philos Trans R Soc Lond B Biol Sci* 366: 2996–3005, 2011. doi:10.1098/rstb.2011.0126.
- Smarandache-Wellmann CR.** Arthropod neurons and nervous system. *Curr Biol* 26: R960–R965, 2016. doi:10.1016/j.cub.2016.07.063.
- Smith JC, Abdala APL, Borgmann A, Rybak IA, Paton JFR.** Brainstem respiratory networks: building blocks and microcircuits. *Trends Neurosci* 36: 152–162, 2013. doi:10.1016/j.tins.2012.11.004.
- Stein W, Büschges A, Bässler U.** Intersegmental transfer of sensory signals in the stick insect leg muscle control system. *J Neurobiol* 66: 1253–1269, 2006. doi:10.1002/neu.20285.
- Talpalar AE, Bouvier J, Borgius L, Fortin G, Pierani A, Kiehn O.** Dual-mode operation of neuronal networks involved in left-right alternation. *Nature* 500: 85–88, 2013. doi:10.1038/nature12286.
- Tass P, Rosenblum MG, Weule J, Kurths J, Pikovsky A, Volkman J, Schnitzler A, Freund H-J.** Detection of n:m phase locking from noisy data: application to magnetoencephalography. *Phys Rev Lett* 81: 3291–3294, 1998. doi:10.1103/PhysRevLett.81.3291.
- Trimmer BA.** Current excitement from insect muscarinic receptors. *Trends Neurosci* 18: 104–111, 1995. doi:10.1016/0166-2236(95)80032-W.
- Wendler G.** [Walking and standing of the stick insect *Carausius morosus*: sensory bristles at the leg joints as parts of closed-loop control circuits]. *Z Vgl Physiol* 48: 198–250, 1964. doi:10.1007/BF00297860.
- Wendler G.** The co-ordination of walking movements in arthropods. *Symp Soc Exp Biol* 20: 229–249, 1966.
- Wilson DM.** Insect walking. *Annu Rev Entomol* 11: 103–122, 1966. doi:10.1146/annurev.en.11.010166.000535.
- Wolf H, Ronacher B, Reichert H.** Patterned synaptic drive to locust flight motoneurons after hemisection of thoracic ganglia. *J Comp Physiol A Neuroethol Sens Neural Behav Physiol* 163: 761–769, 1988. doi:10.1007/BF00604053.
- Wosnitza A, Bockemühl T, Dübbert M, Scholz H, Büschges A.** Inter-leg coordination in the control of walking speed in *Drosophila*. *J Exp Biol* 216: 480–491, 2013. doi:10.1242/jeb.078139.



Erklärung

Ich versichere, dass ich die von mir vorgelegte Dissertation selbstständig angefertigt, die benutzten Quellen und Hilfsmittel vollständig angegeben und die Stellen der Arbeit - einschließlich Tabellen, Karten und Abbildungen -, die anderen Werken im Wortlaut oder dem Sinn nach entnommen sind, in jedem Einzelfall als Entlehnung kenntlich gemacht habe; dass diese Dissertation noch keiner anderen Fakultät oder Universität zur Prüfung vorgelegen hat; dass sie - abgesehen von oben angegebenen Teilpublikationen - noch nicht veröffentlicht worden ist sowie, dass ich eine solche Veröffentlichung vor Abschluss des Promotionsverfahrens nicht vornehmen werde. Die Bestimmungen dieser Promotionsordnung sind mir bekannt. Die von mir vorgelegte Dissertation ist von Prof. Dr. Ansgar Büschges betreut worden.

Köln, den 19.06.2018